ABSTRACT

POLASH, MD MOBARAK HOSSAIN. Modeling of Multistage Nernst-Ettingshausen Coolers. (Under the direction of Dr. Daryoosh Vashaee.)

There are high incentives for using solid-state coolers instead of the existing compression-based technologies, which are bulky, require compressors or cryogenic liquids, and have environmental issues like Ozone depletion potential (ODP) and global warming potential (GWP). Solid-state coolers are still under extensive studies aiming to increase their coefficient of performance (COP). Among the studied solid-state technologies, thermoelectric cooling is widely utilized for the temperature range above 200 K, and thermomagnetic (TM) is found most efficient in the cryogenic temperature range (<200 K). Performance of TM devices, also known as Nernst-Ettingshausen (NE) devices, is material dependent as well as shape dependent. Until now, BiSb material system has been found the most efficient TM material operating with higher thermomagnetic figure-of-merit, ZT, compared to other candidates. Again, for TM operation, some optimized shapes have been proposed to have higher efficiency among which the infinite or exponential shaped NE devices suggested by Harman's model are widely accepted to have the best performance. Harman derived an expression for the optimum shape based on the assumptions of constant current density, constant electric field, temperature independent material properties, and equal COPs for different layers of the material. Among those assumptions, some are non-realistic and lead to errors when predicting or analyzing the experimental data. The focus of this work is to derive a more accurate expression for the infinite stage devices by taking into account more realistic assumptions that can make the model predictive and better matched with experiments. A comparative study is presented that shows how the new model differs from the previous ones and how close the predictions are compared

to the existing experimental data in the literature. The simulations are extended to all suggested geometric shapes such as rectangular, trapezoidal, and exponential shapes to compare their performance. The model calculations compare the maximum temperature gradient as a function current, maximum temperature gradient as a function of device length in the heat flow direction, maximum temperature gradient versus ratio of the dimensions of the hot and cold side areas, maximum heat flow versus device length and geometric ratio, and finally COP versus temperature gradient, length and geometric ratio. As benchmarks, the maximum temperature gradient was obtained for the no-load condition, and the maximum heat flow was obtained for zero temperature gradient conditions. From the comparative analysis, our infinite shape model is found to have superior performance over other shaped devices. Simulation was done for BiSb material system for fixed magnetic field and variable electric field.

A preliminary experimental work was also performed to understand the material properties of $Bi_{95}Sb_5$ alloy and for future works. The samples were synthesized in Argon or vacuum environment to avoid oxidation. The alloy composition was confirmed by X-ray diffraction analysis, and the electrical conductivity and thermopower were measured simultaneously from room temperature down to 173 K. Experimental results are in good agreement with the high-quality samples reported in the literature.

Modeling of Multistage Nernst-Ettingshausen Coolers

by
Md Mobarak Hossain Polash

A thesis submitted to the Graduate Faculty of
North Carolina State University
in partial fulfillment of the
requirements for the Degree of
Master of Science

Material Science and Engineering

Raleigh, North Carolina

2018

APPROVED BY:

Dr. Zlatko Sitar	Dr. Mehmet Ozturk

Dr. Daryoosh Vashaee
Chair of Advisory Committee

DEDICATION

I dedicate this humble effort to my loving Father and Mother whose affection, love and prays make me able to get such success and honor. I also like to thank my amazing wife whose sacrificial care helped me to complete this work.

BIOGRAPHY

Md Mobarak Hossain Polash received his Bachelor of Science in Electrical and Electronic Engineering in 2012 and his Master of Science in Electrical and Electronic Engineering in 2015 from Bangladesh University of Engineering and Technology (BUET), Dhaka, Bangladesh. He joined ECE Department at North Carolina State University in August 2016. He started his Master of Science in Materials Science and Engineering at NC State University in January 2017. Since 2016, he is conducting his research in Nanoscience and Quantum Engineering group under the supervision of Dr. Daryoosh Vashaee.

Mobarak's main research is on investigating the prospect of MnTe material systems with Li and Cr doping as a spin caloritronic systems. His MS thesis is on modeling multistage Thermomagnetic cooling device and measuring transverse magnetic effects in thermomagnetic materials for different shapes. His research interests include thermoelectric and thermomagnetic devices, spin-caloritronics, energy harvesting, etc.

ACKNOWLEDGEMENTS

First and foremost, I would like to express my gratitude to my advisor Dr. Daryoosh Vashaee for his valuable time, resourceful advice, patience, and guidance during my master's thesis at NC State University. I always found him beside me with his constructive feedbacks and definitive direction throughout my thesis work. His philosophies, feedbacks and guidance really helped me to become a better engineer, researcher and professional. I also want to thank my lab fellows Abhishek Malhotra, Michael Hall and Zack Coutant for their continuous support and sharing of their knowledge. Solid-state cooling was a new research topic for me. I can barely survive in this unknown area without their scientific discussions and valuable times to make me familiar with all new tools and machines. You guys really saved me from certain futility by dedicating your valuable time and effort.

I want to express my special thanks to Dr. Beth Dickey for allowing me to pursue this degree from Department of Material Science (MSE), one of the top ranks department in the US. I would also like to thank Edna Deas for her precise and effective help. I always found every information that I need regarding my program, course instructors and official procedures required to keep me on track.

My family, wife, and friends deserve the last, but not least, the gratitude of me. Their well-wishes and continuous encouragement helped me to move forward throughout my life. Thanks go to my friends in the ECE and MSE department for sharing their times with me throughout various activities which helped me to release my pressure and depression.

I would also like to thank my wife for her unwavering support, sacrificial care, and welcome distractions during my mad dash to the finish. Finally, I would like to thank my parents for their support and sacrifices that helped me to succeed in my life. Their perpetual appreciation of the knowledge made me steadfast to achieve my goals. Though

they were not physically around me, I always felt their care and encouraging motivation to accomplish my objectives. I especially would like to thank my mother. Without her, I wouldn't be where I am today. I extend a special token of gratitude to Dr. Paul Franzon, Dr. Shah Alam and Dr. Omer Oralkan. Their advice and support inspired me during my uncertain times and their continued interest in my academic and professional development leave an indelible mark as to what kind of mentor I'd like to be in the future.

TABLE OF CONTENTS

LIST OF TABLES

LIST OF FIGURES

Chapter 1

Introduction

1.1 Motivation

Recently, Solid-state cooling has become a competitive and state-of-the-art technology for cooling application over the conventional cooling method that associated with compressor, condenser, evaporator, and refrigerants. It enables the direct conversion of electricity into a useful form of heat in presence of or absence of magnetic field without using mechanical parts [1, 2]. Solid-state cooling has many salient features like longer lifetime, higher reliability, no moving parts, low maintenance cost, flexible form-factor, smaller size, efficient localized cooling, lightweight, fast and dynamic response, better thermal control, noise-free application, no refrigerants and cost competitive by leveraging the modern semiconductor manufacturing technologies [1, 2]. These features make solid-state coolers more environment friendly and perfect for quiet and sensitive applications like medical appliance cooling, small electronics cooling such as sub-ambient cooling of infrared detectors or charged-coupled cameras [3, 4], laboratories equipment cooling etc. [5]. Moreover, switching between cooling and heating for these coolers can be

done by only reversing the polarity of the driving current. The ultimate drawback of the solid-state cooling devices is its inefficient performance in large-area cooling and need of external magnet for certain applications. Cooling efficiency of the initial solid-state coolers was about 10% of Carnot efficiency while vapor compression-based cooler has 30% efficiency [6]. Low-dimensional devices with doped semiconductor materials later helped to revive the research of the solid-state cooler [7]. Though with current technology, vapor compressed cooler achieve co-efficient of performance (COP) of 3.6 and minimal Ozone depletion potential (ODP) and global warming potential (GWP) [8], modern technology is still driving towards new solid-state based cooling technology which suppressed ODP and GWP. Recent research works on solid-state coolers include the investigation of low-dimensional new material systems with higher thermoelectric and thermomagnetic power factor [9, 10, 11, 12, 13], different process treatments like microwave processing to decrease the thermal conductivity [14, 15, 16], finding of shaped geometry which can improve performance of solid-state coolers [17, 18, 19], new materials with different heat transport mechanisms [20, 21, 22, 23]. Enormous efforts and new discoveries from scientific society make solid-state cooling a prospective and competitive phenomenon for cooling applications. Present research on solid-state cooling mainly concentrated into few topics like a low dimensional thermoelectric cooler for wearable and low power devices, new ideas like spin-caloritronics, electrocaloric etc. Target applications of these research works are making efficient cooling devices at room temperature. But those devices are not efficient in the cryogenic temperature range (< 200K) and very few recent works attribute this field [24, 25]. Until now, thermo-magnetic (TM) coolers are found most efficient in this temperature range [26]. Most of the research on TM coolers were finding efficient material systems [27, 28] and efficient geometric shape for TM cooling application [29, 30]. A very few works showed the comparison between the possible geometric shapes of TM

coolers. Therefore, the main focus of this work is to introduce a new geometric shape function based on realistic assumptions which are not included into previously published works and show characteristics and performance comparisons between different shaped TM devices. Also, an experimental work conducted for the verification of the simulation work.

1.2 Solid-State Cooling

Solid-State cooling devices are the solid-state heat pumps that can pump heat against a temperature difference without a working fluid and no moving parts [31]. Solid-state heat pumps are typically metals or doped semiconductor materials. Most popular pump materials are semiconductors with high mean atomic weights and high figure-of-merit [31]. A typical solid-state cooling device is a doped semiconductor layer or p-n junction device sandwiched between two ceramic plates which act as a heat sink and heat source. Current is passing through the device in transverse or longitudinal direction with respect to heat flow direction to achieve the temperature gradient. Solid-state cooling is achieved by utilizing the Galvano-thermomagnetic effects. These effects help to change the entropy of electron gas of the solid-state pump materials which help to create the temperature difference across the device. Generally, solid-state coolers can be categorized into two types based on the operating Galvano-thermomagnetic effects: thermoelectric (TE) and thermomagnetic (TM) coolers. Due to the absence of working fluid, solid-state coolers have no environmental issues like high Ozone depletion potential (ODP) and global warming potential (GWP). As, solid-state coolers have no thermodynamic losses associated with vapor-compression cycle, they can provide higher cooling efficiency over conventional vapor-compression based cooling systems. Despite the mentioned advantages, solid-state

coolers have their own inherent losses like Joule heating. Therefore, the key challenge of solid-state coolers is to find suitable materials with higher electron and hole mobilities which gives higher conductivity and lower lattice thermal conductivity [5].

1.2.1 Thermoelectric Cooler

Thermoelectric (TE) coolers are the solid-state heat pump operated based on Peltier and Seebeck effects. Seebeck coefficient is also known as thermoelectric power. TE devices need n-type and p-type semiconductor legs to create heating and cooling effect. In TE devices, n-type and p-type semiconductor leg or arrays are connected electrically in series and thermally in parallel between hot and cold side ceramic substrate [26, 31]. Current alternately flow through p and n legs in same the direction shown in Fig. 1.1, which create a temperature gradient across the coolers due to the Peltier effects [26, 31]. In p-type legs, heat flow in the same direction of current and in n-type legs, heat flow is opposite of the current direction.

The figure-of-merit is an important term to evaluate the performance of TE coolers. Generally, higher figure-of-merit, ZT gives higher coefficient of performance (COP). Performance of a TE cooler is limited by two primary losses: electric resistance loss and thermal conduction loss. Electric resistance increases the applied voltage hence increase the required input power and reduces the net heat flow due to the Joule heating. Finite thermal conductivity also limits the net heat flow from cold side to hot side by generating a heat conduction flow in opposite direction. Therefore, thermoelectric figure-of-merit, ZT, a dimensionless term, attributes the strength of thermoelectric effects with respect to the losses from electrical resistivity and thermal conductivity. For good room temperature performance, TE devices with ZT of 4 or higher values are needed [33].

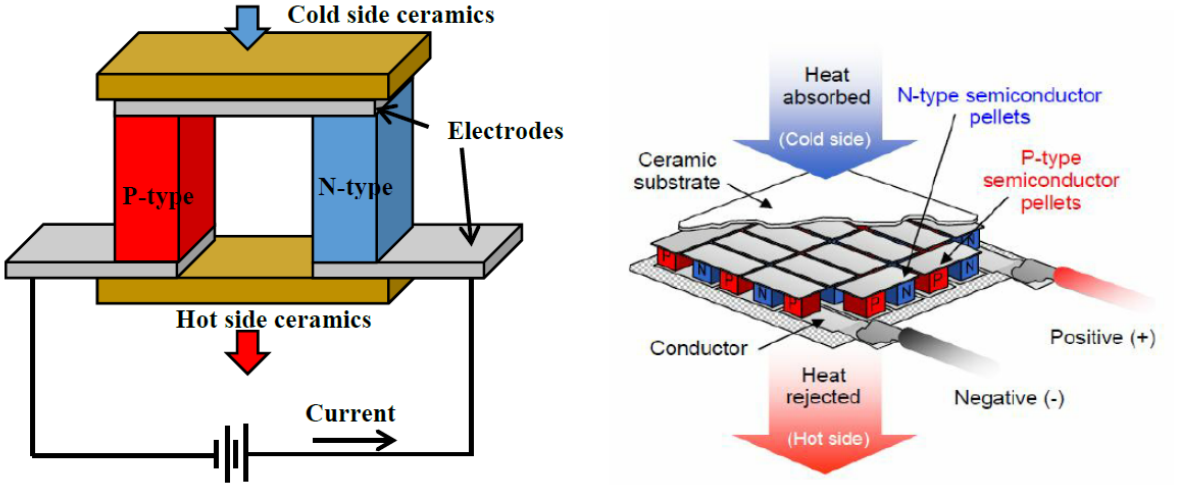

Figure 1.1: Construction and Working mechanism of a single Thermoelectric (TE) cooler (left side) and a TE cooler arrays (right side [32]) made with n-type and p-type semiconductor legs.

1.2.2 Thermomagnetic Cooler

Thermomagnetic (TM) coolers work based on Ettingshausen-Nernst effects and pump heat from cold side to hot side in the presence of magnetic field. Typical construction of a TM cooler (shown in Fig. 1.2), often known as Nernst-Ettingshausen (NE) cooler or only Ettingshausen cooler, is made with a n-type or a p-type doped semiconductor that sandwiched between hot side and cold side ceramics substrate and a magnet with a magnetic field perpendicular to both current flow and heat flow direction.

NE coolers can be both unipolar and bipolar [5]. But presence of both electron and hole can give stronger Ettingshausen effect [5]. In TM devices, magnetic field moves the electron in perpendicular direction to the current flow direction which helps to change the entropy of the electron gas. As like TE devices, a product of Nernst coefficient and magnetic field (NBz) is known as thermomagnetic power. Performance of TM devices depends on the quantity called thermomagnetic figure-of-merit. Performance of the TM

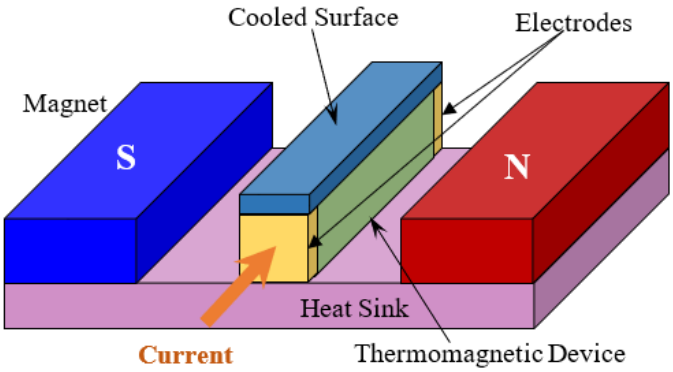

Figure 1.2: Typical Construction of Thermomagnetic devices including magnets, heating and cooling substrate, electrodes and semiconductor TM element.

devices can be tuned by varying the geometry of the device. TM devices are a good replacement for conventional cryogenics with thermodynamic cycles or stored cryogens as those are bulky and expensive. Good application fields of TM devices are on-board electronics in satellites, infrared, X-ray and -ray detectors (shown in Fig. 1.3).

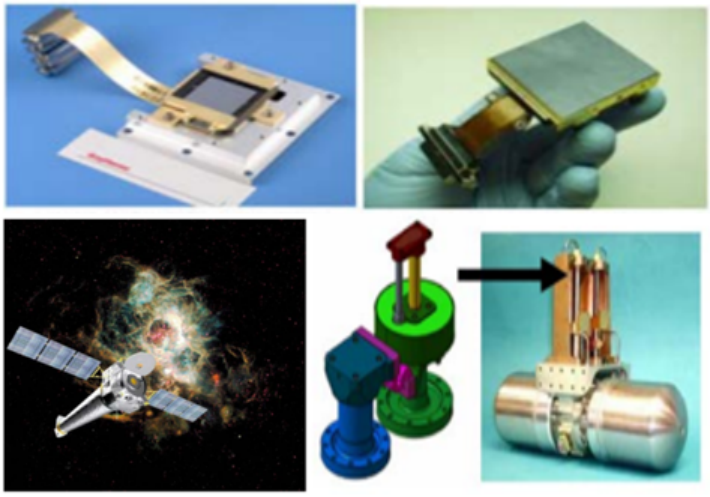

Figure 1.3: Prospective application fields of TM cooler like mid-IR detectors, near-IR detectors, space satellites and cryo-coolers [34].

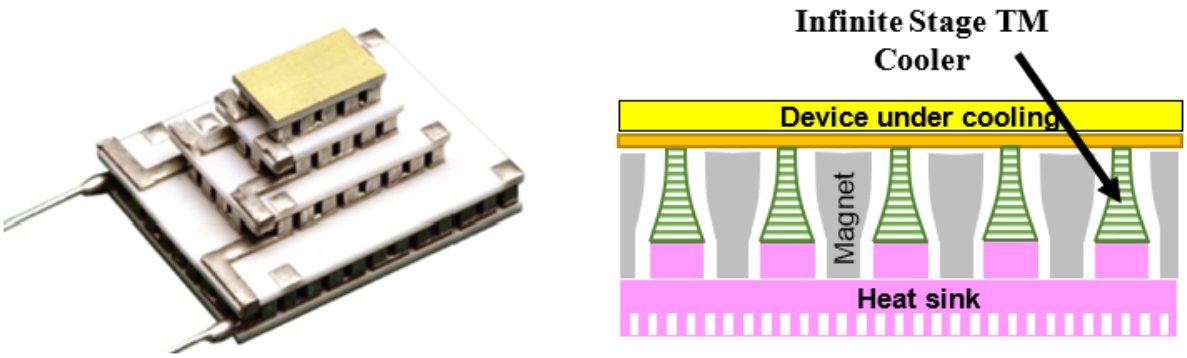

Figure 1.4: (Left side) 4 stage thermoelectric coolers with electrical insulation and separate source connection [35] and (right side) construction of Infinite stage thermo-magnetic cooler arrays with a magnet.

1.3 Multistage TE and TM coolers

Cascading or staging of a number of the individual stages (Fig. 1.4) can provide superior coefficient of performance (COP) and cover a wide range of temperature. Each stage has to pump heat equivalent to the input heat from previous stage plus the input power consumed by its own. Therefore, size and heat pumping capacity of individual stages must increase accordingly towards the heat sink [5]. Heat pumping capacity can be increased by increasing the cross-sectional area of successive stages in the direction of the heat flow. Generally, each stage is electrically separated from other stages by an insulating layer and connected to a separate current source [35]. Staging of TE devices after five or six stages does not provide any further improvement in performance because of the junction losses between the stages, the low thermoelectric figure-of-merit at low temperature, and the need of an enormous number of coupling of TE components to cover a wide range of temperature [5, 26]. Therefore, infinite staging is not possible in TE coolers. As staging

in TM devices can be done without inserting insulating layer in between the stages, the infinite stage is possible for TM coolers. Typical staging shape for TM devices is rectangular, trapezoidal and infinite (exponential) shape. To derive the staging shape for both TE and TM coolers with optimum COP, it has been assumed that individual stage must have equal and optimized COP.

1.4 Other State-of-the-art cooling Technologies

Modern cooling technologies are developed mostly based on entropy change of an internal degree of freedom like magnetic spins, electric dipole, atomic structural arrangement etc. Based on these entropy changes, special materials can perform cooling and heating cycle with external driving forces like magnet field, electrical field, and mechanical stress. Largest cooling can be obtained when these materials undergo a thermodynamic balance between one state to another known as spontaneous phase transition at desired temperature [8]. Among the modern cooling technologies apart from the TE and TM cooling system, magnetocaloric, electrocaloric, elastocaloric and spin-caloritronics are some relevant solid-state technologies. Magnetocaloric effect is the heating and cooling phenomena of magnetic material subjected to an adiabatic variation of the magnetic field which is discovered by Waobourg [20]. When a magnetic field is adiabatically applied to a ferromagnetic material, magnetic moments of the material become ordered and their total entropy is reduced. Therefore, to keep the total entropy constant in an adiabatic process, lattice entropy is increased hence the material heats up. Similarly, cooling occurs when a magnetic field is adiabatically removed. With this effect, entropy changed in an isothermal process while temperature changed in an adiabatic process [8, 20]. Initial magnetic refrigerators achieved 0.25K cooling down and later metallic gadolinium mag-

netic refrigerator gave a temperature reduction from 319K to 272K [8, 36]. Until 1997, all magnetocaloric effects were shown based on second-order phase transition [8, 36]. Later, first-order magnetostructural phase transition was discovered with $Gd_5Si_2Ge_2$ having the magnetocaloric potential of 10 J/kg-K and temperature change of 10 K at 292 K transition temperature which is known as giant magnetocaloric effect [8, 36]. Main limitations of magnetocaloric effect are a requirement of the large magnetic field to activate the effect and need of expensive rare-earth magnet [8]. Recently, many studies [37, 38, 39, 40] are made on other materials to suppress the limitations associated with this effect.

In electrocaloric effect (ECE), a dielectric material changes its polarization with applied electric field which changes the entropy hence the temperature of the material system. ECE can be characterized by two-constant entropy transitions and two constant electric field cooling cycle [21]. This cycle starts with an adiabatically applied E-field by turning it on rapidly to bring the crystal in lower entropy state by arranging the dipoles. As a result, the material heats up due to the lattice vibrational entropy compensation. During the adiabatic removal of E-field, cooling occurs due to decrease in lattice vibrational entropy and increase in dipolar subsystem entropy. In both cases, the total entropy of the system remains constant [41]. Electrocaloric materials are primarily ceramics and polymers which are good electrical insulators as well as thermal insulators. Different material systems are under recent studies for obtaining higher electrocaloric potential [42, 43, 44].

Elastocaloric effect gets the recent attention due to large available latent heat and large adiabatic temperature change associated with martensitic phase transformation [22]. Martensitic transformation is the first-order solid-to-solid diffusionless structural transformation which gives shape memory effect and superelasticity [22]. When a shape memory alloys (SMAs) in austenitic (cube) phase is subjected to adiabatic cyclic uniaxial loading, an exothermic austenitic-martensitic transformation occurs and elastoelec-

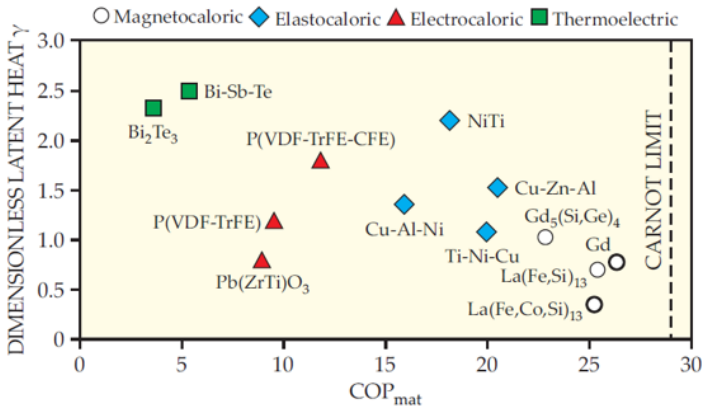

Figure 1.5: Dimensionless latent heat as a function of material co-efficient of performance for various caloric materials. Higher values for both quantities are expected [8].

tric material heats up. During the unloading of the stress, material transforms back to austenitic phase and cools down [45]. Main groups of superelastic alloys are Ni-Ti based, Cu-based and Fe-based alloys with different dopants [22]. Recent studies include different aspects of elastoelectric effect like giant room-temperature elastoelectric effect in thin films [46] and in magnetic shape memory alloy [47], elastoelectric effect in ferroelectric ceramics [48] and CoNiGa single crystal [49], cryogenic superelasticity [50] etc. Fig. 1.5 shows the comparison between the performance of mentioned solid-state cooling devices. Finally, spin-caloritronics is another state-of-the-art cooling technology which relates non-equilibrium thermodynamics of spin, charge, entropy and heat transport in magnetic structures [51]. Recent nano-device physics greatly deals with a fundamental thermodynamic bottleneck known as ohmic energy dissipation which limits the functionalities of both electronics and caloritronics. Electron spin adds an additional degree of freedom to overcome the limitations and helps to increase the thermoelectric figure-of-merit [51]. In spin-caloritronics, spin can control the heat flow in ferromagnetic materials. Several spin-based effects are the fundamental basis for spin-caloritronics: spin-Seebeck effect,

spin-Peltier effect, spin-dependent Seebeck, and Peltier effect. Spin-Seebeck effect (SSE) generates a spin voltage across the ferromagnetic materials due to the applied temperature gradient and then inject spin current from magnetic material to nonmagnetic material via spin pumping process [26]. The spin current creates a transverse voltage in nonmagnetic material via inverse spin-Hall effect (ISHE). SSE typically generates the order of microvolts per kelvin in ferromagnetic metals, semiconductors, and insulators, while giant SSE (GSSE) can produce the range of millivolts per kelvin via intense phonon-electron drag in presence of large magnetic field [26]. In spin-Peltier effect (SPE), a charge current generates a spin current through spin-Hall effect and spin current creates a magnon heat current. Till now, fundamentals of spin-caloritronics [52, 53] are under extensive studies along with the spin-based effect in different materials [54], and structures [55, 56]. No studies are not made to evaluate these devices as an energy conversion device.

1.5 Advantages of TM coolers

Based on applications, each technology has some merits and demerits. In TE devices, achieving high thermoelectric power factor is limited by material properties like electrical conductivity and thermal conductivity. Moreover, TE devices are not suitable for low-temperature application and building a cascade structure. In thermoionic devices, high operating current gives some non-ideal effects which limit the achievable cooling result within 1-4 °C [26]. No detail studies are published on cooling performance and design geometry of spin calorimetric devices [26]. None of the electrocaloric, magnetocaloric and elastocaloric devices are good in cryogenic temperature range operation. In TM devices, main limitations are an inefficient performance in high-temperature region and the need of

magnets. Efficient temperature ranges for different solid-state heat-pumps are illustrated in Fig. 1.6.

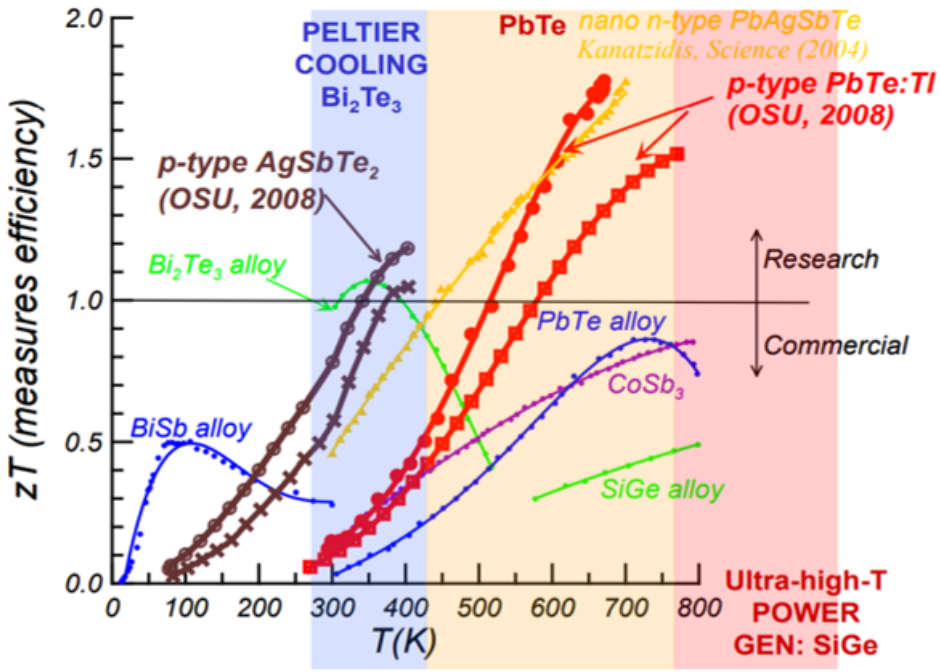

Figure 1.6: Illustration of efficient temperature ranges of different materials with their figure of merit and possible solid-state applications [34].

In TM devices, magnetic field strength can be obtained from $(\mu B)^2 \gg 1$ condition where μ is carrier mobility and B is the magnetic field. With high mobility materials, the requirement of higher magnetic field can be kept in the range of ~0.6 T which can be easily produced from high-filed permanent magnetic materials like Nd_2Fe_14B and SmCo [26]. Also, $(\mu B)^2 \gg 1$ condition limits the operational temperature range for TM device in cryogenic range. Materials for Ettingshausen coolers show good performance with the properties of low band-gap (comparable with thermal energy, k_BT), low lattice thermal conductivity, high thermomagnetic power, and high carrier mobility. Cryogenic tempera-

ture range (< 200K) is suitable for obtaining some of these required material parameters like low thermal conductivity by lowering lattice thermal conductivity contribution. Material optimization is also feasible for TM devices as it contains only single element. TM devices can provide higher cooling power as current flow is perpendicular to heat flow. Hence, it is possible to make the large cross- sectional area for heat flow and a small cross-sectional area for current flow [26]. Moreover, cascading or staging is more feasible in TM devices and infinite staging of TM devices is already made. No electrical isolation is needed between the stages which helps to get unlimited number of cascading and constructs the whole device from a single block material [5].

1.6 The hypothesis of the Work

The main concept of this work is to derive a new geometric shape for the infinite stage with higher performance such as higher temperature gradient and better COP. Our hypothesis is that the commonly used shaping function to get infinite stage proposed by Harman has poor performance due to adopting some ideal considerations. He assumed that current density perpendicular to temperature gradient is constant for individual stages, while electrical conductivity, thermal conductivity and thermomagnetic figure-of-merit are temperature independent. With those assumptions, actual power dissipation in each stage due to Joule heating should be different than the practical values. Therefore, temperature gradient and COP of the device will also be different.

1.7 Accomplishments of this work

In this work, a new shaping function is derived for the infinite stage with the practical consideration that absents in previous works. A numerical analysis is performed to show the performance of the modified infinite stage. A comparative study is also done based on simulation work to analysis the performance different available geometric shapes for infinite staging like rectangular and trapezoidal. An experimental work is conducted to observe the actual performance and evaluate the validation of numerical work. Our target material is Bi_xSb_{1-x}, one of the high-performance materials for NE coolers.

Chapter 2

Background Physics

This chapter presents the fundamentals of Solid-state cooling devices. Chapter is started with the discussion of fundamental Galvano-thermomagnetic effects followed by the discussion of optimum material systems for both thermoelectric and thermomagnetic devices. The following section presents the Galvano-thermomagnetic effects in semiconductors. A brief discussion of irreversible thermodynamics and reciprocal relationship is also provided before moving to the demonstration of explicit expression for TE and TM devices. Finally, discussion on characteristics equations is presented for both devices. The main focus of this work is to present the TM or NE devices as a prospective cooling device at cryogenic temperature range. To get a good understanding of the fundamentals of NE devices, it is better to present the well understood fundamentals of TE devices which has no magnetic field influence. Therefore, in this chapter, we present the physics of TE devices briefly before going for the details of TM devices.

2.1 Fundamental Galvano-thermomagnetic effects

Galvano-thermomagnetic effects are the fundamental physical aspects of the energy conversion process in presence of or absence of magnetic field which does not need any mechanical movement [35]. In presence of magnetic field, effects associated with charged particles (electron or hole) are changed due to the transverse forces that worked on a moving charged particle. These thermodynamic effects are ideally reversible but practically accompanied by irreversible effects related to electrical resistance and thermal conductance [35]. All these effects are arranged in three groups: thermoelectric effects, Galvano-magnetic effects, and thermomagnetic effects.

2.1.1 Thermoelectric effects

The Seebeck effects

The Seebeck effect was discovered in 1821 by T. J. Seebeck. This is one of the basic aspects of thermoelectric devices where electrical power can generate directly from heat. He showed that if two end junctions of two dissimilar conductors are kept at a different temperature, $\nabla_x T$, a voltage, $\nabla_x V$, is developed across the junctions. It is also known as thermoelectric power of one material compare to other. Although this effect observes only at the junction between two materials, this is a characteristic of the bulk rather than surface properties [35]. The Seebeck effect can be used for the temperature measurement. Seebeck coefficient is expressed as

$$S = \frac{\nabla_x V}{\nabla_x T}. \tag{2.1}$$

In a magnetic field, the Seebeck effect is supposed to be same when the field is reversed. But sometimes, a difference is observed in Seebeck co-efficient that known as Umkher

effect [57].

The Peltier effects

The second thermoelectric effect known as the Peltier effect was discovered by J. Peltier in 1834. According to this effect, when a current flow through a junction of two different materials, there is absorption or generation of heat depending upon the direction of the flow. Peltier effect is mostly utilized in cooling devices. Peltier coefficient is defined as

$$\pi = TS = \frac{Q}{I}, \tag{2.2}$$

where Q is the cooling or heating rate and I is current. It is difficult to observe Peltier effect than Seebeck effect due to the irreversible Joule heating [57].

The Thomson effects

The third thermoelectric effect was discovered by Sir William Thomson (also known as Kelvin) in 1855 which is known as Thomson effect. He showed that this effect exists in a homogenous conductor. Thomson effect showed that when a current carrying wire in a steady state has a temperature difference, the heat generation in the wire is greater or less than the Joule heat depending upon the magnitude and direction of the current, temperature and material. Thomson coefficient is expressed as,

$$\tau = \frac{\nabla_x Q}{I \nabla_x T}. \tag{2.3}$$

Utilizing the theory of irreversible thermodynamics, Thomson showed the interdependent relationship between Seebeck and Peltier effect which is known as Kelvin's law [35]. The relationships can be expressed by,

$$\pi = ST. \tag{2.4}$$

$$\tau_A - \tau_B = T\frac{d\alpha_{AB}}{dT}. \tag{2.5}$$

In magnetic field (B), first Kelvin relation is modified as [57, 58],

$$\pi(B) = TS(-B). \tag{2.6}$$

2.1.2 Galvano-magnetic effects

The Hall effects

Hall effect is first detected by E. H. Hall in 1879 which was first predicted by W. Thomson as a rotary power [2]. According to this effect, when a current carrying conductor is subjected to a transverse magnetic field, an electric field known as Hall field is developed across the conductor in perpendicular direction to both current flow and magnetic field. Hall effect has no direct relation to energy conversion but is useful for determining charge carrier's behavior. With zero current condition in the direction of Hall field, EH, Hall coefficient is defined as

$$R_{yx} = \frac{E_y}{J_x B_z}, \tag{2.7}$$

where J_x is the current density in x-direction, E_y is hall field in y-direction and B_z is a magnetic field in z-direction. According to the first law of thermodynamics, it is possible to draw energy by utilizing a conductor in y-direction from the power associated with Hall Effect which is $I_y R I_x B_z/b$. But, I_y current itself will create another Hall Effects in x-direction which is opposite to the applied voltage. So, to maintain constant I_x, additional power of the same amount, $I_y R I_x B_z/b$ is needed. So, the power found from Hall Effect will be coming from primary energy source [59].

The Ettingshausen effects

Ettingshausen effect was first observed by Albert von Ettingshausen along with Walther Nernst in 1887. According to this effect, a transverse temperature gradient is established into a current carrying conductor in presence of a transverse magnetic field. The direction of the temperature gradient is perpendicular to both current flow and magnetic field. The magnitude of the temperature gradient is proportional to the magnetic field density, current, and thickness of the conductor in the direction of magnetic field. Therefore, Ettingshausen coefficient, P can be defined as,

$$P_{yx} = \frac{\nabla_y T}{J_x B_z}. \tag{2.8}$$

This effect is utilized as a means of thermomagnetic refrigeration. To utilize the effect in practical devices, coolers should have a heat sink to hold the hot side of the cooling element to a fixed reference temperature [5]. As the electrodes and the wires are good electrical conductors, they, in general, have a higher thermal conductivity than the thermomagnetic material. Therefore, the thermal loss due to the wires and electrodes are twofold [5]. For these reasons, the length of the cooler along the current direction is made very long compared to its height or width and the main cooling area is taken near the center of the cooling element where the cooler is considered as essentially isothermal in direction of current flow [5].

2.1.3 Thermomagnetic effects

The Nernst effects

Nernst effect was first observed by Ettingshausen and Nernst in 1886 during their study of Hall effect in Bismuth. They found that when a temperature gradient was set across

a conductor that was subjected to a perpendicular magnetic field, an electric potential like Hall effect appeared perpendicular to both temperature difference and magnetic field. In Nernst effect, thermal excitation creates the transverse voltage while in Hall effect, transverse voltage is created by electrical excitation [2]. This Nernst electric field is proportional to the magnetic flux density and temperature gradient. Nernst coefficient is defined by,

$$N_{yx} = \frac{E_y}{B_z \nabla_x T}. \tag{2.9}$$

Nernst voltage sign does not depend on charge carriers like Hall voltage [57]. It is defined by the direction of the magnetic field and temperature gradient. As like Peltier and Seebeck effects, there is a thermodynamic relationship between Ettingshausen and Nernst effects shown by Bridgman in 1925 [5, 60] which can be expressed for anisotropic materials as,

$$N_{yx} T = -P_{xy} \kappa_{xx}, \tag{2.10}$$

where κ_{xx} is the thermal conductivity in x-direction.

The Righi-Leduc effects

The Righi-Leduc effect was independently observed by Righi and Leduc in 1888. They discovered that when a heat current was passed through a conductor that was perpendicular to the magnetic field, in addition to have an electric field by Nernst effect, a transverse Temperature gradient was found which was perpendicular to both heat current and magnetic field. Righi-Leduc coefficient is defined as,

$$L_{yx} = \frac{\nabla_y T}{B_z \nabla_x T}. \tag{2.11}$$

The Righi-Leduc effect is analogous to the Ettingshausen effect where the temperature gradient is set-up by another temperature gradient instead of electrical current [2]. Relations between all transverse effects with the corresponding current, heat flow and magnetic field are shown in Fig. 2.1 for parallelepiped structure In Fig. 2.2, all Galvano-

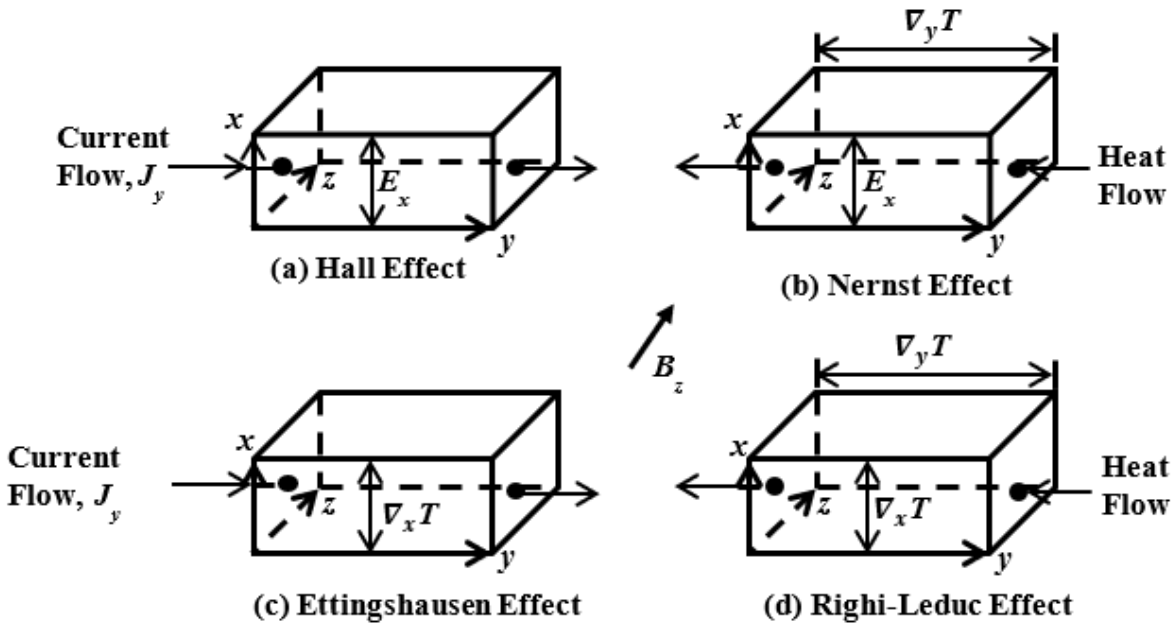

Figure 2.1: Transverse Galvano-thermomagnetic effects along with the direction of heat, current and magnetic field. Diagram directions will provide positive coefficient.

thermomagnetic effects are illustrated along with the longitudinal and transverse relationships of heat flow and current flow with their respective causes like temperature gradient and potential gradient. Transverse effects exist in the presence of magnetic fields.

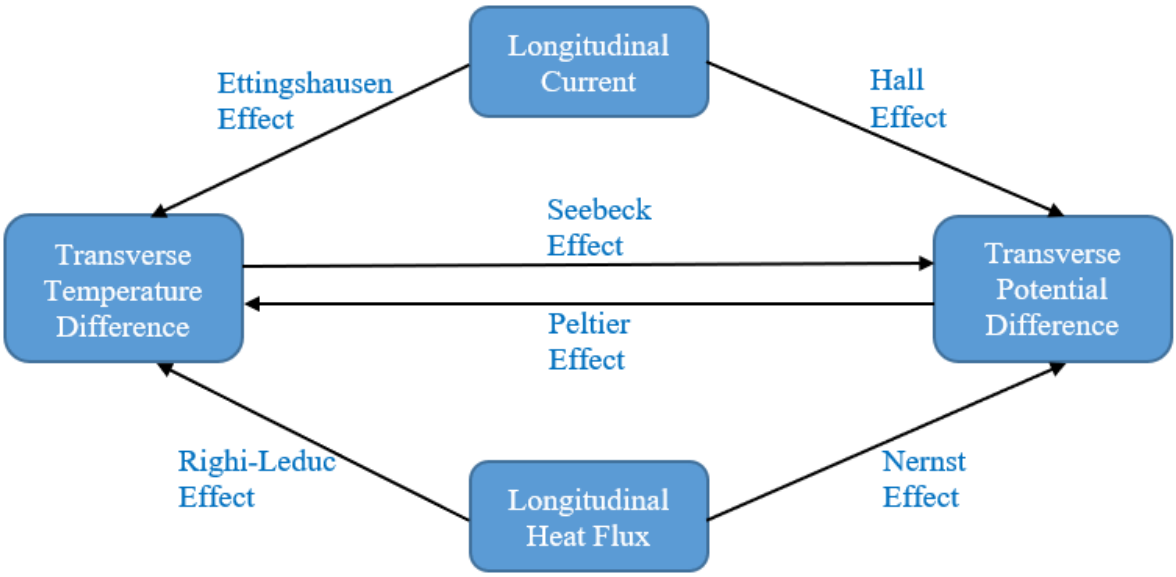

Figure 2.2: The Interrelationship between the Galvano-thermomagnetic effects showing the corresponding connection between causes and outputs.

2.2 Impact of Electrical Resistance and Thermal conductance

Solid-state heat engine would be an ideal reversible energy converter if there is no electrical resistance and thermal conductance associated with the engine. These parameters add the irreversible effects of Joule heating and heat conduction loss. Therefore, in the formalism of the governing equations of solid-state heat engine, electrical and thermal conductivities are included as an essential part. These two parameters also determine the figure-of-merit of solid-state cooling materials. Under zero magnetic field, electrical conductivity is defined as the ratio of current density and electric field which can be expressed as,

$$\sigma = \frac{J}{E} = ne\mu, \tag{2.12}$$

where n is charge carriers concentration and μ is charge mobility. In presence of magnetic field, charged particle is subjected to Lorentz force depending on their velocity. Only particles with a certain average velocity can move in an undeflected path and contribute to the conduction. This reduction of the contribution to conduction causes the increase in resistance in presence of a magnetic field which is known as magnetoresistance. At the low magnetic field, magnetoresistance effect is proportional to the square of the magnetic field [2]. Magnetoresistance effect is more dominant in materials with higher mobility [2]. Another parameter of interest is thermal conductance which refers how well a material conduct thermal energy. Thermal conductivity is given by

$$\kappa = -\frac{QL}{A\Delta T}, \tag{2.13}$$

where Q is the heat flow over a length of L through a cross-sectional area of A at a temperature difference of ΔT. Generally, three mechanisms help to transfer thermal energy in a solid: motion of free electrons in metals, the vibration of molecules in organic solids and lattice vibration (phonon) in crystalline solids [2]. In a semiconductor, thermal energy transformation can be done by multi-mechanism. In metals, the ratio between thermal to electrical conductivity should be same which should be proportional to absolute temperature. This is known as Wiedemann-Franz-Lorenz law which is expressed as

$$\frac{\kappa}{\sigma T} = L_w, \tag{2.14}$$

where L_w is the Lorenz constant (2.45×10^{-3} watt-Ω/K^2 or 155 (μV/K)^2). In a semiconductor, this relation between thermal and electrical conductivity is more complex as multiple mechanisms exist there for thermal energy transportation.

2.3 Selection of Materials

At this stage, it is reasonable to discuss the material systems that most suitable to obtain a considerable amount of Galvano-thermomagnetic effects. Selection criteria for both TE and TM devices are briefly described in this section. Thermoelectric effects can be considered as a small variation of energy and momentum distribution due to temperature gradients [61]. Amount of the effects depend on the energy level and temperature [61]. In metals or degenerate semiconductors, many charge carriers exist near Fermi level which reduces the thermoelectric effects [61]. While, in non-degenerate semiconductors or semi-metals, fewer carriers exist near Fermi which provides higher effects [61]. So, semiconductors and semi-metals are in general a good choice for TE devices. Depending on the doping concentration, semiconductor materials can be two types: degenerate (behaves like a metal) and non-degenerate (can be extrinsic and intrinsic). Choice of the materials for TE elements also depends on several other important material parameters such as power factor and figure-of-merit. These parameters are strongly depended on electrical conductivity, thermal conductivity, and Seebeck Coefficient. Seebeck coefficient and Electrical conductivity is a strong function of carrier density. Seebeck coefficient and carrier concentration are related by Pisarenko relation [62]. Therefore, power factor, $S^2\sigma$ becomes small when Fermi energy moves too far into band gap [57]. Seebeck coefficient varies linearly and conductivity varies exponentially with the Fermi energy for non-degenerate semiconductor [57]. As a result, power factor and figure-of-merit become more electrical conductivity dependent for a semiconductor. In metals, power factor and ratio of thermal conductivity to electrical conductivity increases with the increase in Fermi energy and approaches to the value from Wiedemann-Franz law and then after reaching an optimum value, power factor and Seebeck coefficient reduce [57, 61]. The

relation between Seebeck coefficient or thermoelectric power and Wiedemann-Franz law can be expressed as [61]

$$S = \sqrt{\frac{\kappa}{\sigma T}} = \sqrt{L_w}. \tag{2.15}$$

This relation suggests that a good TE material with negligible phonon thermal conductivity should have a thermopower of 155 μV/K or above. Moreover, the relation between power factor and Fermi energy is also scattering parameter dependent [57, 61]. Typical optimum Fermi energy is close to 0 [57]. On the other hand, dimensionless figure-of-merit for a certain Fermi energy is a function of mobility, effective mass and lattice thermal conductivity [57]. The dimensionless figure-of-merit can be defined as [57]

$$zT = \frac{(\eta - (r + 5/2))^2}{((\frac{k_B}{e})^2 \frac{\sigma_0 T}{\kappa_L} exp(\eta))^{-1} + (r + 5/2)}, \tag{2.16}$$

where η is Fermi energy, σ is electrical conductivity, κ_L is lattice thermal conductivity or phonon thermal conductivity, r is scattering parameter ($r = 1/2$ for acoustic-mode and 3/2 for impurity scattering), e is electron charge and k_B is Boltzmann constant. As electrical conductivity is a strong function of carrier mobility and effective mass, it is observed from above expression that materials with a higher value of the figure-of-merit should have high carrier mobility, high effective mass and low lattice thermal conductivity. But, mobility is lower for the higher effective mass carrier as mobility, $\mu = q\tau/m^*$ where τ is mean time between collisions and m^* is the effective mass. Effective mass is the mass of the carriers inside the crystal where carriers feel themselves a heavier entity with respect to the free carrier mass. Therefore, a good TE materials must have band degeneracy, low effective mass along transport direction and weak electron-phonon scattering [63]. Doping also increase electrical conductivity by adding more carriers in conduction band without decreasing the Seebeck coefficient as impurity-ionized scattering introduced by

doping can increase Seebeck coefficient [64]. Dope acts as an impurity which can modify band structure. Therefore, the carrier concentration in TE material is much higher than that in semiconductors for other application like optical device.

Thermal conductivity, another important quantity for TE devices, is a function of lattice vibration and electronic thermal conduction, $\kappa = \kappa_L + \kappa_e$. Lattice conductivity, κ_L, reduces with the increase in atomic weight [57]. For TE application, materials with low lattice conductivity is always desired. Generally, ionic compounds are not a good choice as they have lower carrier mobility hence lower power factor [57]. Increase in temperature typically generates more electron-hole pairs which can reduce Seebeck coefficient and increases thermal conductivity by bipolar effect [65, 66]. According to the bipolar effect, a more electron-hole pair at elevated temperature will carry more heat from hot side to cold side that will increase the electronic thermal conductivity [66]. Based on the discussion, it can be estimated that a good TE material with large conductivity and Seebeck coefficient and low thermal conductivity, should have minimum energy gap (not less than 6kT [57]) and high mobility.

Like TE materials, semiconductors are also expected to be a good option for TM device. Semiconductors can be either single charge carrier materials of electron-majority (n-type) materials or hole-majority (p-type) materials, or bipolar charge carrier materials. Bipolar carrier system or intrinsic semiconductor material does not provide any advantages for TE application, but it is advantageous for TM devices. Because, it is always important to maximize the number of carriers flowing towards the hot side [61]. If number and velocity of electrons are not equal to those of holes, then charges will accumulate in hot and cold side based on their charge type and create Hall voltage which will reduce the flow of majority carriers or will stop the flow of the carriers in the single carrier system. As a result, the cooling performance of TM device will degrade [61]. Therefore,

Ettingshausen effect is stronger in a bipolar system with e-h symmetry' which have an equal number of electrons and holes with equal mobility, effective masses and mean free path [61]. Fig. 2.3 demonstrates an e-h symmetry' and e-h asymmetry' material system with having conduction band, light and heavy hole band. In e-h symmetry system, if

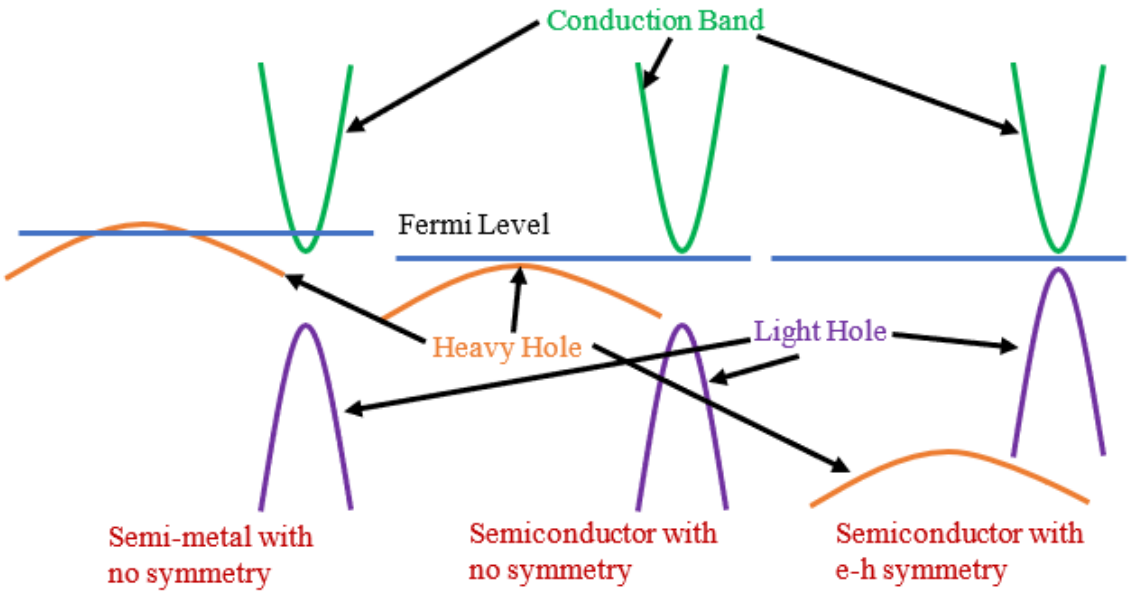

Figure 2.3: Electronic band diagrams of a typical semi-metal and semiconductor showing e-h symmetry.

the heavy hole is not symmetric to electron band structure and is away from Fermi level, heavy holes generally do not get excited thermally which is typically depends on the position of Fermi energy and Fermi energy position depends on effective masses and temperature. Sometimes, doping with other materials can shift the heavy hole from Fermi level and provide the electron-hole symmetry which excel the material properties such as the addition of Sb to Bi with 3∼7% shifts the heavy hole and provides scattering to

phonon to reduce phonon thermal conductivity [61]. Selection of the materials should also depend on the behavior of electrical and thermal conductivity in a magnetic field. Electrical conductivity in a magnetic field is defined as [67]

$$\sigma = \frac{\sigma_n}{1 + \mu_n^2 B_z^2} + \frac{\sigma_p}{1 + \mu_p^2 B_z^2}. \tag{2.17}$$

The behavior of the electrical conductivity can be realized from above equation based on the condition of $(\mu_n B_z)^2 \gg 1 \ll (\mu_p B_z)^2$. On the other hand, thermal conductivity gets better in the presence of magnetic field because temperature dependent electronic thermal conductivity reduces greatly in presence of magnetic field and only phonon dependent term or lattice conductivity becomes dominant [57, 68]. Electronic thermal conductivity is expressed as [57]

$$\kappa_e = \frac{\kappa_e, n}{1 + \mu_{H,n}^2 B_z^2} + \frac{\kappa_e, n}{1 + \mu_{H,n}^2 B_z^2} + \frac{\sigma_n \sigma_p T (\alpha_p - \alpha_n)^2}{\sigma_n (1 + \mu_{H,n}^2 B_z^2) + \sigma_p (1 + \mu_{H,p}^2 B_z^2)}, \tag{2.18}$$

where μ_H is the Hall mobilities. With zero transverse electric field, κ_e tends to zero at the high magnetic field and total thermal conductivity becomes [57]

$$\kappa = \kappa_L (1 + Z_{NE} T). \tag{2.19}$$

It is reported that thermomagnetic figure-of-merit becomes highest, when the bands overlap by around 2kT which indicates semi-metallic materials [57]. Higher band overlapped materials have higher impurity scattering which reduces carrier mobility [57]. So, maintaining the condition of $(\mu B)^2 \gg 1$, thermomagnetic materials should have small band overlap. The thermomagnetic figure-of-merit has the following relation with mobility and

effective masses [57]

$$Z_{NE} \propto (\frac{m_n^* m_p^*}{m^2})^{3/4}((\frac{1}{\mu_n} + \frac{1}{\mu_n})\kappa_L)^{-1}. \tag{2.20}$$

Above expression suggests that if one of the mobility terms is higher than other, Z_{NE} will be dominated by the less mobility term. Therefore, both charge carriers should have equal high mobility. Moreover, effective masses of the carriers should be low and mean free path should be large for TM materials [61]. Under no Hall voltage condition, angles between the electric field and the direction of carrier movement has a relationship which is given [61]

$$\theta_i = tan^{-1}(\omega\tau)_i, \tag{2.21}$$

where ω is the cyclotron frequency which is $\omega = eB/(m_i^* c)$, c is the speed of light and τ is the mean time between collisions and i represents either electron or hole. So, according to the above expression, if the effective mass is lower, then cyclotron frequency will be higher, and tangent of the angle will be around unity. Therefore, low effective mass materials are good for TM device. In summary, above discussion suggests that ideal TM materials should be semi-metal with small band overlapping or semiconductor with small bandgap which should have an equal number of electron and hole, equal but low effective masses of the carriers and higher equal carrier mobilities. Sometimes, Orientation of the applied magnetic field with respect to the crystal axes also influence the thermomagnetic behavior of a TM system.

2.4 Galvanomagnetic Effects in Semiconductor

As above section suggests that semiconductors are in general a good material choice for solid-state cooling application, this section discusses the Galvano-thermomagnetic effects

in semiconductors. Some important properties of semiconductors are [2, 69] -

1. Negative temperature coefficient of resistance (Resistance increases with T).

2. Generally high thermoelectric power (High Seebeck coefficient).

3. Rectifying properties.

In semiconductors, carrier mobility depends on effective mass and relaxation time of electron where relaxation time is scattering dependent. If the crystal is perfect and with no vibration, electrons encounter no resistance. But crystals always have defects which are thermodynamically favored. Common defects are vacancies, interstitials, dislocations and impurity atoms which acts as a scattering site of the lattice. Moreover, the thermal vibration of lattice itself causes scattering of electrons. The probability that an electron has a collision which scatters it into another state in a time dt is dt/τ. Relaxation time is a function of energy and temperature dependent weighting function which is expressed as [2],

$$\tau(E) = \phi(T)E^r, \tag{2.22}$$

where ϕ is the weighting function, E is energy of the carrier and r is a constant depends on the principle mode of scattering which value is between -2 to +2. Average relaxation time is given by [2]

$$\bar{\tau} = \phi(T)(kT)^r \frac{\Gamma(\frac{5}{2}+r)}{\Gamma(\frac{5}{2})}. \tag{2.23}$$

Here, Γ is the gamma function. Hence, mobility can be written as

$$\mu = \frac{e}{m^*}\phi(T)(kT)^r \frac{\Gamma(\frac{5}{2}+r)}{\Gamma(\frac{5}{2})}. \tag{2.24}$$

A crystal with N atoms has 3N independent mode of lattice vibrations which are called lattice waves. There are two transverse waves (vibration is perpendicular to direction of propagation of the wave) and one longitudinal wave. If in a unit cell, there are M atoms, there are M kinds of a wave of each of the three types. Optic modes in long wavelength limit move two adjacent atoms in the unit cell almost exactly out of phase with each other. On the other hand, acoustic modes in same limit move adjacent atoms in phase with each other. Each vibrational mode can be represented by a quasi-particle known as phonon. In acoustic mode scattering, relaxation time is proportional to the energy as $E^{-1/2}$ and the mobility varies with temperature and effective mass as $T^{-3/2}m^{*-5/2}$, while in optical mode scattering relaxation time depends on charges carried by atoms and electrical polarization of lattice produced by vibration [2, 70]. In general, relaxation time depends on energy and mobility depends on temperature.

Ideal assumption is electron flow and phonon flow can be treated as independent which is not the case at low temperature. Generally, phonon has longer mean free path. Hence, phonon-phonon scattering is more unlikely in crystal which gives higher phonon-phonon relaxation time. In contrast, phonon-electron relaxation time is shorter, and long-wavelength phonon can exchange its energy with electron. This phonon-electron interaction is known as phonon drag which means that phonon carries electrons in the direction of heat flow due to the temperature gradient. Phonon drag can improve Seebeck coefficient at low temperature. Also, it is expected to be strongest at low carrier concentration [57]. As, TM devices are operated into low temperature regime, phonon-drag also plays an important role in determining longitudinal Nernst-Ettingshausen effect [71]. Above mentioned semiconductor properties and effects determined the nature of Galvano-thermomagnetic effects in semiconductors. Different Galvano-thermomagnetic effects in semiconductor are discussed in the following sections.

Peltier Coefficient and Seebeck Coefficient

In a non-degenerate semiconductor, Peltier coefficient depends on the Fermi energy level and relaxation time related the scattering nature of the charge carriers. By convention, Peltier coefficient is considered as negative for n-type semiconductor and as positive for p-type semiconductor. For semiconductors, Peltier coefficient can be expressed as [2]

$$\pi = \pm\frac{1}{e}[(\frac{5}{2} + r)kT - E_F], \tag{2.25}$$

where E_F is the Fermi energy level. From the first Kelvin's relation, Seebeck coefficient for semiconductors can be given by [2]

$$S = \pm\frac{k}{e}[(\frac{5}{2} + r)kT - \frac{E_F}{kT}]. \tag{2.26}$$

Hall Coefficient

If there is only one type charge carrier or there are two charge carriers with one dominating carrier in semiconductor, carriers experienced a transverse force due to Lorentz force in presence of magnetic field. Therefore, carriers are deflected to one end in a transverse direction which is dependent on the charge of the carrier. Accumulation of one type charge in one side will cause the transverse electric field which is known as Hall field and the generated voltage is called Hall voltage. Due to the defection of the carriers, longitudinal current flow is changed which also change the resistance. This phenomenon is known as magnetoresistance. In a semiconductor, Hall Coefficient is defined by [2]

$$R = \pm\frac{3\pi}{8}\frac{1}{ne}. \tag{2.27}$$

Hall coefficient has also the dependency on diffusion mechanism and degeneracy of electron gas. For both electron and hole, Hall coefficient is [2]

$$R = \pm \frac{3\pi}{8e} \frac{nb^2 - p}{(nb + p)^2}, \tag{2.28}$$

where $b = \mu_e/\mu_h$. This equation is applicable when minority carriers have a significant role.

Ettingshausen Coefficient

In a semiconductor, Ettingshausen effect depends on the relaxation time of the carriers with certain energy [2]. At any certain temperature, carriers are distributed in certain quasi-continuous energy levels known as energy band. Mean value of drift velocity of a carrier at a certain energy level is determined by the relaxation time, . And the Lorentz force on the carriers due to the magnetic field is directly proportional to the mean drift velocity. So, higher energy carriers have higher mean drift velocity and experience larger Lorentz force and deflect toward one side. But, lower energy carriers are deflected on the other side due to the higher transverse electric force with respect to Lorentz force. Force on the carrier can be expressed by [5]

$$F(\epsilon) = -[e\nu(\epsilon) \times B - eE_H], \tag{2.29}$$

In single carrier system or extrinsic semiconductor, electrons (or hole) and phonons are at a similar temperature at steady state. When the magnetic field is turned on (shown in Fig. 2.4), fast electrons are deflected quickly to the bottom. They create a coulomb field that pushes the low energy electrons, who experience smaller Lorentz force due to their lower speed, to the top side. The population of fast electrons at the bottom increases

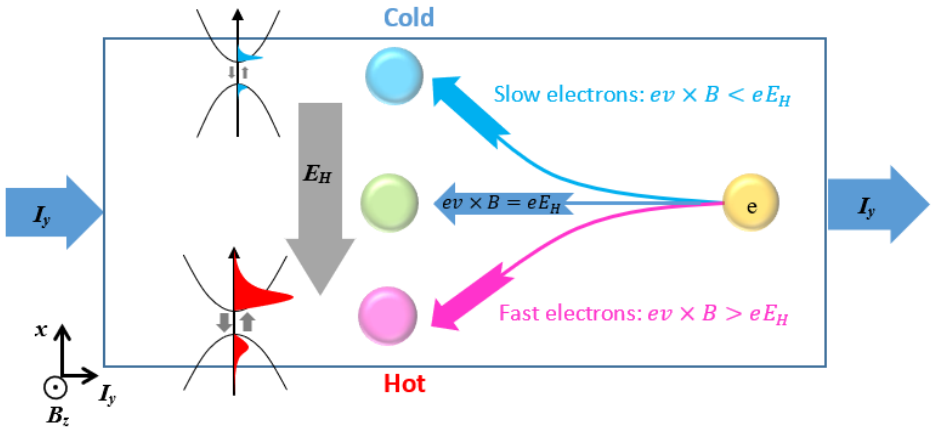

Figure 2.4: Schematic illustration of Ettingshausen cooling effects in single carrier or extrinsic Semiconductor material system.

the temperature of the electron gas above the lattice temperature. Therefore, they start giving energy to the lattice and heating up the lattice. On the other side of the material, the population of low energy electrons reduce the temperature of the electron gas, so heat transfer happens from the lattice to electron gas. That results in lower temperature than before the application of the magnetic field. Generation and recombination rates are functions of temperature. At the bottom, the temperature rise increases the steady state generation and recombination rates, and an opposite trend happens at the top side of the material.

In a two-carrier system with equal carrier numbers which is intrinsic semiconductor, although the Lorentz force can lead to a similar process for electrons and holes as in the intrinsic materials, a more dominant process controls the temperature profile. At steady state, electrons, holes and phonons are all at a similar temperature. When the magnetic field is turned on, electrons and holes moving in opposite directions, both experience Lorentz forces towards the bottom of the material (Fig. 2.5). That increases the population of electrons and holes at the bottom, which in turn increases the recombination

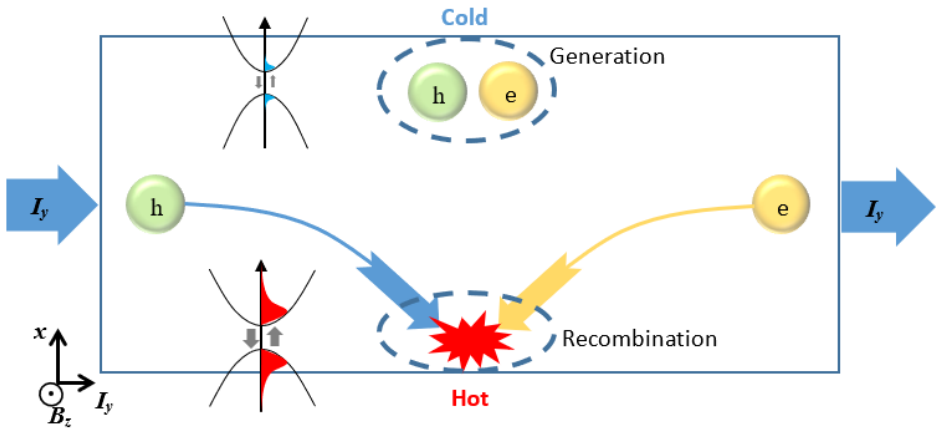

Figure 2.5: Schematic illustration of Ettingshausen cooling effects in two carrier or intrinsic Semiconductor material system.

rate. The energy from electron and hole recombination is given to phonon system leading to the rise of the lattice temperature. With the increase of the lattice temperature, the generation rate also increases until the recombination and generation rates are balanced out. At this time, the lattice temperature, as well as the carrier temperature, reaches a steady state. On the top side of the material, the population of the electrons and holes reduces due to their deflection to the bottom side. Therefore, the generation rate exceeds the recombination rate. The excess generation rate will take energy from the phonon system leading to the reduction of the lattice temperature. As the temperature drops, the generation rate also reduces until it balances the recombination rate. At this time, the lattice and carriers reach a lower steady state temperature. Ettingshausen effect is stronger in intrinsic semiconductors due to more efficient energy transfer by electrons and holes. In the case of single carrier system, the separation of the slow and fast electrons is not very efficient especially at low electric field or high temperature when the drift velocity is small compared to the thermal velocity. Assuming classical statistics and pure lattice scattering by acoustic modes (r = 1/2), Ettingshausen coefficient for n-type

semiconductor is [2],

$$P = \frac{-3\pi}{16e}\frac{kT}{\kappa}\mu_n. \tag{2.30}$$

And, for p-type semiconductor [2],

$$P = \frac{-3\pi}{16e}\frac{kT}{\kappa}\mu_h. \tag{2.31}$$

Nernst Coefficient

Considering the free electron in a semiconductor as a perfect gas, if one side is heated, electrons (or charge carriers) at the hot side will try to establish equilibrium in energy with cold side electrons (or charge carriers). Therefore, hot electrons will flow towards the cold side and in presence of magnetic field, they will deflect by Lorentz force to one side of transverse direction. As a result, a transverse electric field will appear which is known as Nernst voltage. Nernst coefficient can be obtained from Bridgeman relation. So, Nernst coefficient for n-type can be defined as [2]

$$N = \frac{-3\pi k}{16e}\mu_n. \tag{2.32}$$

And for p-type semiconductor, the expression is [2]

$$N = \frac{-3\pi k}{16e}\mu_h. \tag{2.33}$$

For mixed carrier system, Nernst coefficient becomes [2],

$$N = \frac{-3\pi k}{16e}\frac{(n^2\mu_n^3 + p^2\mu_h^3) - np\mu_n\mu_h(\mu_n + \mu_h)(7 + 2\Delta E/kT)}{(n\mu_n + p\mu_h)^2}, \tag{2.34}$$

where ΔE is the energy gap.

Righi-Leduc Coefficient

In the same process of Nernst effect, when hot electrons deflect in one side, a transverse temperature gradient will also appear which is called Righi-Leduc temperature difference. Considering lattice scattering by acoustic modes, Righi-Leduc coefficient for n-type is [2]

$$L = -\frac{21\pi}{32}\frac{k^2T}{e\lambda}n\mu_n^2 \tag{2.35}$$

And for p-type [2],

$$L = +\frac{21\pi}{32}\frac{k^2T}{e\lambda}p\mu_h^2. \tag{2.36}$$

2.5 Thermodynamics Expressions for TE and TM device

Thermodynamics expressions for TE and TM devices are derived based on irreversible thermodynamics. Generally, reversible thermodynamics deal with the reversible process, or ideal process in which system and its surroundings can be restored to the initial state (equilibrium) from the final state by reversing the direction of the process without any change in thermodynamics properties like entropy, enthalpy, etc. The reversible process can be defined by two characteristics: first, the system will change infinitely slowly due to the infinitesimal gradient in thermodynamic force and second, initial and final state should be in equilibrium with each other. On the other hand, irreversible thermodynamics only deals with the irreversible process or natural process where system spontaneously moves from initial state to final state due to the finite gradient like current flow due to voltage gradient and heat flow due to a temperature gradient. Irreversible processes can

be restored in their initial state only be changing the thermodynamic properties and most common change is the change in entropy which is defined by the second law of thermodynamics. Hence, the second law of thermodynamics can classify the reversible and irreversible process.

Irreversible thermodynamics can be defined based on two postulates: equilibrium thermostatics which deal with all equilibrium states at different entropies and time reversal symmetry of physical laws [72]. Time reversal symmetry suggests that physical laws remain unchanged if time is replaced with negative time and if the magnetic field is present then replaced it by its negative value. Typically, time is asymmetric in irreversible thermodynamics as the dynamic equation is variant under the time reversal condition. One of the powerful theorems for irreversible thermodynamics is Onsager Reciprocity Theorem. The reciprocal relation is the cross-effects between two or more irreversible transport processes that occur simultaneously in a thermodynamic system like coupling effects between heat conduction and electric conduction, the relation between electric conduction and diffusion or relation between heat conduction and diffusion [73, 74]. Here, heat conduction, electric conduction and diffusion can be defined as thermodynamic flux or displacement which are associated with thermodynamic forces or gradients like temperature gradient, potential gradient and concentration gradient [72]. Onsager gave the Reciprocity theorem based on microscopic reversibility assumption and law of least dissipation of energy which stated that the rate of increase in entropy plays the role of potential [73]. According to Onsager, any fluctuation in thermodynamic process returns to the initial equilibrium state which suggests a macroscopic reversibility for irreversible processes [73, 74, 75]. Onsager's reciprocal relations are valid for a system where flux and force have linear relation [74]. According to the Onsager reciprocal relation, kinetic coefficients, L_{ij} has following

relations [72],

$$L_{ij} = L_{ji}. \tag{2.37}$$

$$L_{ij}(B) = L_{ji}(-B). \tag{2.38}$$

Equation 2.38 is also derived in detail for anisotropic materials by Fieschi et. al. with the consideration of vector or tensor quantity instead of considering scalar quantity [76, 77, 78].

From these concepts of thermodynamics, all thermodynamics expressions for thermoelectric and thermomagnetic devices can be derived. In TE or TM systems, temperature gradient and potential gradient plays the role of thermodynamic forces which causes the displacement of the system from equilibrium state and produce thermodynamic fluxes; entropy flow and current flow for TE and TM systems. From the consideration of the linear relationship between force and flux, a general formula can be written as [72],

$$J_i = \sum_j L_{ij} X_j, \tag{2.39}$$

where, J is the flux, X is the force and L is the scalar quantity named as a kinetic coefficient. Now, for two flux coupled system, reciprocal relation suggests the following thermodynamic equation of motion [72]

$$J_1 = L_{11} X_1 + L_{12} X_2. \tag{2.40}$$

$$J_2 = L_{21} X_1 + L_{22} X_2. \tag{2.41}$$

Now, Law of least dissipation of energy suggests that entropy production has a relation with thermodynamic forces which can be defined by [72]

$$\dot{S} = \sum_k F_k J_k, \tag{2.42}$$

where, $\dot{S}$ is the rate of change in entropy and F is affinity given by X/T where T is temperature. Now, for a TE or TM system, with thermal and electrical force in x and y plane and magnetic field in the z-direction (for TE system, magnetic field term will be 0 or magnetic field associated terms will be replaced by corresponding TE terms), above expression can be written as [72]

$$\dot{S} = Q_x \frac{X_{qx}}{T} + Q_y \frac{X_{qy}}{T} + J_x \frac{X_{jx}}{T} + J_y \frac{X_{jy}}{T}, \tag{2.43}$$

where Q is the heat flow density, X_q is the thermal gradient, J is the current flow density and X_j is the electrical gradient. Replacing the forces, X with corresponding gradient quantities, above equation can be rewritten as [72]

$$\dot{S} = Q_x \frac{\nabla_x T}{T} + Q_y \frac{\nabla_y T}{T} - J_x \frac{\nabla_x \psi}{T} - J_y \frac{\nabla_y \psi}{T}, \tag{2.44}$$

where ψ is electric potential, the negative sign represents the relation between electric field and electric potential. According to equation 2.39, we can write the complete thermodynamic equations for TE or TM system as [2]

$$-J_x = L_{11} \frac{\nabla_x \psi}{T} + L_{12} \frac{\nabla_y \psi}{T} + L_{13} \frac{\nabla_x T}{T} + L_{14} \frac{\nabla_y T}{T} \tag{2.45}$$

$$-J_y = L_{21} \frac{\nabla_x \psi}{T} + L_{22} \frac{\nabla_y \psi}{T} + L_{23} \frac{\nabla_x T}{T} + L_{24} \frac{\nabla_y T}{T} \tag{2.46}$$

$$Q_x = L_{31}\frac{\nabla_x \psi}{T} + L_{32}\frac{\nabla_y \psi}{T} + L_{33}\frac{\nabla_x T}{T} + L_{34}\frac{\nabla_y T}{T} \tag{2.47}$$

$$Q_y = L_{41}\frac{\nabla_x \psi}{T} + L_{42}\frac{\nabla_y \psi}{T} + L_{43}\frac{\nabla_x T}{T} + L_{44}\frac{\nabla_y T}{T} \tag{2.48}$$

For isotropic materials, symmetry in x and y direction provides $L_{11} = L_{22}$, $L_{33} = L_{44}$, $L_{12} = L_{21}$ etc., modify the above expressions as [2]

$$-J_x = L_{11}\frac{\nabla_x \psi}{T} + L_{12}\frac{\nabla_y \psi}{T} + L_{13}\frac{\nabla_x T}{T} + L_{14}\frac{\nabla_y T}{T} \tag{2.49}$$

$$-J_y = L_{12}\frac{\nabla_x \psi}{T} + L_{11}\frac{\nabla_y \psi}{T} + L_{14}\frac{\nabla_x T}{T} + L_{13}\frac{\nabla_y T}{T} \tag{2.50}$$

$$Q_x = L_{31}\frac{\nabla_x \psi}{T} + L_{32}\frac{\nabla_y \psi}{T} + L_{33}\frac{\nabla_x T}{T} + L_{34}\frac{\nabla_y T}{T} \tag{2.51}$$

$$Q_y = L_{32}\frac{\nabla_x \psi}{T} + L_{31}\frac{\nabla_y \psi}{T} + L_{34}\frac{\nabla_x T}{T} + L_{33}\frac{\nabla_y T}{T} \tag{2.52}$$

In TM system, L_{11}, L_{13}, L_{31}, and L_{33} are even functions of the magnetic field and L_{12}, L_{14}, L_{32} and L_{34} are odd functions of magnetic field. Utilizing Onsager relation for magnetic field, we will get, $L_{13}(B) = L_{31}(B)$, $L_{31}(B) = L_{13}(B) = L_{13}(B)$ [as odd function], $L_{14}(B) = L_{41}(B) = L_{32}(B) = L_{32}(B)$ [due to odd function]. Utilizing these relations between kinetic coefficients and considering even odd functions, thermodynamic expression will become [2]

$$-J_x = L_{11}\frac{\nabla_x \psi}{T} + L_{12}\frac{\nabla_y \psi}{T} + L_{13}\frac{\nabla_x T}{T} + L_{14}\frac{\nabla_y T}{T} \tag{2.53}$$

$$-J_y = L_{12}\frac{\nabla_x \psi}{T} + L_{11}\frac{\nabla_y \psi}{T} + L_{14}\frac{\nabla_x T}{T} + L_{13}\frac{\nabla_y T}{T} \tag{2.54}$$

$$Q_x = L_{31}\frac{\nabla_x \psi}{T} + L_{32}\frac{\nabla_y \psi}{T} + L_{33}\frac{\nabla_x T}{T} + L_{34}\frac{\nabla_y T}{T} \tag{2.55}$$

$$Q_y = L_{32}\frac{\nabla_x \psi}{T} + L_{31}\frac{\nabla_y \psi}{T} + L_{34}\frac{\nabla_x T}{T} + L_{33}\frac{\nabla_y T}{T} \tag{2.56}$$

Rearranging these expressions will give the finalize thermodynamic relations as [2]

$$-\nabla_x \psi = L_{11}^{'} J_x + L_{12}^{'} J_y - L_{13}^{'} \nabla_x T - L_{14}^{'} \nabla_y T \tag{2.57}$$

$$-\nabla_y \psi = L_{12}^{'} J_x + L_{11}^{'} J_y + L_{14}^{'} \nabla_x T - L_{13}^{'} \nabla_y T \tag{2.58}$$

$$Q_x = -TL_{13}^{'} J_x - TL_{14}^{'} J_y - L_{33}^{'} \nabla_x T - L_{34}^{'} \nabla_y T \tag{2.59}$$

$$Q_y = -TL_{14}^{'} J_x - TL_{13}^{'} J_y - L_{34}^{'} \nabla_x T - L_{33}^{'} \nabla_y T \tag{2.60}$$

Here, $L_{ij}^{'}$'s are the new kinetic coefficients. From these above relations, we can identify the Galvano-thermomagnetic coefficients and thermal conductivity and electrical resistivity with proper conditions. All the coefficients with their corresponding conditions are given below [2] -

Seebeck Coefficient ($J_x = J_y = \nabla_y T = 0$): $S = -\frac{-\nabla_x \psi}{\nabla_x T} = -L_{13}^{'}$.

Isothermal Electric resistivity ($J_y = \nabla_x T = \nabla_y T = 0$): $\rho_i = \frac{-\nabla_x \psi}{J_x} = L_{11}^{'}$.

Adiabatic Electric resistivity ($J_y = \nabla_x T = Q_y = 0$): $\rho_a = \frac{-\nabla_x \psi}{J_x} = L_{11}^{'} - T(L_{13}^{'})^3 / L_{33}^{'}$.

Isothermal thermal conductivity ($J_x = J_y = \nabla_y T = 0$): $\kappa_i = \frac{-Q_x}{\nabla_x T} = L_{33}^{'}$.

Adiabatic thermal conductivity ($J_x = J_y = Q_y T = 0$): $\kappa_a = \frac{-Q_x}{\nabla_x T} = (L_{33}^{'2} + L_{34}^{'2})/L_{33}^{'}$.

Isothermal Hall Coefficient ($\nabla_x T = \nabla_y T = J_y = 0$): $R_i = -\frac{-\nabla_y \psi}{J_x B} = -L_{12}^{'}/B$.

Adiabatic Hall Coefficient ($\nabla_x T = Q_y = J_y = 0$): $R_a = -\frac{-\nabla_y \psi}{J_x B} = -\frac{(L_{12}^{'} + TL_{13}^{'} L_{14}^{'} / L_{33}^{'})}{B}$.

Isothermal Nernst Coefficient ($J_x = J_y = \nabla_y T = 0$): $N_i = \frac{-\nabla_y \psi}{\nabla_x T B} = L_{14}^{'}/B$.

Adiabatic Nernst Coefficient ($J_x = J_y = Q_y = 0$): $N_a = \frac{-\nabla_y \psi}{\nabla_x T B} = (L_{14}^{'} - L_{13}^{'} L_{34}^{'} / L_{33}^{'})/B$.

Ettingshausen Coefficient ($J_y = Q_y = \nabla_x T = 0$): $P = \frac{\nabla_y T}{B J_x} = TL_{14}^{'}/BL_{33}^{'}$.

Righi-Leduc Coefficient ($J_x = J_y = Q_y = 0$): $L = \frac{\nabla_y T}{B \nabla_x T} = L_{34}^{'}/BL_{33}^{'}$.

2.6 Characteristics equations of TE devices

Most important characteristic of the thermoelements is the coefficient of performance (COP), the ratio between the heat extracted from the source and the expenditure of electrical energy to extract that heat. COP will reach to ideal value of Carnot limit when there are no losses from electrical resistance and heat conduction [57]. Higher COP is desirable to reduce the electrical energy consumption and to able to use smaller capacity heat sink [57]. Heat extraction rate or Cooling power of TE devices are obtained from Peltier cooling which must compensate the heat conduction rate and Joule heating occurred due to thermal conductivity and electrical resistance, respectively [79]. COP depends on both current and cooling power which can be expressed as [57]

$$COP = \frac{(S_p - S_n)IT_c - (T_h - T_c)(\kappa_p + \kappa_n) - I^2\frac{(R_p+R_n)}{2}}{(S_p - S_n)I(T_h - T_c) + I^2(R_p + R_n)}, \tag{2.61}$$

where S is the Seebeck coefficient, I is the current, T_c and T_h is the cold and hot side temperature, respectively, κ is the thermal conductivity, R is the resistance and p and n represents the p and n legs of TE devices. From the expression, it is seen that Peltier cooling power is a function of I whereas Joule heating is a function of I^2. The equation also suggests that COP will be reached at a maximum when Peltier cooling power is twice of the Joule heating reached at the cold end [57].

In TE devices, there are two types of important current values: one is for maximum cooling power and other is for maximum COP. COP for maximum cooling power depends on ZT which is known as the dimensionless thermoelectric figure-of-merit. Z is equal to $(S_p - S_n)^2/((\kappa_p + \kappa_n)(R_p + R_n))$. For TE devices, Z is approximately average of z_p and z_n. Maximum COP is also known as optimum COP [57]. Practically, cooling power at optimum COP is much lower than maximum cooling power. Optimum COP is economical

in term of electrical energy consumption but uneconomical for thermoelectric application [57]. Another important quantity of a TE device is maximum temperature gradient which is obtained for zero cooling power as well as zero COP. Maximum temperature gradient is defined by [5, 57]

$$\Delta T_{max} = \frac{1}{2} Z T_c^2. \tag{2.62}$$

Final important characteristic is the heat flow rate delivered to the heat sink by TE device. This is equal to cooling power and electrical power consumption by the TE elements. Heat delivery rate can be defined as [57]

$$Q_{out} = Q_{in} + P_{in} = P_{in}(COP + 1). \tag{2.63}$$

Heat delivery rate should be greater that the electric power to obtain the cooling application.

2.7 Characteristics equations of TM devices

Expressions for COP and cooling power of a TM device are analogous to the expressions of TE device [80]. In TM devices, transverse heat flow is perpendicular to both current and magnetic field. Therefore, heat source and sink are thermally connected not electrically [57]. In presence of magnetic field, equipotential surfaces bend at the center of TM device toward the perpendicular surface due to the Hall effect. But at the ends, those are perfectly normal to the plane. To avoid the end effects, TM devices should be longer along the current flow direction than the dimension along heat flow direction [5, 57, 80]. Peltier heat flow can be realized with analogous Ettingshausen heat flow term which is defined by the product of Nernst coefficient, magnetic field, current and temperature.

The product of magnetic field and Nernst coefficient is also known as thermomagnetic power similar to the thermoelectric power or Seebeck coefficient. In TM devices, heat flow is opposed by thermal conduction and Joule heating. The cooling power of TM devices is defined as [57]

$$Q_{in} = \frac{NB_z I_x T_c L_x}{L_y} - \frac{\kappa(T_h - T_c)L_x L_z}{L_y} - \frac{I_x^2 \rho L_x}{2L_y L_z}, \tag{2.64}$$

where N is Nernst coefficient, B is magnetic field, L is the device length and x, y, z

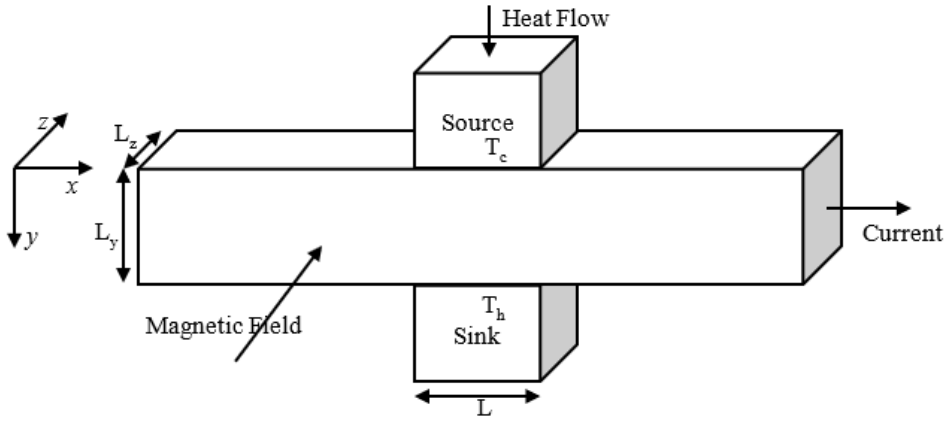

Figure 2.6: Basic structure of Ettingshausen coolers with the dimensions and the directions of current flow, heat flow and magnetic field.

represents the axes where x is in current flow, y is in heat flow and z is in magnetic field direction (see Fig. 2.6). As like TE device, TM device has the term, ZNE, known as a thermomagnetic figure-of-merit which is given by, $Z_{NE} = (NB_z)^2/\rho\kappa$. There are two types of figure-of-merit in TM devices: one is isothermal thermomagnetic figure-of-merit and other is adiabatic thermomagnetic figure-of-merit. Isothermal Z_{NE} is obtained for zero electric current and zero transverse temperature gradient which has theoretical

limits of 0 and 1 [57]. On the other hand, adiabatic Z_{NE} is obtained for zero transverse temperature gradient, zero transverse current and zero longitudinal heat flow [57] which value lies between 0 and ∞.

Thermomagnetic devices need only one material for the cooling application. It is also possible to make the TM device with the small cross-sectional area in the current flow direction and the large cross-sectional area in heat flow direction, as the current flow and heat flow are in a different direction and more precisely are perpendicular. This advantage of TM device helps to make a thin film of TM material which gives higher sensitivity and fast response [81] and to make infinite cascading or staging devices [80]. Similar to the TE device, input electrical power can be given by the summation of Ettingshausen cooling power and Joule heat. From the definition of COP, we can define the COP as [57]

$$COP = \frac{\frac{NB_z I_x T_c L_x}{L_y} - \frac{\kappa(T_h - T_c) L_x L_z}{L_y} - \frac{I_x^2 \rho L_x}{2 L_y L_z}}{\frac{NB_z I_x T_c L_x}{L_y} + - \frac{I_x^2 \rho L_x}{L_y L_z}}. \tag{2.65}$$

Also, we can define the optimum COP for an NE element as [57]

$$COP_{opt} = \frac{T_c}{\Delta T} \frac{(1 + Z_{NE} T)^{1/2} - 1}{(1 + Z_{NE} T)^{1/2} + 1}, \tag{2.66}$$

where $T = (T_c + T_h)/2$ and $(1 + Z_{NE}T)^(1/2) = \delta$. This optimum COP is also needed to derive the expression for infinite staging. Current for obtaining optimum COP is expressed by [5]

$$I_{y,COP_{opt}} = \frac{NB_z(T_h - T_c)L_z}{\rho(1 - \delta)}. \tag{2.67}$$

The maximum temperature gradient, another important characteristic, can be obtained with the same condition of TE device which can be given by [5]

$$\Delta T_{max} = \frac{1}{2} Z T_h^2. \tag{2.68}$$

Current associated with the maximum temperature gradient is expressed as [5]

$$I_{y,\Delta T_{max}} = \frac{N B_z T_h L_z}{\rho}. \tag{2.69}$$

Finally, the heat delivery towards hot side can be found by the summation of cooling power and half of the Joule heating towards hot side. Maximum heat pumping power of a NE device can be written as [5]

$$Q_{max} = \kappa \frac{\Delta T}{L_y} (\frac{\Delta T_{max}}{\Delta T} - 1). \tag{2.70}$$

Chapter 3

Analytical Model of Modified Infinite Geometry

3.1 Introduction

Cascading or staging for improving device performance has been reported in different publications for both thermoelectric and thermomagnetic devices [29, 80, 82]. For thermomagnetic, Infinite cascading or staging is reported as a maximum efficient device in several published works [29, 83, 84, 85, 86]. In those works, an exponential shape has been also derived to realize the infinite staging. Later, several works introduced infinite staging for transverse thermoelectric devices [83, 87], as cascading in longitudinal TE devices over 6 stages doesn't provide further improvement in performance [57, 87]. Most of the works derived the expression for infinite staging based on constant current density and temperature independent material parameters [29, 83, 84]. Among those, an expression derived by Harman [29] was widely used for making infinite thermomagnetic or NE devices. In this chapter, a detail derivation is presented to obtain a new expression

for Infinite shaped NE devices which is a modified version of Harman's infinite model. The modification was performed based on practical assumptions which were ignored by Harman for simplicity. The ignored assumptions ware later addressed in various works [5, 83, 85] but few works [83] were done to make the change for the expression of the infinite stage. One of the reason is that Harman's model is approximately correct for low-efficiency devices [5]. Here, a correction factor is derived which takes care of the practical assumptions. For better understanding, a brief section is written on O'Brien [84] and Harman's model [29] with the limitations that taken care in our derivation and then in following sections, corrected assumptions and complete derivation are presented.

3.2 O'Brien Model for Infinite Staging

O'Brien and Wallace derived the infinite stage shape (shown in Fig. 3.1) based on constant magnetic field, temperature independent material properties, and constant current density assumptions. They proposed that thin block ($y \ll x$) of the Infinite shaped block could be operated more efficiently. Thin block help to absorb the generated Joule heat by Ettingshausen effect at the sides of the block at a higher temperature. Moreover, if the sides are thermally insulated, then thin block helps to assume isothermal surface at constant x. From that assumptions, they showed [84],

$$T_0 - T_1 = \sum \Delta x t(x) = \Delta x \sum t(x). \tag{3.1}$$

And [84]

$$log(\frac{Q_0}{Q_1}) = \sum_x log(\frac{Q_0^1}{Q_1^1}) \approx \sum \frac{Q_0^1 - Q_1^1}{Q_1^1}, \tag{3.2}$$

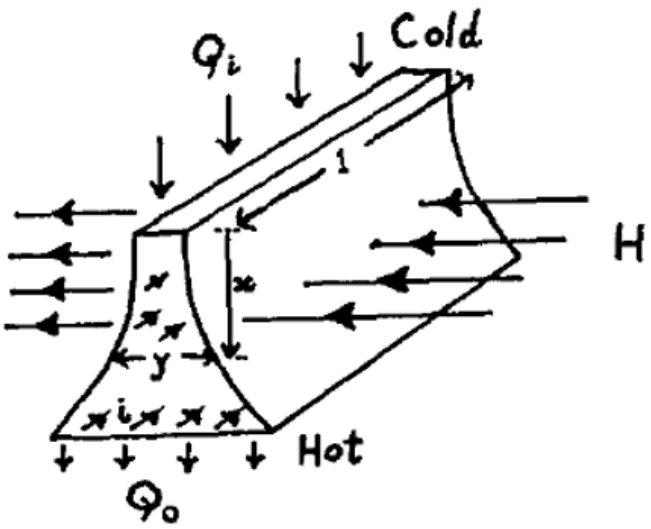

Figure 3.1: Infinite shape Ettingshausen device derived by OBrien and Wallace [84].

where $t(x)$ is the thermal gradient in x-direction, Q_0 and Q_1 are the rates of heat emission and absorption per unit length at hot and cold ends, T_0 is the hot side temperature and T_1 is the cold side temperature. With detail derivation, they finally obtained [84],

$$y = Aexp(2tx/\Delta T_0), \tag{3.3}$$

where A is a constant. Utilizing y_0 and y_1, the hot side and cold side widths, respectively, above expression was simplified by [84]

$$\frac{y_0}{y_1} = exp(\frac{2(T_0 - T_1)}{\Delta T_0}). \tag{3.4}$$

Here, ΔT_0 is the maximum temperature difference for an unloaded rectangular block. This model had some restrictions like $Z_{NE}T$ and $\Delta T/T$ were independent of x and $Z_{NE}T \ll 1$ which were addressed in Harman's work [29].

3.3 Harman's Model for Infinite Staging

Harman also derived an exponential function to realize the infinite stage NE device. Fig. 3.2 shows the device coordinates and temperatures of the ends of n-stage NE devices. In his derivation, he assumed a constant current density and constant electric field along y-direction. Other constant parameters were y-length, L_y, cold side temperature, T_0 and hot side temperature, T_L. Derivation was based on two principles: energy conservation principle and Equal coefficients of performance (COP) in each stage. In his work, COP of the individual stage (ith stage) was considered as [88],

$$COP^i = C^i(T)C^i(\delta) = \frac{T_0^i}{\Delta_x T^i} C^i(\delta) = \frac{\dot{\varepsilon}_{x=x_{i-1}}}{\dot{\varepsilon}_{x=x_i} - \dot{\varepsilon}_{x=x_{i-1}}} = \frac{\dot{\varepsilon}_{x=x_{i-1}}}{P^i} \tag{3.5}$$

Here, $C(T)$ is Carnot COP, $\Delta_x T = T_L - T_0$, $\dot{\varepsilon}_{x=x_i}$ is the energy flow rate and T_i is the temperature at $x = x_i$, P^i is the input power and $C^i(\delta)$ has an expression of $C^i(\delta) = (1-\delta)/(1+\delta)$ where $\delta = (1 - Z_{NE}T)^(1/2)$ and $Z_{NE} = (H_z N_{yx})^2/\kappa_{xx}\rho_{yy}$. H_z is the magnetic field in z direction, N_{yx} is the Nernst coefficient, κ_{xx} is thermal conductivity and ρ_{yy} is electrical resistivity. According to the energy conservation law, energy flow rate at hot junction of a stage is equal to the sum of incoming energy flow rate from cold junction of previous stage and power input in the present stage. Hot junction of one stage is also the cold junction for next stage. With the mentioned considerations, Harman showed the basic formula of interest as [29],

$$\frac{dP}{P} = \frac{d\dot{\varepsilon}}{\dot{\varepsilon}} = \frac{dT}{TC^i(\delta)} \tag{3.6}$$

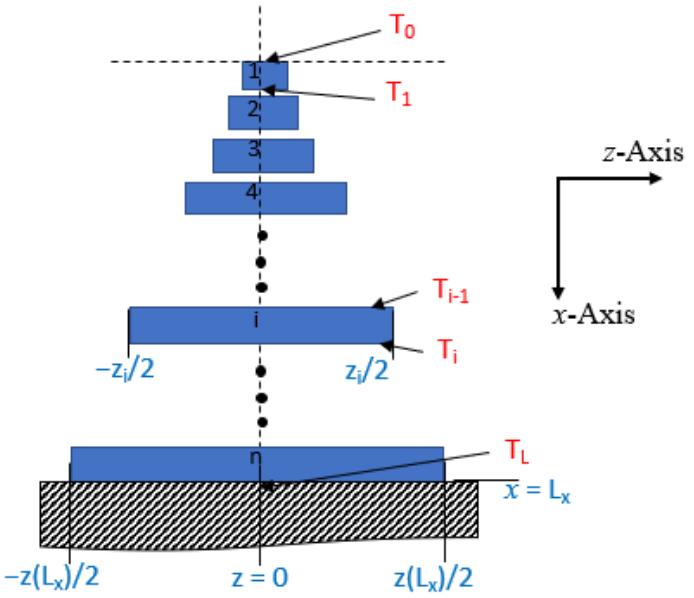

Figure 3.2: Schematic diagram of n-stage NE device in x-z plane with dimensions and temperatures of the individual stage in Harman's Model.

With the assumption of no heat flow in the z-direction, input power for ith and $(i+1)$th stage was expressed as [29],

$$P^i = \dot{\varepsilon}^i_{x=x_i} - \dot{\varepsilon}^i_{x=x_{i-1}} = 2z\Delta x^i L_y \nabla_y \psi^i J^i_y \tag{3.7}$$

and,

$$P^{i+1} = \dot{\varepsilon}_{x=x_{i+1}}{}^{(i+1)} - \dot{\varepsilon}_{x=x_i}{}^{(i+1)} = 2(z+\Delta z)\Delta x^{(i+1)} L_y \nabla_y \psi^{(i+1)} J^{(i+1)}_y, \tag{3.8}$$

where $\nabla_y \psi$ is the voltage gradient or electric field. Now, for a physically connected multistage devices, the electric field can be considered constant. With the assumption of constant current density, Harman showed the expression [29]

$$\frac{P^{i+1} - P^i}{P^i} = \frac{\Delta x^{(i+1)}}{\Delta x^{(i)}} - 1 + \frac{\Delta z}{z}\frac{\Delta x^{(i+1)}}{\Delta x^{(i)}}. \tag{3.9}$$

From, $\Delta x^{(i)} = \Delta x^{(i+1)}$, above expression was simplified as [29],

$$\frac{P^{i+1} - P^i}{P^i} = \frac{\Delta P}{P} = \frac{\Delta z}{z}. \tag{3.10}$$

To obtain maximum COP in staging device, COP of each stage should be equal, and COP of the individual stage should be optimized with respect to current density. A required condition for obtaining the same COP is [29]

$$\frac{\Delta_x T^{(i)}}{T_{i-1}} = \frac{\Delta_x T^{(i+1)}}{T_i}. \tag{3.11}$$

From $\nabla_y \psi^{(i)} = \nabla_y \psi^{(i+1)}$, it was shown that [29]

$$\frac{\Delta_x T^{(i)}}{\Delta x^{(i)}} = \frac{\Delta_x T^{(i+1)}}{\Delta x^{(i+1)}}. \tag{3.12}$$

Harman showed the relation between $ln(T)$ and x by [29]

$$\frac{dT}{T} = b^{'} dx. \tag{3.13}$$

Finally, he derived the complete exact derivative relation which was [29]

$$\frac{dT}{T} = \frac{dP}{P} = \frac{d\dot{\varepsilon}}{\dot{\varepsilon}} = \frac{dT}{TC^i(\delta)} = bdx. \tag{3.14}$$

where b is the arbitrary constant. From integration and boundary conditions of $x = 0$ at $z = z(0)$ and $x = L_x$ at $z = z(L_x)$, Harman derived two equations for infinite shaped device as [29]

$$\frac{z(x)}{z(0)} = (\frac{z(L_x)}{z(0)})^{x/L_x}. \tag{3.15}$$

And

$$z(T) = z(L_x)exp \int_{T_L}^{T} \frac{dT}{TC^i(\delta)}. \tag{3.16}$$

Though Harman successfully derived a simplified expression addressing some limitations of O'Brien and Wallace work, still, Harman's model has some serious approximations like constant current density for all stage and temperature independent material parameters. As the temperature in NE cooling device should be increased towards hot side, each stage should have different current densities which are the result of a temperature dependent electrical resistivity. With those idealistic approximations, exact infinite shaped NE device can't be obtained with optimum performance. Therefore, a detail derivation is demonstrated in the next section which takes care of the idealistic approximations of Harman's model.

3.4 New Model for Infinite shaped device

From the previous section, it is seen that Harman's model has no temperature dependency which is the result of constant current density and temperature independent material properties assumptions. Before moving to detail derivation for modified shape function, 3.1 is given here to show why it is important to considered temperature dependent parameters for the derivation of device geometry of a TM device. The table presents all the relationship between temperature and important material properties for degenerately doped narrow-gap semiconductors which defines the thermomagnetic figure-of-merit. To take care the approximation of constant current density, we start our derivation from the expressions of optimized current density and voltage gradient or electric field for individual stages. As mention before, to obtain maximum COP for multi-staged devices,

Table 3.1: Approximate relation between temperature and material properties for low band-gap degenerate semiconductors [34, 70]

Material Parameters	Relationship with temperature
Lattice thermal conductivity	$\kappa_L \propto T^{-1}$
Nernst Coefficient	$S \propto T^{-1}$
Relaxation time (Acoustic phonon scattering)	$\tau \propto T^{-1/2}$
Electrical conductivity	$\sigma \propto T^{1.5}$

current density and electric field should be optimized. Optimized current density and electric field can be defined as [29]

$$J_y^i = -\frac{\kappa_{xx}}{H_z N_{yx}} \frac{\Delta_x T^i}{T^i} \frac{(1+\delta)}{\Delta x^i}. \tag{3.17}$$

And

$$E_y^i = -H_z N_{yx} \frac{\Delta_x T^i}{\Delta x^i} \frac{\delta}{(1-\delta)}. \tag{3.18}$$

As NE devices are assumed as a longitudinally isothermal cooling device, there is no heat flow in y and z-direction. So, the power input to the ith stage which is the difference between the input and output energy flow rate, can be expressed as [29]

$$P^i = \dot{\varepsilon}^i_{x=x_i} - \dot{\varepsilon}^i_{x=x_{i-1}} = 2z\Delta x^i L_y E_y^i J_y^i \tag{3.19}$$

Similarly, for next stage ((i+1)th stage), power input is [29]

$$P^{i+1} = \dot{\varepsilon}^{i+1}_{x=x_{i+1}} - \dot{\varepsilon}^{i+1}_{x=x_i} = 2z\Delta x^{i+1} L_y E_y^{i+1} J_y^{i+1}, \tag{3.20}$$

Now, from equation 3.17 and 3.18, we have derived the relationship between current density and electric field which is known as Ohm's relation. Ohm's relation for NE devices can be expressed as,

$$J_y = \sigma_{yy} E_y = \frac{\kappa_{xx}}{(H_z N_{yx})^2} \frac{1}{T} \frac{(1-\delta^2)}{\delta} E_y, \tag{3.21}$$

where σ_{yy} is the electrical conductivity. From this expression, a temperature dependent relationship is obtained for electrical conductivity. Therefore, different current densities should be obtained for different stages based on the temperature dependent σ. Now, current densities for ith and $(i+1)$th stages are,

$$J_y^i = \sigma_{yy}^i E_y^i = \frac{\kappa_{xx}}{(H_z N_{yx})^2} \frac{1}{T^i} \frac{(1-\delta^2)}{\delta} E_y^i \tag{3.22}$$

$$J_y^{i+1} = \sigma_{yy}^{i+1} E_y^{i+1} = \frac{\kappa_{xx}}{(H_z N_{yx})^2} \frac{1}{T^{i+1}} \frac{(1-\delta^2)}{\delta} E_y^{i+1}. \tag{3.23}$$

For two successive stages, we can get the following temperature relationship,

$$T^{i+1} = T^i + \Delta T. \tag{3.24}$$

Hence, according to equation 3.24, equation 3.23 can be modified as

$$J_y^{i+1} = \frac{\kappa_{xx}}{(H_z N_{yx})^2} \frac{1}{T^i + \Delta T} \frac{(1-\delta^2)}{\delta} E_y^{i+1} = \frac{\kappa_{xx}}{(H_z N_{yx})^2} \frac{1}{T^i(1+\frac{\Delta T}{T^i})} \frac{(1-\delta^2)}{\delta} E_y^{i+1}. \tag{3.25}$$

Therefore, from equation 3.23 and 3.25, we can write,

$$J_y^{i+1} = \sigma_{yy}^{i+1} E_y^{i+1} = \sigma_{yy}^i (1+\frac{\Delta T}{T^i})^{-1} E_y^i. \tag{3.26}$$

Taking binomial expansion and ignoring higher order term from second order power, we can simplify the above equation as,

$$J_y^{i+1} = \sigma_{yy}^i(1 - \frac{\Delta T}{T^i})E_y^i = (1 - \frac{\Delta T}{T^i})J_y^i. \tag{3.27}$$

Now, following Harman's derivation steps, we obtained the following equation.

$$\frac{P^{i+1} - P^i}{P^i} = \frac{2(z + \Delta z)(1 - \frac{\Delta T}{T^i})\Delta x^{i+1} L_y E_y^i J_y^i - 2z\Delta x^i L_y E_y^i J_y^i}{2z\Delta x^i L_y E_y^i J_y^i}. \tag{3.28}$$

Considering similar height for each stage, $\Delta x^i = \Delta x^{i+1}$, we can simplify the above expression as

$$\frac{P^{i+1} - P^i}{P^i} = \frac{\Delta P}{P} = \frac{2\Delta x^i L_y E_y^i J_y^i[(z + \Delta z)(1 - \frac{\Delta T}{T^i}) - z]}{2z\Delta x^i L_y E_y^i J_y^i} = (1 + \frac{\Delta z}{z})(1 - \frac{\Delta T}{T}) - 1. \tag{3.29}$$

Or,

$$\frac{\Delta P}{P} = \frac{\Delta z}{z} - \frac{\Delta T}{T}. \tag{3.30}$$

From equation 3.30 and the complete exact derivative relation from Harman's model, we can write the new expression for exact derivative as follows

$$\frac{dP}{P} = \frac{dz}{z} - \frac{dT}{T} = \frac{d\dot{\epsilon}}{\dot{\epsilon}} = \frac{dT}{TC^i(\delta)}. \tag{3.31}$$

Rittner [82] showed that to operate the multi-stage devices at its maximum C.O.P., we can adjust the intermediate stage temperatures according to the following relationship,

$$\frac{\Delta_x T^i}{T^{i-1}} = \frac{\Delta_x T^{i+1}}{T^i} = \frac{T^i - T^{i-1}}{\Delta x^i T^{i-1}} = \frac{T^{i+1} - T^{i-1}}{\Delta x^{i+1} T^i} = b'. \tag{3.32}$$

where, $b^{'}$ is an arbitrary constant that equal to $bC(\delta)$. We can write a generalized expression for equation 3.32 as

$$\frac{\Delta T}{\Delta x T} = b^{'}. \tag{3.33}$$

Or,

$$\frac{\Delta T}{T} = b^{'}\Delta x. \tag{3.34}$$

Substituting the value of $b^{'}$ into equation 3.34, we get the following expression as

$$\frac{dT}{TC(\delta)} = bdx. \tag{3.35}$$

From 3.32 and 3.35, we obtain,

$$\frac{dz}{z} - \frac{dT}{T} = bdx. \tag{3.36}$$

Or,

$$\frac{dz}{z} = \frac{dT}{T} + bdx. \tag{3.37}$$

Denominator T can be expressed by initial temperature or cold side temperature of NE device, T_0, and spatial temperature gradient, dT/dx, which is

$$T = T_0 + x\frac{dT}{dx} = T_0(1 + \frac{x}{T_0}\frac{dT}{dx}). \tag{3.38}$$

Substituting equation 3.38 into equation 3.37, we can write,

$$\frac{dz}{z} = bdx + \frac{dT}{T_0(1 + \frac{x}{T_0}\frac{dT}{dx})}. \tag{3.39}$$

Utilizing binomial expansion for the above expression and ignoring the higher order terms except the first order term, we get,

$$\frac{dz}{z} = bdx + \frac{1}{T_0}(1 - \frac{x}{T_0}\frac{dT}{dx})dT. \tag{3.40}$$

From the boundary conditions, $z = z(0)$ at $x = 0$ and $T = T_0$ and $z = z(L_x)$ and $T = T_L$ at $x = L_x$, we can write the following linear temperature gradient profile along x-direction as

$$\frac{dT}{dx} = \frac{T_L - T_0}{L_x}. \tag{3.41}$$

Therefore, equation 3.40 becomes

$$\frac{dz}{z} = bdx + \frac{1}{T_0}(1 - \frac{x}{T_0}\frac{T_L - T_0}{L_x})(\frac{T_L - T_0}{L_x})dx. \tag{3.42}$$

Taking integration on both sides of above equation, finally we get,

$$ln\frac{z(x)}{z(0)} = bx + (\frac{T_L - T_0}{T_0})\frac{x}{L_x} - (\frac{T_L - T_0}{T_0})^2\frac{x^2}{2L_x^2}. \tag{3.43}$$

Utilizing the boundary conditions shown above, from equation 3.43, we can write,

$$ln\frac{z(L_x)}{z(0)} = bL_x + (\frac{T_L - T_0}{T_0}) - \frac{1}{2}\frac{T_L - T_0}{T_0})^2. \tag{3.44}$$

From equation 3.44, we can find the expression for constant b as

$$b = \frac{ln\frac{z(L_x)}{z(0)} - (\frac{T_L - T_0}{T_0}) + \frac{1}{2}(\frac{T_L - T_0}{T_0})^2}{L_x}. \tag{3.45}$$

Substituting b into 3.43, we obtain

$$ln\frac{z(x)}{z(0)} = (ln\frac{z(L_x)}{z(0)} - (\frac{T_L - T_0}{T_0}) + \frac{1}{2}(\frac{T_L - T_0}{T_0})^2)\frac{x}{L_x} + (\frac{T_L - T_0}{T_0})\frac{x}{L_x} - (\frac{T_L - T_0}{T_0})^2\frac{x^2}{2L_x^2}. \tag{3.46}$$

Finally, we can rewrite the above equation as,

$$ln\frac{z(x)}{z(0)} = \frac{x}{L_x}ln\frac{z(L_x)}{z(0)} + \frac{1}{2}\frac{x}{L_x}(\frac{T_L - T_0}{T_0})^2 - \frac{1}{2}\frac{x^2}{L_x^2}(\frac{T_L - T_0}{T_0})^2. \tag{3.47}$$

This is the modified temperature dependent shaping function for infinite shaped geometry whereas Harman's derived shaping function was

$$ln\frac{z(x)}{z(0)} = \frac{x}{L_x}ln\frac{z(L_x)}{z(0)}. \tag{3.48}$$

Therefore, we can generalize our derived expression as,

$$ln\frac{z(x)}{z(0)} = \frac{x}{L_x}ln\frac{z(L_x)}{z(0)} + C.F., \tag{3.49}$$

where $C.F.$ is the temperature dependent correction factor and is defined as

$$C.F. = \frac{1}{2}\frac{x}{L_x}(\frac{T_L - T_0}{T_0})^2 - \frac{1}{2}\frac{x^2}{L_x^2}(\frac{T_L - T_0}{T_0})^2. \tag{3.50}$$

The temperature terms of $C.F.$ expression actually take care of the temperature dependent material parameters which are another focus of this derivation work. Those Temperature terms are obtained from the expression containing material parameters given in the next chapter. Therefore, the derived model for the infinite stage is based on practical consideration and give the actual shape for optimum performance of NE device.

3.5 Comparison between new model and Kooi's Model

As mentioned earlier, Kooi et. al. [83] also addressed the idealistic approximation of Harman's and derived another expression for infinite stage devices. The expression derived in [83] is

$$\frac{z}{z_c} = (\frac{T}{T_c})^{\frac{1}{\delta-1}}. \tag{3.51}$$

In this expression, δ is also considered as a constant which is contradictory as it is a function of $Z_{NE}T$ hence a function of temperature. So, it is another ideal assumption that δ is a temperature independent term although they were able to show the Carnot limit from their expressions, which is $COP = \frac{T_c}{(T_h - T_c)}$ at $Z = \infty$, $\delta = \infty$, and equal hot and cold side areas. They also showed that at $Z = 0$ and $\delta = 0$, COP is zero and the ratio between the hot and cold side areas is infinity. Comparing to Kooi's model, our derived model has no temperature independent term. Moreover, Carnot limit can also be applied to our model but in a different way. According to Kooi's work, when hot side area is equal to cold side area or $z(0) = z(Lx)$ or $\Delta z = 0$, COP is $T_c(T_h - T_c)$, and when $\Delta z = \infty$, COP is 0. From equation (3.30) and (3.31), we can write,

$$\frac{dP}{P} = \frac{dz}{z} - \frac{dT}{T} = \frac{d\dot{\epsilon}}{\dot{\epsilon}} = \frac{1}{COP}. \tag{3.52}$$

Now, at $\Delta z = 0$,

$$\frac{1}{COP} = -\frac{dT}{T} = \frac{T_h - T_c}{T_c}. \tag{3.53}$$

And at $\Delta z = \infty$,

$$\frac{1}{COP} = \infty. \tag{3.54}$$

Above expressions show that our derived model also able to gives proper Carnot limit as like Kooi's model.

Chapter 4

Numerical Model for Multistage TM Cooler

4.1 Introduction

In this section, a numerical model has been presented for comparing the performance of different geometry for NE devices. Several works were published on the performance analysis [29, 83, 89, 90, 91], but most of them are on rectangular and Infinite stage NE devices. Common geometries for NE devices are rectangular, trapezoidal and exponential infinite stage. Geometries are shown in Fig. 4.1. Few works were performed on trapezoidal NE devices [92]. Comparison of performance between the available geometric shaped NE devices is rarely published. Therefore, another focus of this work is to develop a complete numerical model to perform the comparative analysis of the existing geometric shaped TM devices. Numerical model is developed from the refs [5, 88, 93, 94, 95, 96].

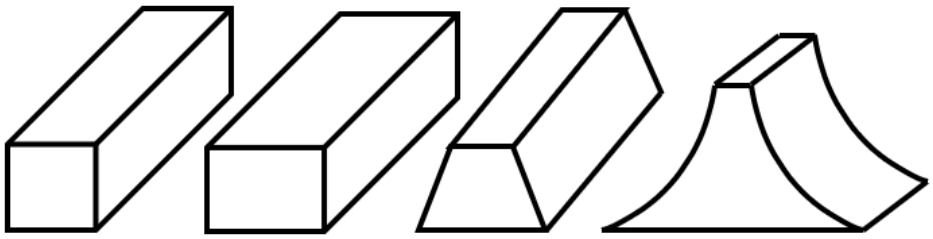

Figure 4.1: Different geometric shape for NE devices: thin rectangular, thick rectangular, Trapezoidal and exponential (Infinite) shape.

4.2 A Mathematical model for single stage NE element

Numerical modeling is started with the thermodynamic expressions for entropy flux density and voltage gradient based on the Galvano-thermomagnetic effects. These relations are based on irreversible processes in a magnetic field for isotropic and homogeneous materials. These phenomenological relations are expressed as [93]

$$J_x^S = -(\frac{\kappa_I}{T})\nabla_x T - (\frac{B_z L_I \kappa_I}{T})\nabla_y T + S_I J_x - B_z N_I J_y. \tag{4.1}$$

$$J_y^S = (\frac{B_z L_I \kappa_I}{T})\nabla_x T - (\frac{\kappa_I}{T})\nabla_y T + B_z N_I J_x + S_I J_y. \tag{4.2}$$

$$E_x = S_I \nabla_x T - B_z N_I \nabla_y T + \rho_I J_x - B_z R_I J_y. \tag{4.3}$$

$$E_y = B_z N_I \nabla_x T + S_I \nabla_y T + B_z R_I J_x + \rho_I J_y. \tag{4.4}$$

Here, J^S is entropy flux density, E is electric field, T represents temperature, J is the current density, B is magnetic field, S is Seebeck coefficient, ρ is electrical resistivity, κ is thermal conductivity, L is Righi-Leduc coefficient, N is Nernst coefficient, R is Hall coefficient, subscript I represent isotropic medium and x, y, z represents the coordinates

of the device. All these expressions are for single stage parallelepiped NE device. Now, above relationships can be extended for anisotropic material systems and can be represented in a matrix expression. Thermodynamic relationship matrix for an anisotropic material system is given by [88, 96]

$$\begin{pmatrix} J_x^S \\ J_y^S \\ E_x \\ E_y \end{pmatrix} = \begin{pmatrix} -\frac{\kappa_{xx}}{T} & -\frac{\kappa_{yx}}{T} - \frac{B_z L_y x \kappa_{yy}}{T} & S_{xx} - B_z N_{xx} & S_{yx} - B_z N_{yx} \\ -\frac{\kappa_{yx}}{T} + \frac{B_z L_y x \kappa_{yy}}{T} & -\frac{\kappa_{yy}}{T} & S_{xy} - B_z N_{xy} & S_{yy} - B_z N_{yy} \\ S_{xx} + B_z N_{xx} & S_{xy} - B_z N_{yx} & \rho_{xx} & \rho_{yx} - B_z R_{yx} \\ S_{yx} + B_z N_{yx} & S_{yy} + B_z N_{yy} & \rho_{yx} + B_z R_{yx} & \rho_{yy} \end{pmatrix} \begin{pmatrix} \nabla_x T \\ \nabla_y T \\ J_x \\ J_y \end{pmatrix} \tag{4.5}$$

This matrix can be the fundamental basis for any material system operated in any conditions like isothermal and adiabatic. Moreover, this can be extended to the 6×6 matrix [88] by introducing z components for entropy flux and electric field, but for typical NE devices, $\nabla_z T = J_z = 0$ and J_x^S and E_z are negligible due to the negligible associated Galvano-thermomagnetic effects. Generally, isothermal condition means $\nabla T = 0$ and adiabatic condition indicates $J^S = 0$ [97]. So, in longitudinally isothermal thermomagnetic coolers, $\nabla_y T = 0$ and $J_x = 0$ because of no electrical connection in x direction. Most of the studied NE devices are longitudinally isothermal TM device. Therefore, applying the conditions into the matrix representation will make the 4×4 matrix into a simple 2×2 matrix. From the 2×2 matrix, with proper sign conventions, expressions for $\nabla_x T$ and J_y can be found as

$$\nabla_x T = \frac{1}{(1 + \frac{(S_{yx}^2 - (B_z N_{yx})^2)T}{\kappa_{xx}\rho_{yy}})}(-\frac{Q_{in}}{\kappa_{xx}} + \frac{S_{yx} E_y T}{\kappa_{xx}\rho_{yy}} + \frac{B_z N_y x E_y T}{\kappa_{xx}\rho_{yy}}), \tag{4.6}$$

and

$$J_y = \frac{E_y}{\rho_{yy}} + \frac{B_z N_{yx} \nabla_x T}{\rho_{yy}} + \frac{S_{yx} \nabla_x T}{\rho_{yy}}, \tag{4.7}$$

where Q_{in} is the input heat flow density which can be obtained from the output heat flow density of previous stage and the power input of current stage. Joule heating plays an important role to determine both input and output heat flow density. Joule heating is a result of the collisions between charge carriers and lattice imperfections like impurity, defects and lattice vibrations and Joule energy is uniform throughout the system. Therefore, it is considered and proved that half of the total generated Joule heating will be transported by heat conduction towards both ends of a NE element [5, 79, 93]. With this consideration, we can get the expressions for input and output heat flow densities as below -

$$Q_{in} = \frac{B_z N_{yx} E_y T_c}{\rho_{yy}} + \frac{S_{yx} E_y T_c}{\rho_{yy}} - \frac{1}{2}\frac{E_y^2 da}{\rho_{yy}} - (1 + \frac{(S_{yx}^2 - (B_z N_{yx})^2)\bar{T}}{\kappa_{xx}\rho_{yy}})\kappa_{xx}\nabla_x T, \quad (4.8)$$

$$Q_{out} = \frac{B_z N_{yx} E_y T_h}{\rho_{yy}} + \frac{S_{yx} E_y T_h}{\rho_{yy}} + \frac{1}{2}\frac{E_y^2 da}{\rho_{yy}} - (1 + \frac{(S_{yx}^2 - (B_z N_{yx})^2)\bar{T}}{\kappa_{xx}\rho_{yy}})\kappa_{xx}\nabla_x T, \quad (4.9)$$

Here, $\bar{T} = (T_h + T_c)/2$. In multistage devices, output heat flow density of one stage should be the input heat flow density for next stage but it should be scaled with respect to the area of input end. From the obtained results of each stage, final outputs of $\nabla_x T$ and J_y for multistage NE device can be performed. To obtain the COP, ratio between input heat flow at the cold surface and input power, of a single stage NE device, we can utilize the following expression -

$$COP = \frac{Q_c}{P_{in}} = \frac{Q_c bc}{P_{in}} = \frac{T_c}{T_h - T_c}, \quad (4.10)$$

where b and c are the dimensions perpendicular to the current flow direction. For multistage devices, COP can be calculated from the following relationship,

$$1 + \frac{1}{COP} = 1 + \frac{P_{in}}{Q_c} = \frac{Q_c + P_{in}}{Q_c} = \frac{Q_h}{Q_c}, \quad (4.11)$$

where Q_h and Q_c are the heat flow at hot side and cold side of the multistage device, respectively. We can get the relationship between the COPs of individual stages and the total COP from Fig. 4.2. The expression for the relation is given by

$$(1 + \frac{1}{COP_T}) = \frac{Q_h}{Q_{cn}} \times \frac{Q_{hn-1}}{Q_{cn-1}} \times ... \times \frac{Q_{hi}}{Q_{ci}} \times ... \times \frac{Q_{h1}}{Q_c}, \tag{4.12}$$

where COP_i is the COP of the ith stage. COPs can be defined with respect to maximum input heat flux, COP_{max} and optimum input power, COP_{opt}. Optimum COP of the individual stage is expressed as [5],

$$COP_{opt} = \frac{1}{2}(\frac{T_h}{T_c})(1 - \frac{\Delta T}{\Delta T_{max}}). \tag{4.13}$$

4.3 Flowchart for the Simulation model

To perform the analysis on the multi-stage device, whole NE device is considered as the collection of many single stage NE elements with a uniform height. In our simulation model, height resolution is set at 10^{-3} cm, where whole device dimensions are taken in cm. The simulation model is developed for four different modules for different analyses. Heart of the analysis is same for all modules and that is calculating the performance parameters like heat flow, cold side and hot side temperatures for a single stage and then sum up them to obtain the collective performance of the multistage devices. In this simulation model, five geometric shapes are considered; thin rectangular, thick rectangular, trapezoidal, Harman's infinite shape and infinite shape derived in this work. Device lengths are taken from some previously published works to verify the results produced

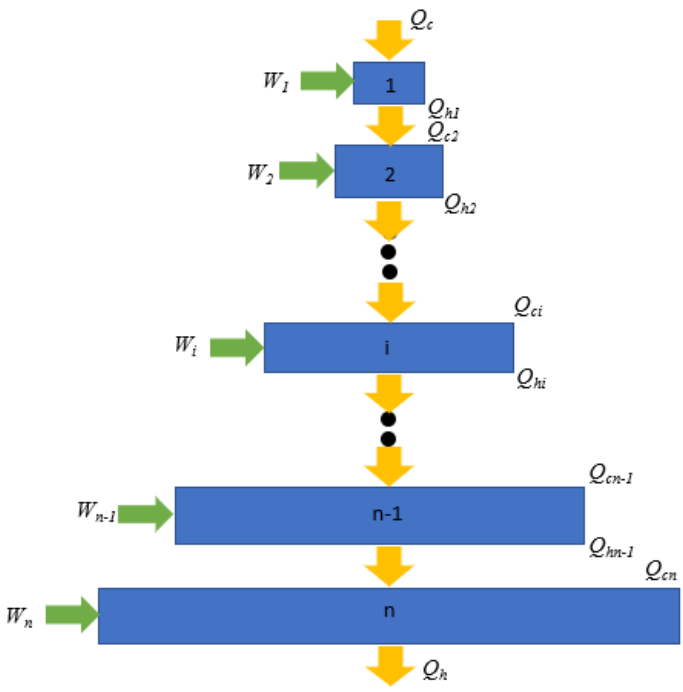

Figure 4.2: Schematic diagram showing the relations of input and output heat flow between the individual stages of the multi-stage device.

by our model [5, 91]. For all modules, maximum electric field, magnetic field and hot side temperature inputs are same. For our model, we considered the maximum electric field of 1 Vcm^{-1}, the magnetic field of 1 T and hot side temperature of 150 K. The simulation model is also capable of calculating the device characteristics taking cold side temperature as an input.

The focus of this simulation model is to calculate the device characteristics of different geometric shaped TM devices and compare the performance of our infinite shaped model with another geometric shape mainly with Harman's model. For the purpose of analysis, we have calculated different device characteristics like, maximum temperature gradient as a function of current and height, spatial temperature profile, maximum temperature

gradient as a function of geometric shape variation, maximum heat flow as a function of height and shape variation and finally, COP as a function of height and shape variation. For the calculation, a self-consistent model is developed, where a linearly distributed temperature profile is considered, and that temperature distribution is updated from the calculation of all the heat components. Fig. 4.3 shows all the heat fluxes associated with individual stages. The cooling performance of an NE device can be obtained from the

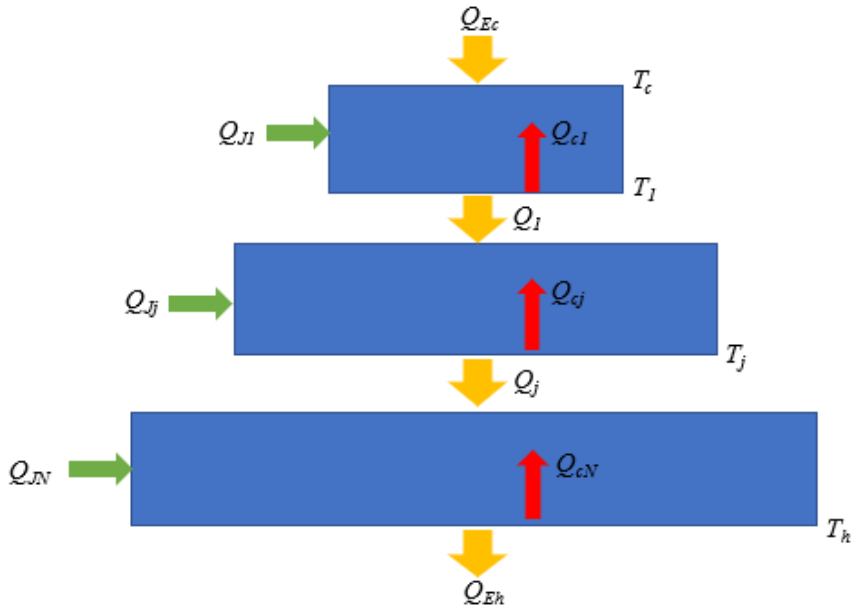

Figure 4.3: Interrelations between different heat fluxes and Temperature of different stages used in Multistage Calculation.

Joule heating, conduction heat flow, and Ettingshausen heat flow. As discussed earlier, Joule heating is divided into two and flow towards the cold and hot side of each stage, respectively. Generally, Joule heat and conduction heat oppose the cooling performance of an NE device which can be understood from 4.8 and 4.9. For better understanding,

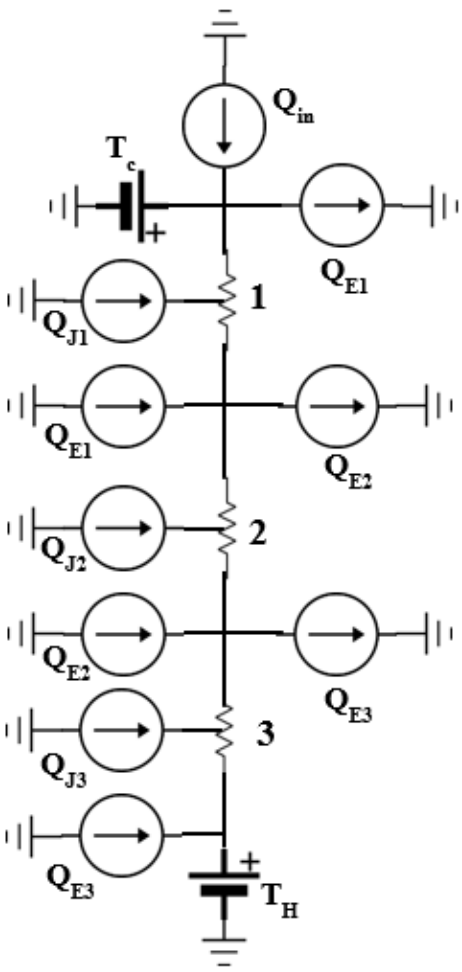

Figure 4.4: Circuit model for the representing all fluxes and forces in 3 staged NE device.

a circuit model with voltage and current sources are illustrated in Fig. 4.4. Here, heat fluxes are modeled with current sources, temperature gradient is modeled with voltage sources and material properties associated with the corresponding heat flux is represented with resistance such as resistance in the figure can be treated as thermal resistance for conduction heat and can be treated as electrical resistance for Joule heat.

A self-consistent model is controlled with a tolerance which is calculated from the difference between the summation of old temperature distribution assumption and new

temperature distribution obtained based on circuit model calculation. Fig. 4.5 the flow chart of calculation for multistaged devices with a different shape. From the calculated temperature distribution and heat fluxes of the multistaged device, different performance parameters are calculated based on different conditions. To obtain the maximum $\nabla_x T$, simulation is performed at no-load condition ($Q_i n = 0$) with the desired variation. On the other hand, to obtain the maximum input heat flow density, Q_{max}, towards hot side, Q_{max} is obtained from $\nabla_x T_{max}$ condition. COPs are also calculated during the calculation of Q_{max}. Fig. 4.5 shows the flowchart representing the algorithm for mathematical calculation of multistage device, while Fig. 4.6 illustrates the flowchart for the complete simulation model to obtain the device characteristics based on mentioned conditions.

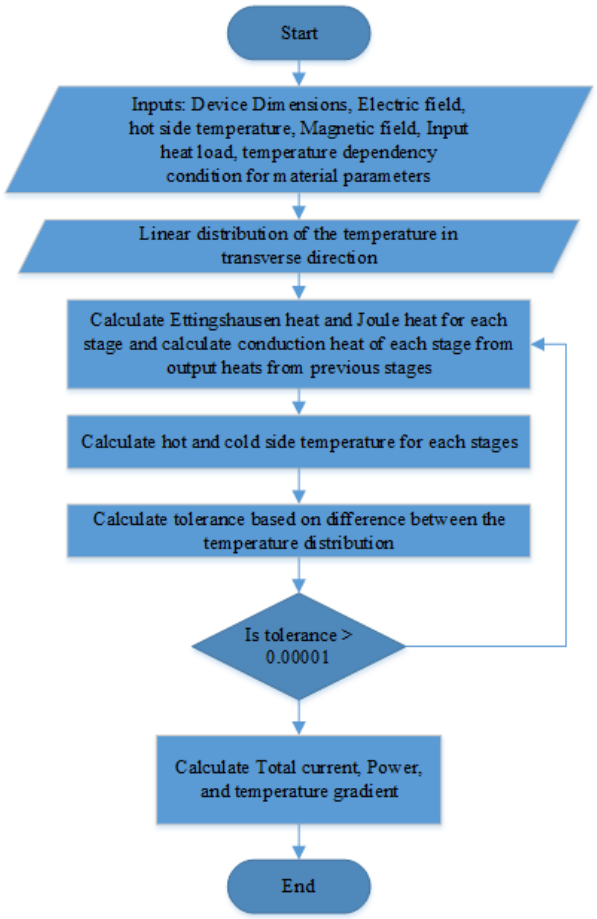

Figure 4.5: Schematic diagram showing the relations of input and output heat flow between the individual stages of the multi-stage device.

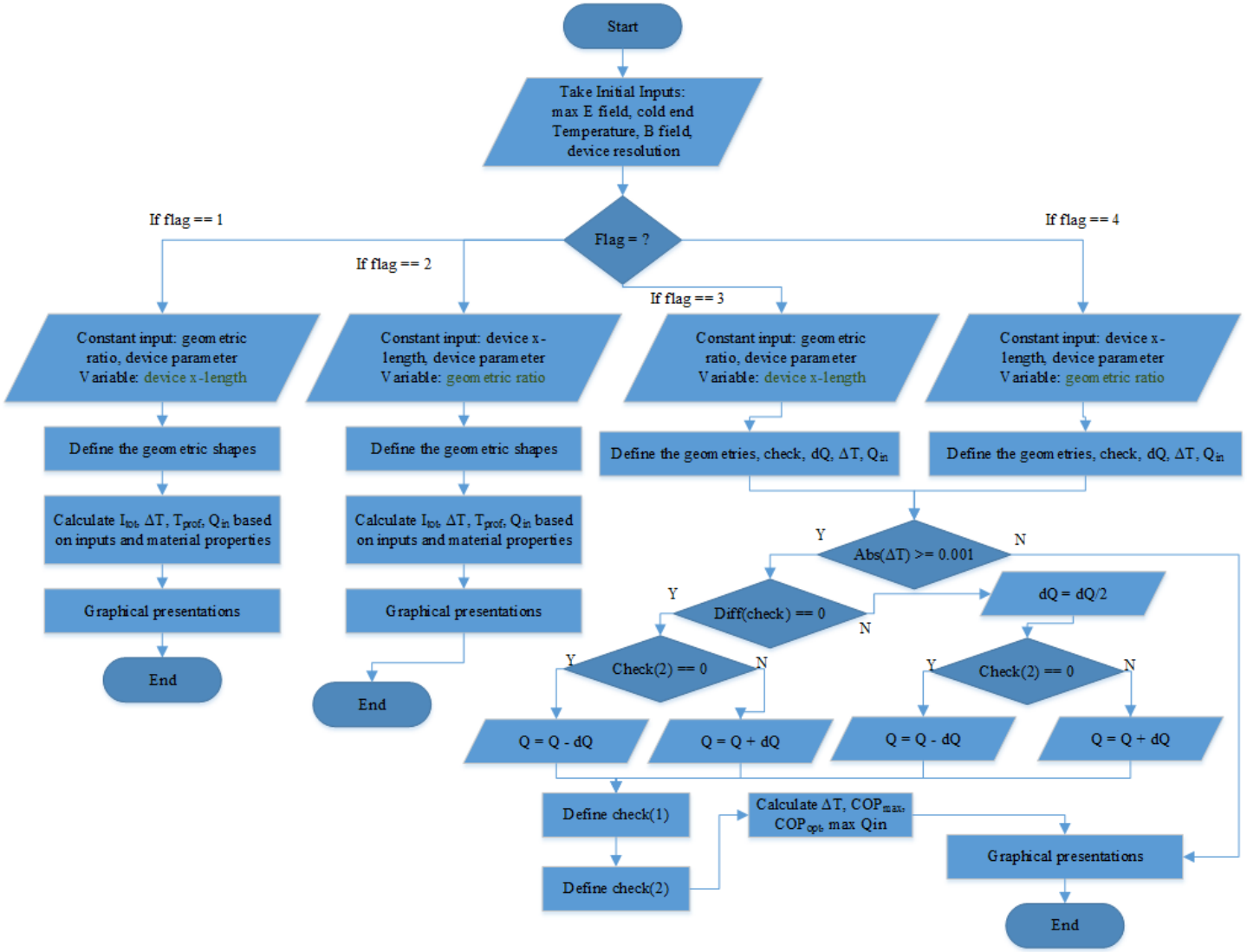

Figure 4.6: Schematic diagram showing the relations of input and output heat flow between the individual stages of the multi-stage device.

Chapter 5

Experimental Works on Multistage TM Cooler

5.1 Introduction

An experimental work is performed to obtain the practical results and analysis those result with the theoretical works. This chapter provides the details about the motivation behind experimental works, description about sample preparation and steps of experimental work. Till now, most of the theoretical and experimental works are performed on thermoelectric devices. And for thermomagnetic, most of the works are theoretical, few works are done based on experimental data. One of the reasons is the difficulties to do the experimental setup to calculate the transverse effect in presence of magnetic field with the variation of temperature and current flow. With this motivation, we have performed the experimental works on BiSb material system, one of the most efficient TM material systems with higher thermomagnetic figure-of-merit. Many published results [27, 85, 90, 91, 98] are also available for this material system which is beneficial for

verifying our obtained results.

5.2 Sample Preparation and Characterization

For performing the experimental work, we have prepared four samples with two different BiSb material systems. Two samples are made with $Bi_{97}Sb_3$ and other two are $Bi_{95}Sb_5$. All samples are made from the elemental elements of Bi and Sb. Samples are prepared inside the glovebox which is always kept under positive pressure with Argon environment. Inside environment is always maintained with < 0.01 ppm H_2O and < 0.01 O_2 molecules which ensures the preparation of pure BiSb system without forming any oxide. First, we measured Bi droplets and Sb powder to make 10g of BiSb alloy. Measurement error kept within 1$\sim$3 mg range so that we can control our material composition precisely. Then, a 10g mechanical mixture of BiSb alloy was transferred to a glass tube under argon environment. Glass tubes were cleaned with IPA sonication for 10 min before the use. Glass tubes and the sealing valves are taken inside the glovebox with vacuum and purging of Ar to ensure that everything happened in an inert environment. Glass tubes were then sealed tightly with the valve inside the glovebox and then take out from the glovebox. A vacuum system is used to remove the argon from the tube. Then, under vacuum, tubes are sealed in the middle with an oxyacetylene torch. After sealing, material system is melt with the oxyacetylene torch for 5 mins with aggressive movement so that a uniform alloy system can be obtained. A rapid quenching was done after melting to avoid the undesired phase transformation and to obtain a better crystalline structure. Fig. 5.1 demonstrates the sample preparation steps sequentially.

After the preparation of the BiSb material systems, we cut the samples with a diamond wire saw. We only made rectangular and trapezoidal shaped samples, as making these

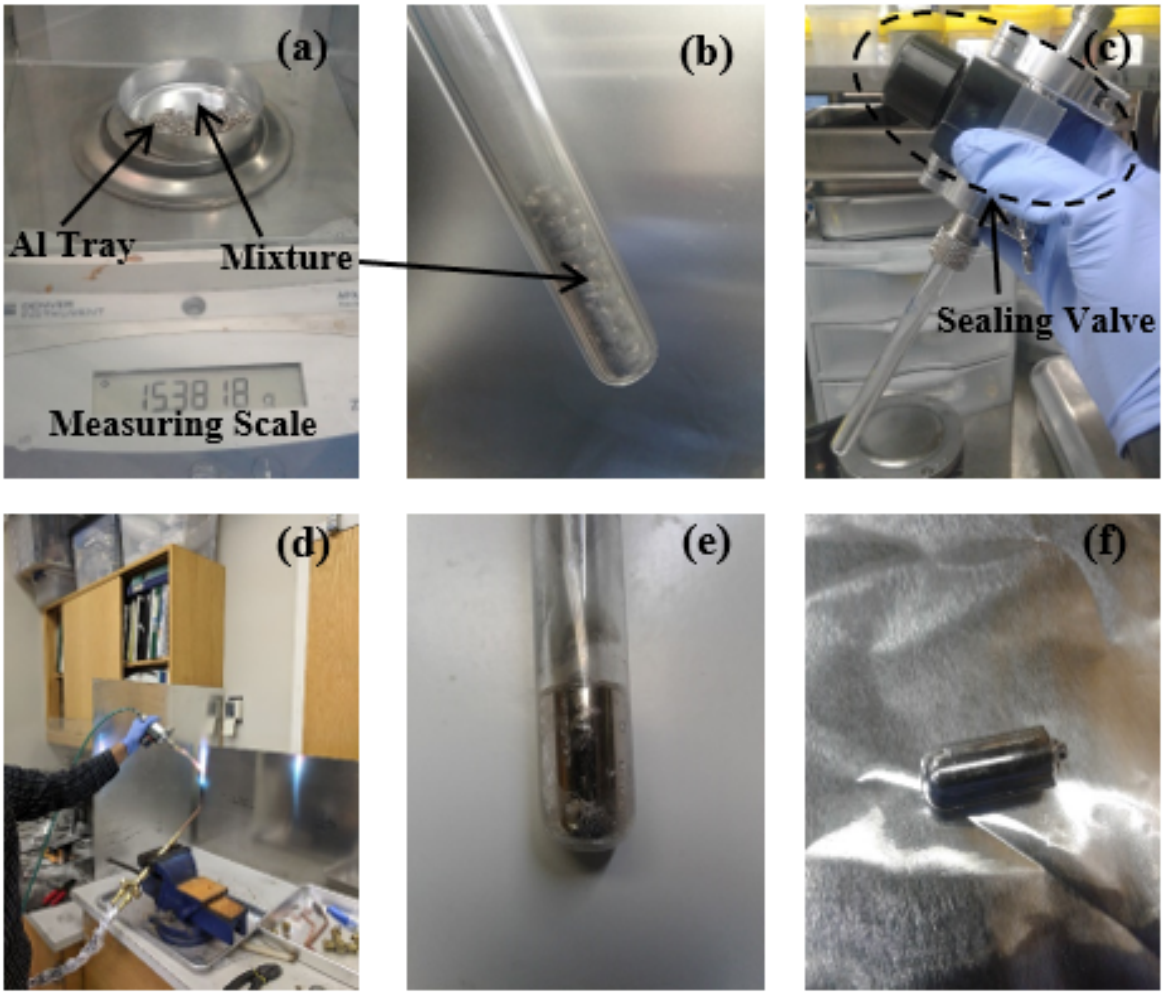

Figure 5.1: Sample preparation steps: (a) measuring the elements of sample inside glove box, (b) Sample mixture in glass tube, (c) Glass tube sealing with valve, (d) Melting the sample in torch, (e) Sample after quenching and (f) final ingot of sample.

structure is simple. Making infinite shaped device is ignored because of the difficulties to make that shape with the existing setup. To prepare samples with a smooth surface, we kept the cutting speed at 1 mm-min^{-1}. Surface smoothness was observed under a microscope and was found satisfactory.

Fig. 5.2 shows the picture of the surface of the sample. After cutting the samples, samples

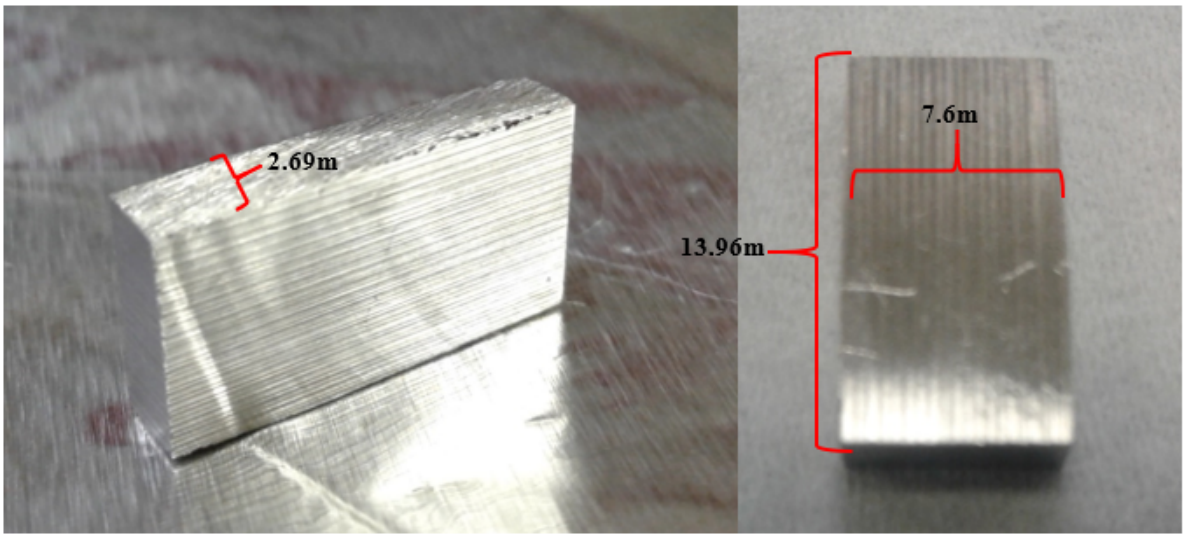

Figure 5.2: Rectangular shaped sample shown with the dimensions after wire saw cutting.

are cleaned with Acetone and IPA by 20 min sonication to remove the wax used to set up the sample in the wire saw tool and an oily surface that might be coming from the machine and used gloves. Samples are kept in glovebox after every treatment performed on the sample.

To check the formation of BiSb alloy, we took the diffraction pattern in XRD using Rigaku Miniflex XRD machine. XRD was performed with Cu K radiation with 0.154 nm wavelength. Fig. 5.3 shows the XRD peaks for both $Bi_{95}Sb_5$ and $Bi_{97}Sb_3$. XRD results show a good formation of BiSb alloy.

From the above figures, it is seen that both samples give first peak and dominant peak for the crystal plane of (0,0,3) and (0,1,2), respectively. But peak positions of $Bi_{95}Sb_5$ are shifted with respect to those values for $Bi_{97}Sb_3$. From the data, it is found that the first peak position is 22.54° for $Bi_{95}Sb_5$, while for $Bi_{97}Sb_3$, it is at 22.51°. Therefore, the interplanar distances are also different. The interplanar distance of (0,0,3) planes is 3.941

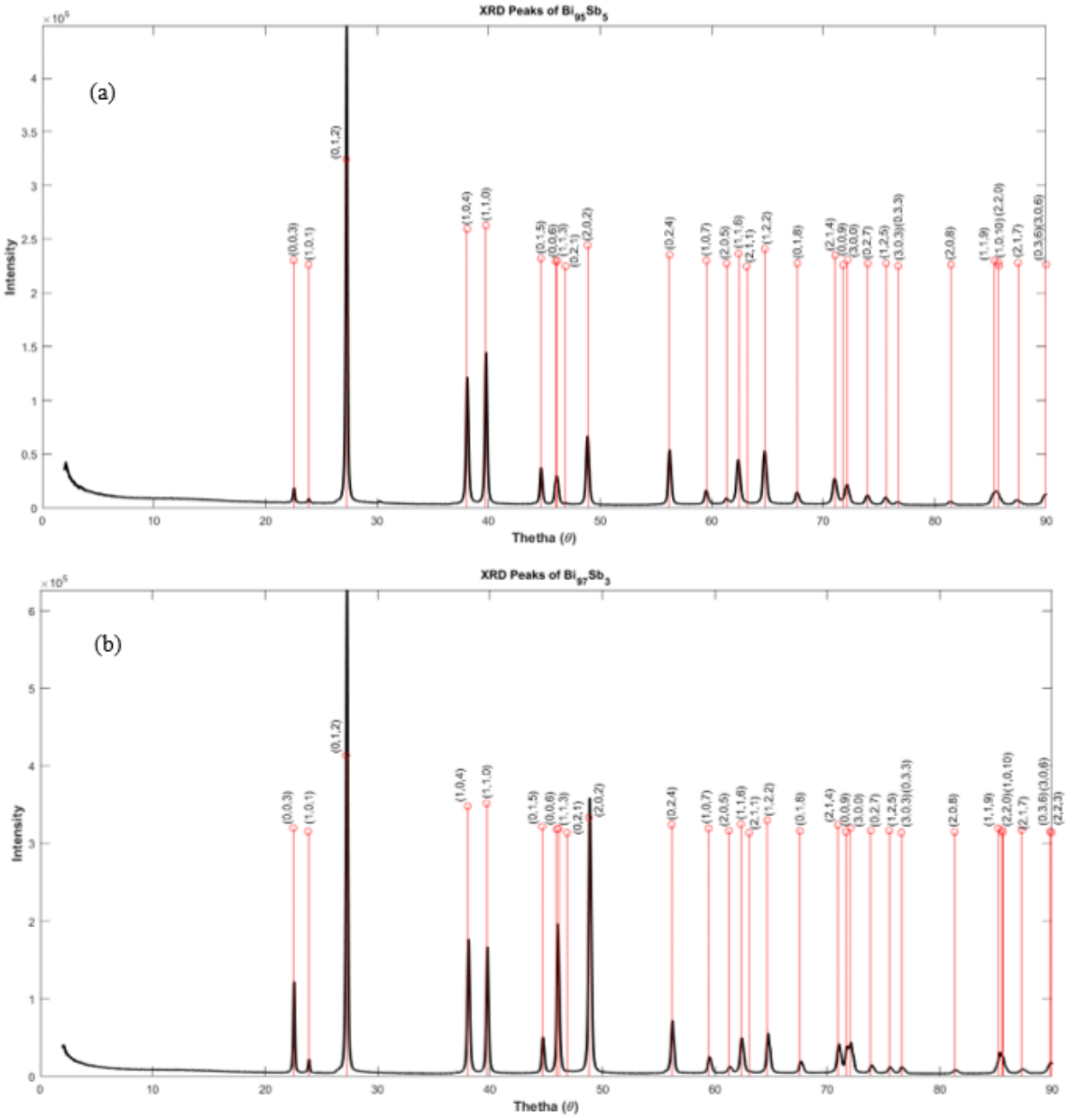

Figure 5.3: XRD patterns for (a) $Bi_{95}Sb_5$ sample and (b) $Bi_{97}Sb_3$ sample.

Table 5.1: Material characteristics of the synthesized samples: $Bi_{95}Sb_5$ and $Bi_{97}Sb_3$

Parameters	$Bi_{95}Sb_5$	$Bi_{97}Sb_3$
Density (g/cm^3)	8.81	9.468
Ideal density (g/cm^3)	9.4	9.73
First Peak location of XRD	22.54°	22.51°
Millar plane for first peak	(0,0,3)	(0,0,3)
d_{003} ($\AA$)	3.941	3.947

$\AA$ for $Bi_{95}Sb_5$, and 3.947 $\AA$ for $Bi_{97}Sb_3$. From the relation between interplanar distance and lattice constant, it can be understood that lattice constant of $Bi_{97}Sb_3$ is higher than that of $Bi_{95}Sb_5$. From the measurement of the physical dimensions of the samples and weight, their densities are also measured. From the measurement, it is found that $Bi_{95}Sb_5$ sample is 94% dense with respect to its ideal density and $Bi_{97}Sb_3$ is 97.3% dense. Table 5.1 shows the general properties of two BiSb samples which are calculated from measurements.

Finally, for the measurement of the thermopower and electrical resistivity were measured simultaneously using LSR machine. LSR machine is mainly made to measure thermoelectric figure-of-merit by measuring Seebeck coefficient, and electrical resistivity. It has a wide operating temperature range from 100 °C to 1500 °C. It measures Seebeck coefficient with static dc method and electrical resistance with the four-point method. Samples should be in cylindrical, disk or rectangular shape with the range of 6∼23 mm long and 2∼8 mm diameter. Two heater systems are used to create a temperature gradient into the sample and two thermocouples (TC) are used to measure the voltage. Separation between the TCs can be 4 or 6 mm. Fig. 5.4 shows a typical setup of a sample along with

the different parts associated with the measurement [99].

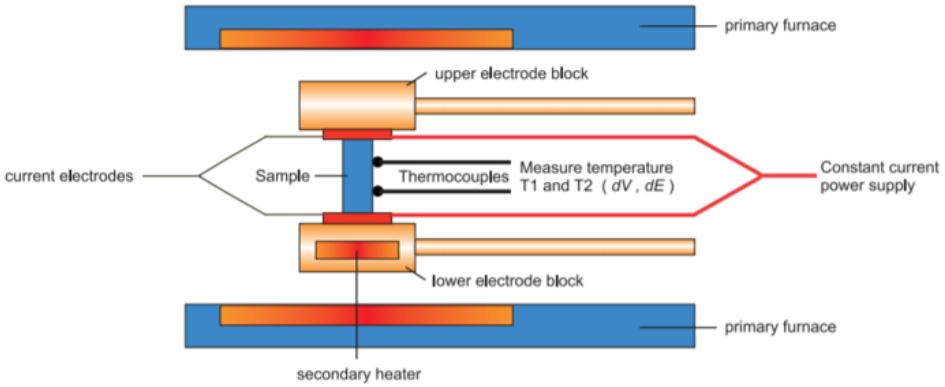

Figure 5.4: Schematic diagram of LSR tools with connection between different parts and with sample setup inside the tool [99].

Chapter 6

Results and Discussions

6.1 Results from Simulation Work

The simulation model is developed based on the mathematical model presented in chapter 4. To make the analysis more practical and verify the developed model, device dimensions and other required parameters are taken from the previously published results [5, 91]. In the simulation, hot side temperature is assumed constant as typically there is a heat sink attached to that end. The magnetic field is kept constant for simplicity and time constraint. Table 6.1 shows the parameters that used for the simulation.

Simulation is performed for all available geometric shape: thin rectangular, thick rectangular, trapezoidal, Harman's infinite shape and derived shape in this work. Thin and thick rectangular shapes are defined with respect to the dimension of the shaped devices like trapezoidal and infinite. In thin rectangular, transverse length with respect to heat flow always keeps constant at cold side length of the shaped device, while in thick rectangular, the hot side length of the shaped device is taken as transverse length.

Fig. 6.1 illustrated the geometries of the different NE devices that considered for the

Table 6.1: Input parameters used for the model

Parameters	Value
Device Dimension	Length in current flow direction 2.54 cm Length in B field direction 0.031 cm (cold side) Length in heat flow direction 0.428 cm
Shape factor or a geometric ratio	13
Sample materials	$Bi_{97}Sb_3$
Maximum Electric Field	2 Vcm^{-1}
Individual stage height	0.001 cm
Hot side temperature	150 K

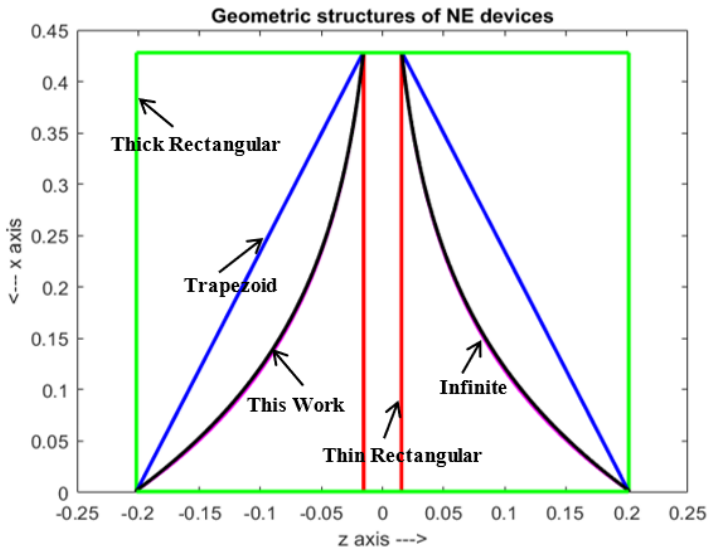

Figure 6.1: All geometric shaped NE devices considered into the simulation model along with their dimensions.

simulation. It is seen from the above figure that, both infinite models that derived in Harman's work and in this work have almost similar shape, but corrected model gives little bit wider side than Harman's model. This difference can be more noticeable for the

material systems which material properties are changed aggressively with temperature. This difference is caused by the ideal assumptions taken in Harman's model where he assumed constant input power density for each stage. In reality, power density will change with temperature which will be illustrated by next figures. Both models give the same shape for low-efficiency material system.

To observe the effect of temperature dependent material parameters on device performance, simulation is performed based on both temperature dependent and independent material properties. As shown in prior chapters, all material properties like Nernst coefficient, electrical resistivity, and thermal conductivity are a strong function of temperature and these parameters determines the important elements of cooling performance like Ettingshausen heat, Joule heat, and conduction heat. According to the circuit model demonstrated in chapter 4, temperature distribution into the devices is also depended on these heat components. In Fig. 6.2, an illustration is showed that how the temperature is distributed throughout the device length. Devices are considered as longitudinally isothermal. Therefore, the only temperature distribution map is seen along heat flow direction. The temperature distribution is illustrated with a color map in Fig. 6.2.

Distribution color map gives an overall idea of the temperature profile. But, it doesn't give the understanding of temperature gradient profile created at each stage. According to the circuit model, it is seen that all stages don't carry or pump the same amount of heat. So, it is expected to get a non-linear temperature gradient profile along the x-axis. In our simulation, initially a linear temperature distribution model is assumed and then from the self-consistent method, the temperature values are updated. This update is done with heat component calculation which are material properties dependent. Temperature gradient profile along the x-axis for all NE devices are presented in Fig. 6.3 and Fig. 6.4. Fig. 6.3 shows gradient profile considering temperature dependent

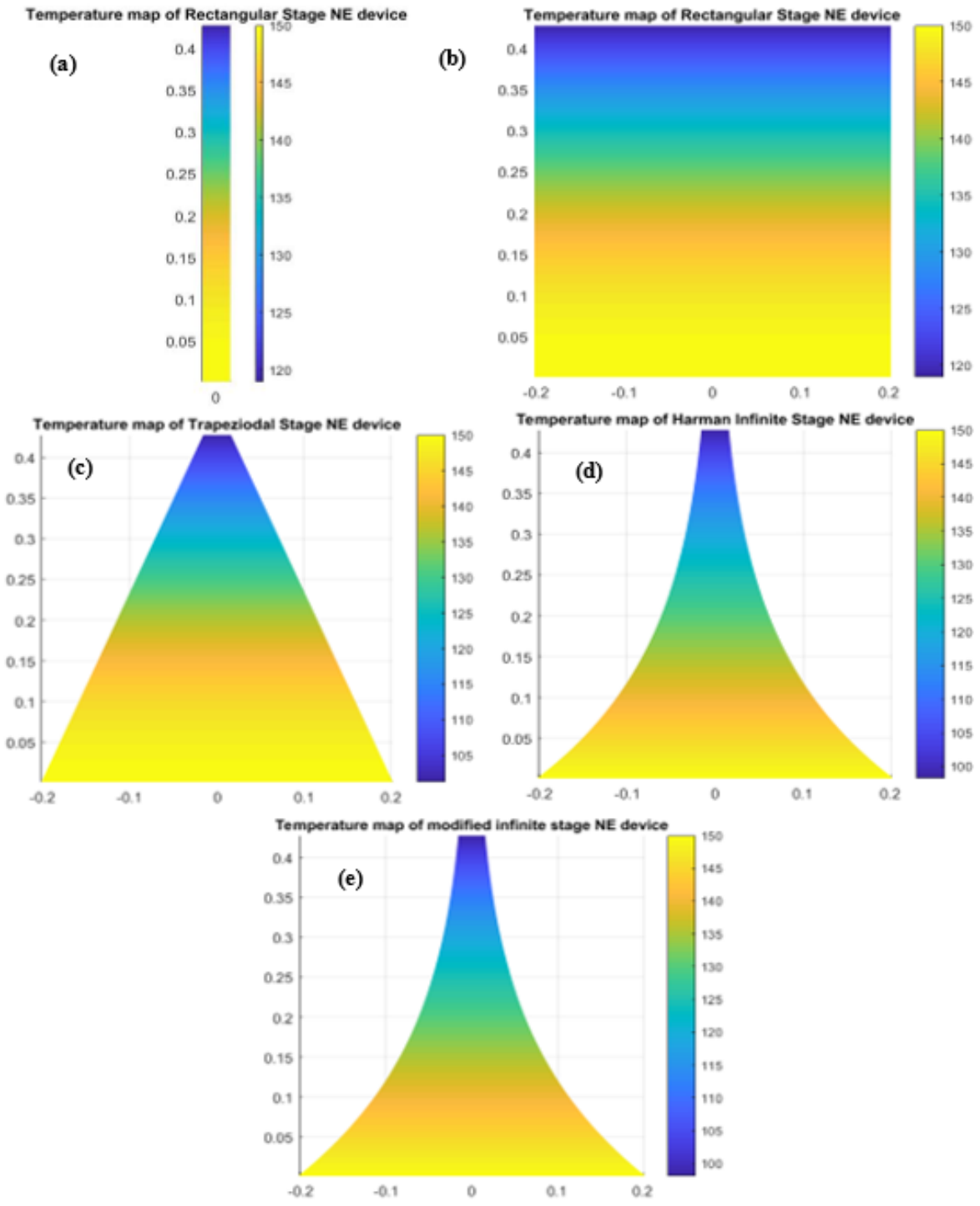

Figure 6.2: Color-bar illustration of spatial temperature distribution for all NE devices: (a) thin rectangular, (b) thick rectangular, (c) trapezoidal, (d) Harman's infinite shape and (e) corrected shape proposed in this work.

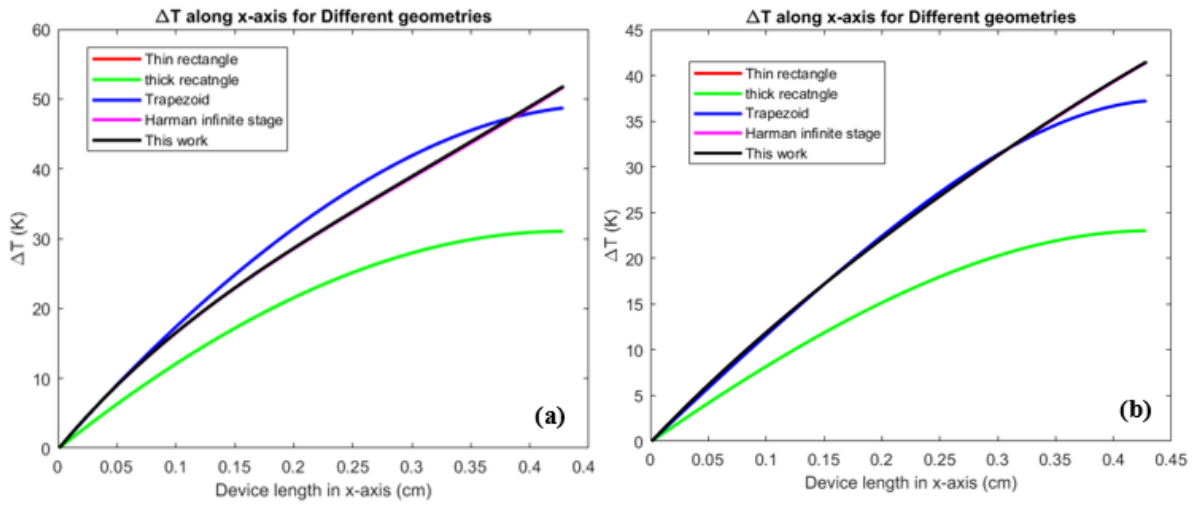

Figure 6.3: Temperature gradient profile along x-axis considering: (a) temperature independent material properties, and (b) temperature dependent material properties.

and independent material properties, separately. And, Fig. 6.4 demonstrates the impact of temperature dependent properties on gradient profile by showing all gradient profile collectively.

From Fig. 6.4, it is found that with the consideration of temperature dependent properties, the rectangular geometric shaped device shows 27.07% drop in a temperature gradient across the device while trapezoidal shape shows 23.62%, Harman's infinite shape has 19.89% and our derived shape geometry shows 19.98% drop in the temperature gradient. This actually shows the importance of consideration of temperature dependent material properties.

The temperature profile and gradient profile of the NE devices are the output of the heat components existed into the device. According to the discussion in prior chapters, two heat components plays an important role to determine the cooling performance of an NE device: Ettingshausen heat and Joule heat. Theoretically, Ettingshausen heat is a linear function of current. According to Fig. 6.5, NE devices show a linear relation

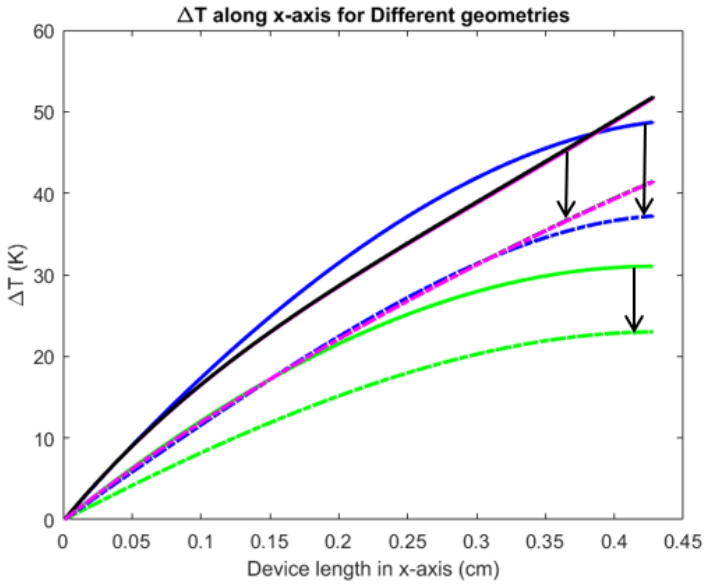

Figure 6.4: Temperature gradient profile along x-axis showing the decrement in gradient with temperature dependent material properties consideration. Solid lines represent gradient obtained from temperature independent material properties consideration and dash-dot lines represent temperature dependent consideration.

for a certain region with temperature independent material properties study and show a perfect linear relation while temperature dependent material parameters are considered. Comparing both figures, it is also seen that Ettingshausen heat has a linear relation with current up to 6000W.

On the other hand, Joule heating is proportional to the square of the current and it is always increased with the increase in current. Both temperature dependent and independent studies show the trends of the theoretical relation between Joule heating and current that is shown in Fig. 6.6. In temperature-dependent material properties study, less Joule heating is found because of the less temperature drop across the NE devices is lower and the resistivity is almost inversely related to the temperature.

Both Ettingshausen and Joule heat along with conduction heat loss define the cooling

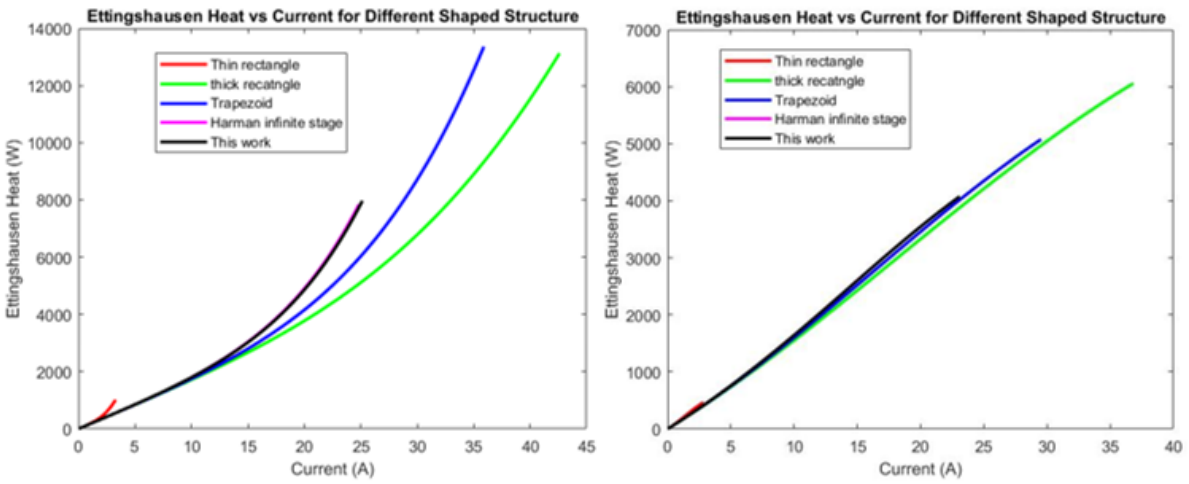

Figure 6.5: Ettingshausen heat flow in a different geometric device with considering (left) temperature independent properties and (right) temperature dependent properties.

power of the NE devices. To analysis the cooling power of a heat pump, it is important to know the performance of the device at the no-load condition. In no-load condition means zero input heat, NE devices generally give maximum temperature gradient which is named as ΔT_{max}. Though no devices are operated in a no-load condition, this condition gives the idea of maximum device performance. It is generally expected that shaped geometry will generate a maximum temperature gradient in comparison with the rectangular geometry, as shaped geometries can pump more heat than rectangular geometry. From both studies of temperature dependent and independent material properties, similar behaviors are found which is shown in Fig. 6.7.

Fig. 6.8 shows the combined results to illustrate the effect of the temperature dependent properties. From the figure, it is seen that maximum temperature gradient is decreased from 31.04 K to 23.01 K for both rectangular devices, while in trapezoid, maximum gradient is decreased from 48.73 K to 37.22 K, in Harman's infinite shaped devices, drop is from 51.77 K to 41.47 K and finally in our derived shape device, maximum temperature

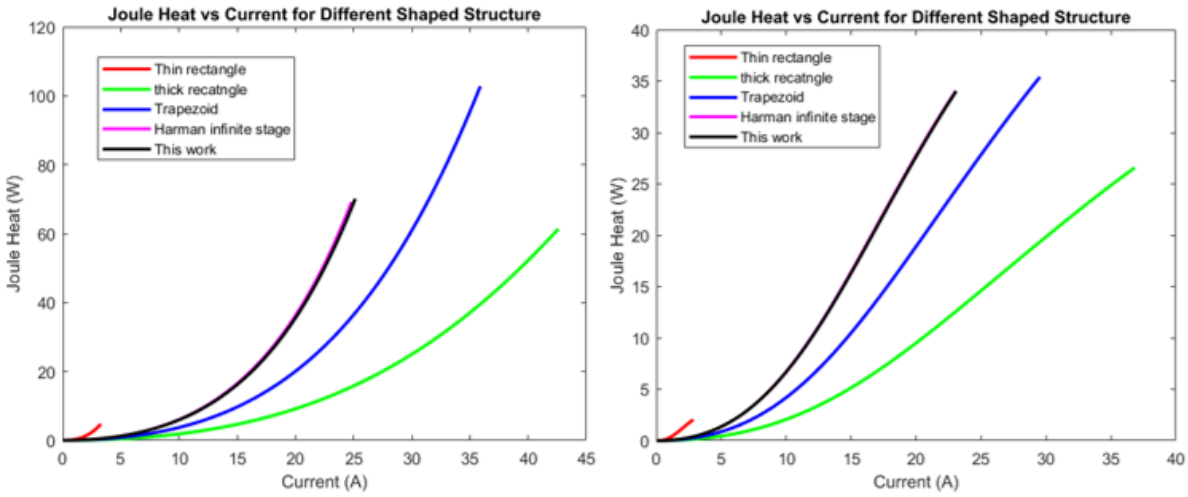

Figure 6.6: Joule heating in different geometric device with considering (left) temperature independent properties and (right) temperature dependent properties.

gradient is decreased from 51.9 K to 41.52 K.

As geometric ratio or shape function plays the important role to increase device performance in terms of obtaining maximum temperature. It is expected that with the increase in shape factor maximum temperature gradient should also increase. But this is true for certain range of shape factor. After that range, maximum temperature gradient shows a constant behavior which is due to the fact of Carnot limit so that the efficiency doesn't go to ideal Carnot limit. Moreover, at higher shape factor, the device will operate under high current which will generate the higher Joule heating which will limit the cooling performance as well as the maximum temperature gradient. Moreover, a higher temperature gradient will generate higher conduction heat so to reach the optimum value, maximum temperature gradient should be saturated after certain range. Fig. 6.9 and Fig. 6.10 show the expected behavior as mentioned.

From Fig. 6.9, it is seen that after the geometric ratio of 40, a maximum temperature gradient is increased by a small amount, hence giving the saturation behavior. But, from

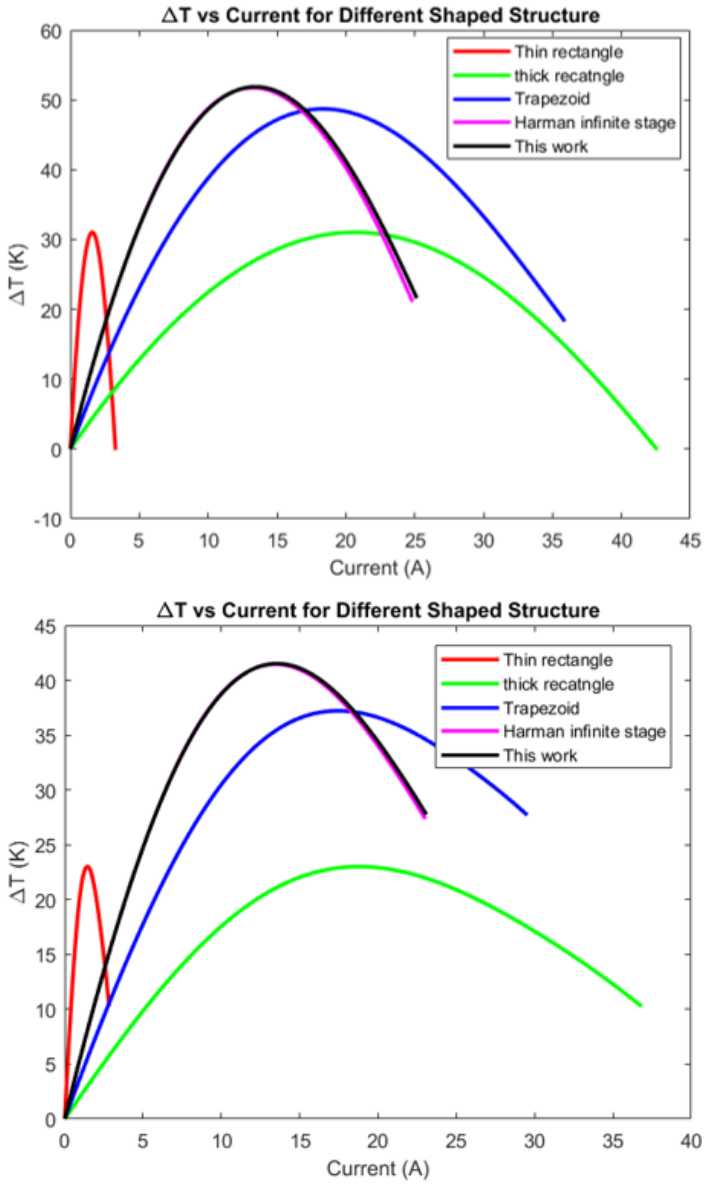

Figure 6.7: Maximum temperature gradient as a function of current for the consideration of (up) temperature independent properties and (down) temperature dependent properties.

Fig. 6.10 it is found that current is increased almost linearly with respect to shape factor.

Both figures also show the effects of temperature dependent and independent material

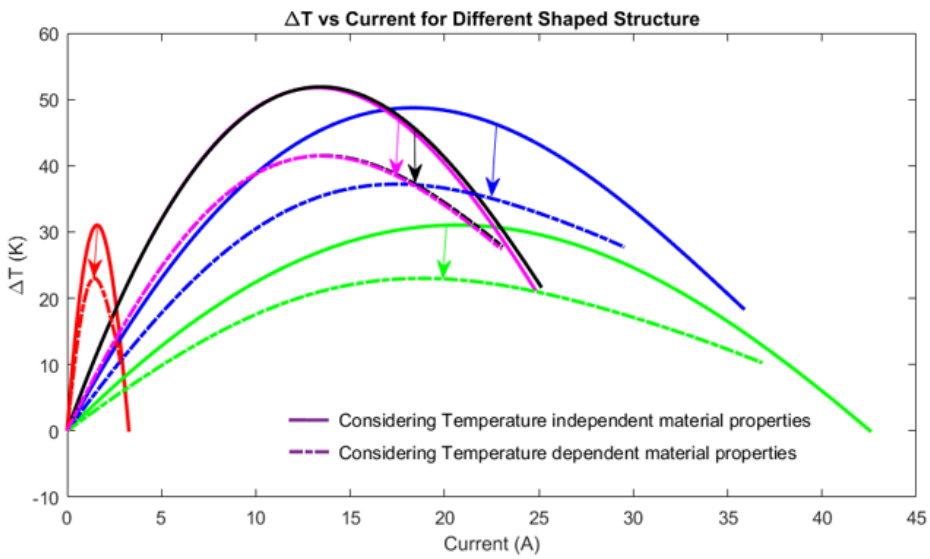

Figure 6.8: Maximum temperature gradient considering (solid) temperature independent properties and (dash-dot) temperature-dependent properties for different geometries.

properties on the results.

6.2 Results from Experimental Work

With the mentioned process in chapter 5, we performed our experiment based on the availability of the equipment in the lab. We measured the electrical conductivity and thermopower versus temperature. Then the carrier concentration was estimated from the thermopower values. Knowing the carrier concentration and the electrical conductivity, we estimated the carrier mobility and the electronic part of the thermal conductivity of the synthesized BiSb sample. Those characteristics of BiSb are presented in Fig. 6.11. It can be seen that the power factor of the synthesized BiSb sample is close to the best-reported data in the literature for this material system [100].

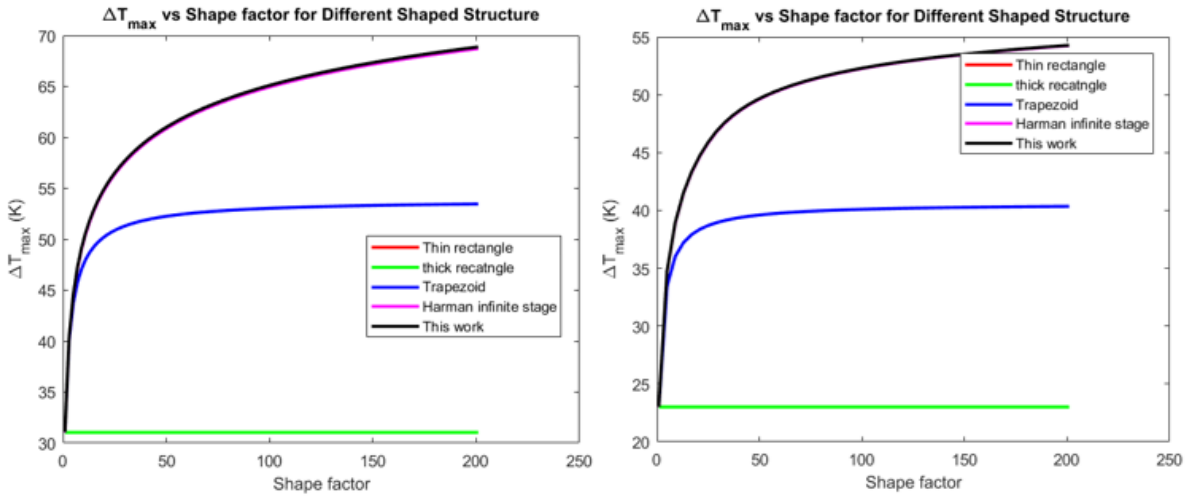

Figure 6.9: ΔT_{max} as a function of shape factor with considering (left) temperature independent properties and (right) temperature-dependent properties for different geometries.

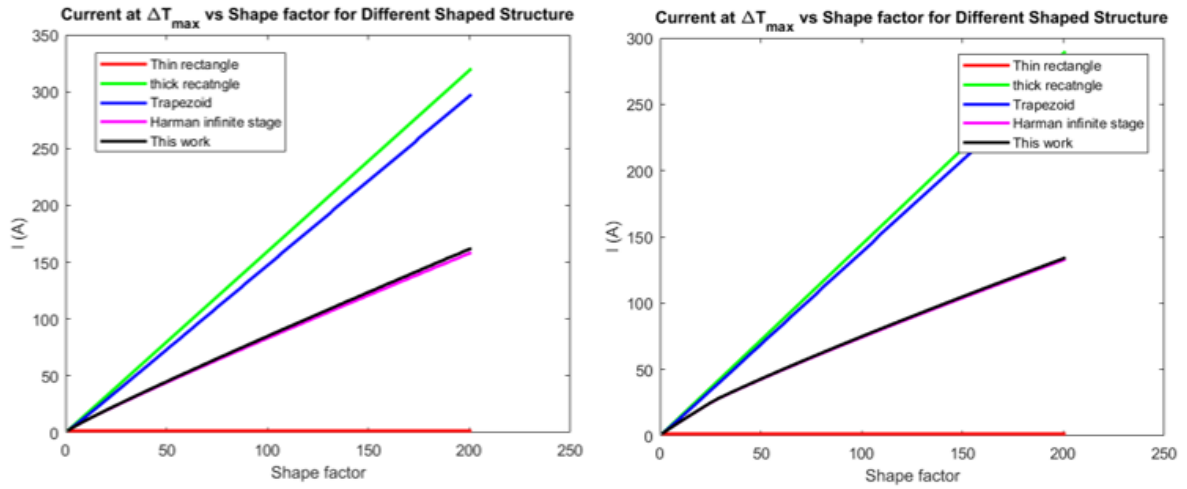

Figure 6.10: Current versus shape factor with considering (left) temperature independent properties and (right) temperature-dependent properties for different geometries.

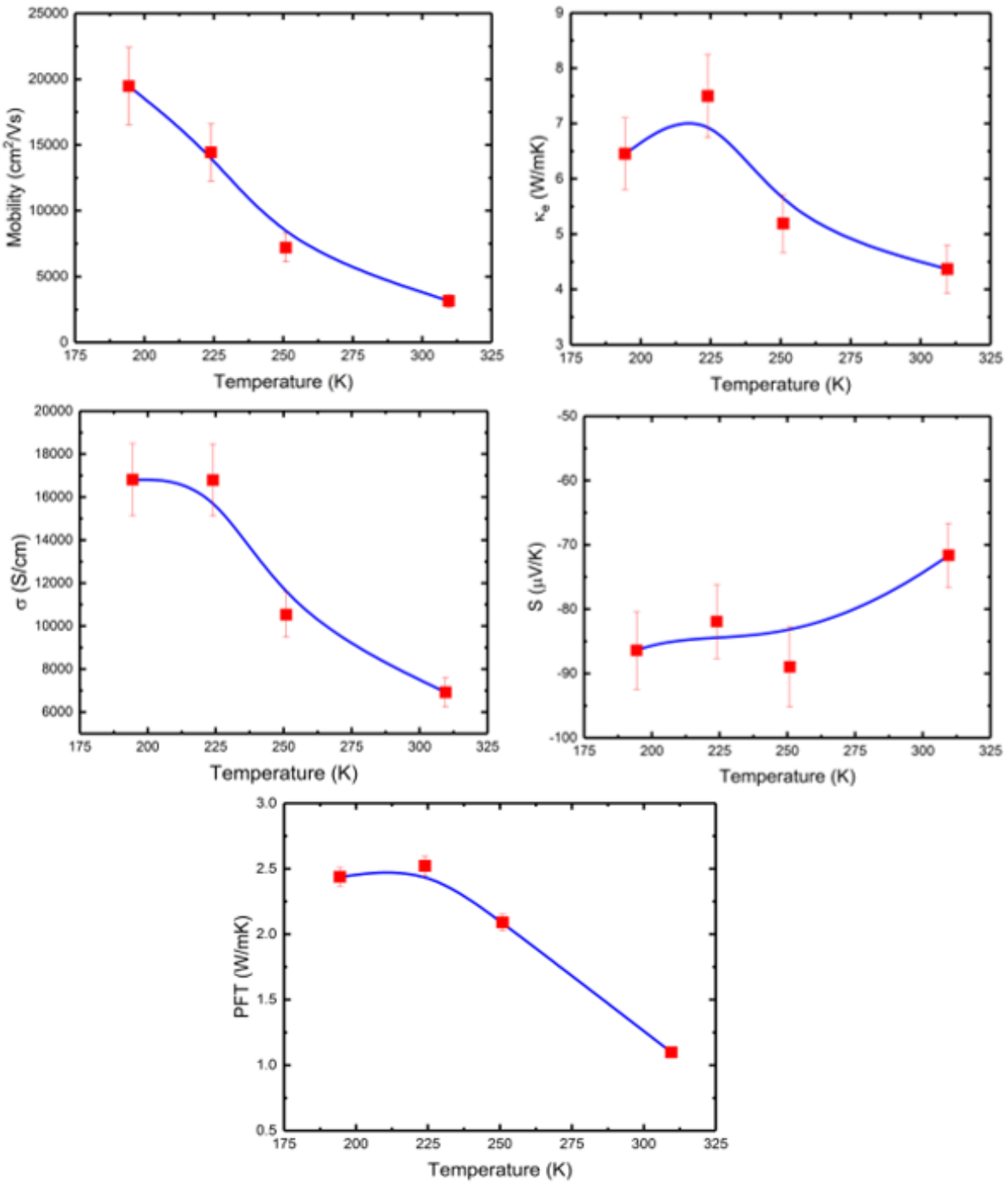

Figure 6.11: Mobility, electrical conductivity, thermal conductivity due to electronic contribution, Seebeck co-efficient and thermoelectric figure of merit of $Bi_{95}Sb_5$ materials with respect to temperature.

Table 6.2: Comparison of performances between different geometric shapes for both temperature dependent (TD) and temperature independent (TID) material properties

Performance parameters	Thin Rectangle	Thick Rectangle	Trapezoid	Harman's Infinite stage	This work
ΔT_{max} (K) @ shape factor (S.F.) = 13	31 (TD) 23 (TID)	31 (TD) 23 (TID)	48.7 (TD) 37.2 (TID)	51.8 (TD) 41.5 (TID)	51.9 (TD) 41.5 (TID)
Current (A) @ ΔT_{max}	1.57 (TD) 1.43 (TID)	20.5 (TD) 18.8 (TID)	17.9 (TD) 17.5 (TID)	13.4 (TD) 13.6 (TID)	13.4 (TD) 13.6 (TID)

6.3 Analysis and Discussions

To compare the obtained results from the simulation model, all performance characteristics are summarized in Table 6.2. From the details of the simulation model, it is found that the less efficient NE device is thick rectangular device and most efficient one is infinite stage device. As discussed in chapter 2, making the area bigger along the heat flow direction and making the area smaller in the current flow direction give a more efficient performance in NE devices. This statement can be verified by comparing the performance of thin and thick rectangular geometry.

On the other hand, among the shaped geometries, infinite staged devices are superior to trapezoidal shaped device due to the increment trends of the area along heat flow direction. This is the optimized way to build the device. Though, making trapezoidal shaped NE device is more practically feasible than the infinite shaped devices. Infinite shape derived in this work shows a little improvement than Harman's infinite staged device in terms of performance as shown in the table. This is because of the nature of temperature dependent material properties. If these properties change aggressively with the change

Table 6.3: Published results on different shaped thermomagnetic devices with corresponding materials and dimensions

Reference	Material	Dimensions (cm) and geometry	ΔT_{max} (@1T)
Scholz et. al. [91]	$Bi_{97}Sb_3$	2.8×1.6(hot side)× 0.1(cold side)×0.9, Infinite	42 K
Hawkins et. al. [5]	$Bi_{97}Sb_3$	2.62×0.2×0.6, Rectangular	25 K
Horst et. al. [92]	$Bi_{97}Sb_3$	2.54×0.394(hot side)× 0.031(cold side)×0.428, trapezoid	38 K
OBrien et. al. [80]	$Bi_{99}Pb_1$	5×3×0.8, Rectangular	0.25 K
This work	$Bi_{97}Sb_3$	Horst's trapezoid device Scholz infinite device	37.22 K 41.47 K

in temperature, it is expected to get a significant difference between two models. To compare the results obtained in this simulation work with previously published results, Table 6.3 presents the results of those published works.

Scholz et. al. found 42 K experimentally for Harman's infinite shaped device and Horst et. al. found 38 K in trapezoidal shape. From our simulation, we found 41.47 K for infinite shape device and 37.22 K for trapezoidal shape. Scholz also presented a result showing the maximum temperature gradient as a function of geometric ratio. Our obtained result (shown in Fig. 6.9) also agree with their result. The difference between the results of Scholz work and this work is caused by the consideration of different geometric shape.

Almost no prior works demonstrated the results for maximum heat load and coefficient of performance for different geometries. Most of the work avoid these calculations due to the complexity in the calculation. In this work, we performed those characteristics based on the assumptions shown in previous chapters. But, we can't provide any reference for the verification. We considered those values as reasonable from the verifications of other

characteristics and the trends of those outputs.

6.4 Findings from this Work

From this study and the performance of the simulation work, we have demonstrated the device characteristics of Nernst-Ettingshausen coolers. One of the important findings of this work is the proposed new model for infinite staged devices which is actually a temperature dependent corrected model of Harman's proposed model. This new model shows a little improvement in a maximum temperature gradient, maximum input heat load, and coefficient of performance than those of Harman's model. As discussed earlier, this model takes care of the limitations in Harman's model and can show the Carnot's limit for performance.

We demonstrated a complete flowchart and a suitable circuit model which are used to develop simulation models. Our self-consistent model for the multistaged device is later utilized for the performance analysis of the devices. From our simulation model, we successfully reproduce the similar results which actually provides the verification of our developed model. Throughout the simulation performance, we obtained all the device characteristics associated with the NE coolers. We also demonstrated the characteristics of maximum heat pumping capacity as a function of both device length and shape factor as well as COP versus length and shape factor which is less addressed in the previously published results.

Finally, we developed an experimental setup for measuring transverse thermomagnetic effects with our existing characterizing tools. Measurements of thermomagnetic effects in the presence of magnetic field are always challenging. We designed the magnet which must be modified for LSR measurement. We also made thermomagnetic elements for the

measurement and characterize those sample. Our characteristics illustrations show that our samples are in good for reliable measurements.

Chapter 7

Conclusion and Future Works

7.1 Conclusion

The aim of this work is to develop a new infinite shape expression which will take care of the ideal assumption made in Harman's work for deriving the exponential shape for the infinite stage. Improving the performance of Nernst-Ettingshausen (NE) coolers by cascading the individual stages was first demonstrated by O'Brien and Wallace. They also gave the expression for infinite staging. Later, Harman modified their expression and Kooi et. al. proposed another model for addressing the limitation of Harman's model. In this work, a brief study was made on the previous model and then a details derivation was presented with all the practical considerations which are ignored in other models. Carnot limits are also demonstrated for the derived model. To provide the better understanding of the motivation of this derivation work, a literature review is also presented addressing all recent and widely used solid-state cooling technologies with their pros and cons. Detail theoretical study is done and provided to present the fundamental background that required for the analytical work.

A simulation work is performed to obtain the performance of NE devices in terms of maximum temperature gradient obtained across the device, maximum heat flow and coefficient of performance. Performance of the devices is calculated as a function of current, device length and the geometric ratio between cold side area to a hot side area. Simulation work is performed for all available geometric shape such as rectangular, trapezoidal and infinite shaped devices. Material system, chosen for the simulation work is BiSb, mostly studied material system with higher thermomagnetic figure-of-merit. Comparisons between the performance of the devices with different geometric shape are presented. It is found that infinite shaped devices are more efficient than other geometric shaped devices which agrees the previously published results. Moreover, our derived model for infinite shaped device showed better performance than Harman's model. Due to the idealistic approximation, Harman's model overestimated the Joule heating and COPs for individual stages which causes the difference between Harman's model and our model. We presented the correction factor that should be included in Harman's model.

In addition to the simulation work, an experimental work is also done to get the practical idea over TM devices. To perform the experiment, we used LSR tools along with a modified N52 Neodymium permanent magnet and four type-K thermocouples. The aim of this experimental work is to measure the Nernst coefficient, Ettingshausen coefficient, electrical resistivity and thermal conductivity in presence of magnetic field. The experiment is performed for the temperature range of 100 °C to 30 °C at 0.6T magnetic field. For the experiment, four samples are made with $Bi_{95}Sb_5$ and $Bi_{97}Sb_3$. Samples are made in a glovebox under Argon environment with a negligible amount of oxygen and water particles. Samples are melt under vacuum and quenched them in cold water to achieve a good crystal profile. Samples are characterized by XRD and found in the desired condition. For the experimental work, only two geometric shaped devices are prepared for

simplicity and available equipment. Prepared samples are of rectangular and trapezoidal shape. Measurements are performed in He environment and low-temperature range is obtained with liquid nitrogen flow. Measurement results are found to be in good agreement with simulation work and previously published results.

7.2 Future Works

There is a lot of scopes to extend this work as this work tried to present the prospect of thermomagnetic devices as a solid-state refrigerator. As, modern and future society is moving towards green technologies which have no Ozone depletion potential (ODP) and global warming potential (GWP) issues, development of efficient solid-state cooling technologies will fulfill the demand. Till now, the thermoelectric device is found to be efficient for above 200 K temperature range and thermomagnetic devices are found to be efficient for cryogenic temperature range. But, the coefficient of the performance (COP) of these devices is still low which actually obstructs the solid-state cooling devices to replace the compression-based cooling technologies. This study is made to address the prospect of the solid-state technologies. Therefore, this works has lots of options for future works.
First and foremost is the extension of the simulation work. Our simulation model is limited to constant magnetic field analysis. But, as discussed in chapter 2, the magnetic field has a significant influence on the material properties like electrical resistivity, thermal conductivity, and all transverse thermomagnetic coefficients, the variable magnetic field-based study should be beneficial for scientific society. Magnetic field-based study should include the variation in material properties due to the variation in magnetic field and effects of magnetic field on the performance of the NE devices. Performance analysis needs to include maximum temperature gradient, maximum heat flow and COP as a function

of current, device length and geometric ratio. For developing the extended simulation model, flowchart presented in chapter 4 can be utilized for developing the algorithm for the simulation. Moreover, our simulation model is limited to one material system, BiSb. An extension can be made to include more material systems into the simulation model. This will provide several benefits. First, new material systems will be studied for obtaining thermomagnetic cooling and second, a comparison can be made between the different material systems to select the optimum material for certain operating conditions and certain geometric shape.

Another important future aspect of this work is to directly measure the other thermomagnetic effects like Righi-Leduc effect and Hall effect with the same experimental setup of measuring Nernst and Ettingshausen effects. This will open the opportunity to study the other material systems for thermomagnetic cooling and other solid-state cooling technologies like spin-caloritronics and magnetocaloric technology. Especially, this direct measurement technique will be beneficial for studying the spin-based materials for thermoelectric and thermomagnetic applications.

Perhaps the most important future extension of this work is to make the infinite shaped samples based on Harman's model and our derived model to observe the practical comparison between this two-geometric shaped device. This will be helpful to obtain higher COP NE device. To provide the exponential shape with defined expression, programmable machining tools are needed. A possible solution is to use CNC machining to create the shape with the desired geometric ratio. Moreover, recently studied materials can be used to make the new samples to observe their practical performances. Table 7.1 summarizes the recent works accomplished by studying different transverse thermomagnetic effects of different materials at different temperature range. Those studies showed that these materials can be utilized for thermomagnetic application with higher thermomagnetic power.

Table 7.1: Recent studies of transverse thermomagnetic effects in different materials

Reference	Material	Studied effect
Behnia et. al. [106]	URu_2Si_2, $PrFe_4P_{12}$	Nernst effect
Cohn et. al. [107]	$Li_{0.9}Mo_6O_{17}$	Nernst effect
Alisultanov et. al. [108]	Graphene	Nernst-Ettingshausen effect
Nemov et. al. [109]	SnTe:In	Nernst-Ettingshausen effect

Some of the other prospective material systems can be BiSbTe, BiTe, SbTe, BiSeTe and BiSbTeSe [101, 102, 103, 104, 105]. Those material systems are extensively studied for thermoelectric and found to be competitive for thermoelectric applications.

REFERENCES

[1] G. N. Hatsopoulos and J. Kaye. Analysis and Experimental Results of a Diode Configuration of a Novel Thermoelectron Engine. *Proceeding of the IRE*, 46(9):1574–1579, 1958.

[2] S. W. Angrist. *The direct conversion of heat to electricity by means of a Nernst effect thermomagnetic generator*. The Ohio State University, Columbus, OH, 1961.

[3] A. Shakouri. Recent Developments in Semiconductor Thermoelectric Physics and Materials. *Annu. Rev. of Mater. Res.*, 41(1):399431, 2011.

[4] A. Shakouri and Y. Zhang. On-Chip Solid-State Cooling for Integrated Circuits Using Thin-Film Microrefrigerators. *IEEE Trans. Components and Packaging Technol.*, 28(1):65–69, 2005.

[5] S. R. Hawkins, C. F. Kooi, K. F. Cuff, J. L. Weaver, R. B. Horst, and G. M. Enslow. *Low-Temperature Ettingshausen Coolers* in Advances in Cryogenic Engineering, vol 9. Springer, Boston, 1964.

[6] F. J. DiSalvo. Thermoelectric Cooling and Power Generation. *Science*, 285(5428):703–706, 1999.

[7] L. D. Hicks, T. C. Harman, and M. S. Dresselhaus. Use of QuantumWell Superlattices to Obtain a High Figure of Merit from Nonconventional Thermoelectric Materials. *Appl. Phys. Lett.*, 63(23):32303232, 1993.

[8] I. Takeuchi and K. Sandeman. Solid-state cooling with caloric materials. *Phys. Today*, 68(12):48–54, 2015.

[9] M. S. Dresselhaus, G. Chen, M. Y. Tang, R. Yang, H. Lee, D. Wang, Z. Ren, J. P. Fleurial, and P. Gogna. New directions for low-dimensional thermoelectric materials. *Adv. mater.*, 19(8):1043–1053, 2007.

[10] W. Xie, X. Tang, Y. Yan, Q. Zhang, and T. M. Tritt. High thermoelectric performance BiSbTe alloy with unique low-dimensional structure. *J. Appl. Phys.*, 105(11):113713, 2009.

[11] L. P. Hu, T. J. Zhu, Y. G. Wang, H. H. Xie, Z. J. Xu, and X. B. Zhao. Shifting up the optimum figure of merit of p-type bismuth telluride-based thermoelectric materials for power generation by suppressing intrinsic conduction. *NPG Asia Mater.*, 6:1–8, 2014.

[12] N. Neophytos. Prospects of low-dimensional and nanostructured silicon-based thermoelectric materials: findings from theory and simulation. *The European Phys. J. B*, 88(4):86, 2015.

[13] F. Tseng, S. Li, C. Wu, Y. Pan, and L. Li. Thermoelectric and mechanical properties of ZnSb/SiC nanocomposites. *J. Mater. Sci.*, 51(11):5271–5280, 2016.

[14] W. Zhao, Z. Liu, Z. Sun, Q. Zhang, P. Wei, X. Mu, H. Zhou, C. Li, S. Ma, D. He, P. Ji, W. Zhu, X. Nie, X. Su, X. Tang, B. Shen, X. Dong, J. Yang, Y. Liu, and J. Shi. Superparamagnetic enhancement of thermoelectric performance. *Nature*, 549(7671):247–251, 2017.

[15] W. Zhao, Z. Liu, P. Wei, Q. Zhang, W. Zhu, X. Su, X. Tang, J. Yang, Y. Liu, J. Shi, Y. Chao, S. Lin, and Y. Pei. Magnetoelectric interaction and transport behaviours in magnetic nanocomposite thermoelectric materials. *Nature Nanotechnol.*, 12(1):55–60, 2017.

[16] D. Li, S. T. Huxtable, A. R. Abramson, and A. Majumdar. Thermal Transport in Nanostructured Solid-State Cooling Devices. *J. Heat Transfer*, 127(1):108–114, 2005.

[17] M. A. Korzhuev and E. S. Avilov. Use of the Harman Technique for figure of merit measurements of cascade thermoelectric converters. *J. Electron. Mater.*, 39(9):1499–1503, 2010.

[18] S. Lin and J. Yu. Optimization of a trapezoidal-type two-stage Peltier couples for thermoelectric cooling applications. *Int. J. Refrig.*, 65:103–110, 2016.

[19] G. S. Hwang, A. J. Gross, H. Kim, S. W. Lee, N. Ghafouri, B. L. Huang, C. Lawrence, C. Uher, K. Najafi, and M. Kaviany. Micro thermoelectric cooler: Planar multistage. *Int. J. Heat and Mass Transfer*, 52(7-8):1843–1852, 2009.

[20] N. A. D. Oliveira and P. J. V. Rnake. Theoretical aspects of the magnetocaloric effect. *Phys. Rep.*, 489(4-5):89–159, 2010.

[21] J. F. Scott. Electrocaloric materials. *Annu. Rev. Mater. Res.*, 41(1):229–240, 2011.

[22] J. Tusek, K. Engelbrecht, R. M. Solsona, L. Manosa, E. Vives, L. P. Mikkelsen, and N. Pryds. The Elastocaloric Effect: A Way to Cool Efficiently. *Adv. Energy Mater.*, 5(13):1500361, 2015.

[23] S. R. Boona, R. C. Myers, and J. P. Heremans. Spin caloritronics. *Energy & Environ. Sci.*, 7(3):885–891, 2014.

[24] T. Luo, S. Wang, H. Li, and X. Tang. Low temperature thermoelectric properties of melt spun $Bi_{85}Sb_{15}$ alloy. *Intermetallics*, 32:96–102, 2013.

[25] S. S. Waldrop, D. Morelli, and D. Morelli. Low-Temperature Thermoelectric Properties of $PtSb_{2-x}Te_x$ for Cryogenic Peltier Cooling Applications. *J. Electron. Mater.*, 44(6):1562–1565, 2015.

[26] A. Ziabari, M. Zebarjadi, D. Vashaee, and A. Shakouri. Nanoscale solid-state cooling: a review. *Rep. Prog. Phys.*, 79(9):095901, 20116.

[27] P. Jandl and U. Birkholz. Thermogalvanomagnetic properties of Sn-doped $Bi_{95}Sb_5$ and its application for solid state cooling. *J. Appl. Phys.*, 76(11):7351–7366, 1994.

[28] M. Zebarjadi. Thermomagnetic transport in Polycrystalline Samples. *J. Electron. Mater.*, 44(10):3827–3832, 2015.

[29] T. C. Harman. Theory of the infinite stage Nernst-Ettingshausen refrigerator. *Adv. Energy Convers.*, 3(4):667–676, 1963.

[30] L. D. Medici. Thermomagnetic mechanism for self-cooling cables. *Phys. Rev. Appl.*, 5(2):024001, 2016.

[31] J. Dieckmann, A. Cooperman, and J. Brodrick. Solid-State Cooling, Part I. *ASHRAE J.*, 53(3):82–84, 2011.

[32] G. Y. Karapetyan and V. G. Dneprovski. *Research of Opportunity to Use MISM Structures for Cooling of Light-Emitting Diodes* in Physics and Mechanics of New Materials and their Applications. Nova Science Publishers, New York, 2013.

[33] M. Zhou, M. S. H. Al-Furjan, J. Zou, and W. Liu. A review on heat and mechanical energy harvesting from human Principles, prototypes and perspective. *Renew. Sust. Energy Rev.*, 482(3):3582–3609, 2017.

[34] H. Jin. Materials for Thermoelectric Energy Conversion. *Res Metallica 2015*, KU Leuven, May 27, 2015.

[35] H. J. Goldsmid. *The Physics of Thermoelectric Energy Convertion.* Morgan & Claypool Publishers, San Rafael, CA, 2017.

[36] B. G. Shen, J. R. Sun, F. X. Hu, H. W. Zhang, and Z. H. Cheng. Recent progress in exploring magnetocaloric materials. *Adv. Mater.*, 21(45):4545–4564, 2009.

[37] J. Liu, T. Gottschall, K. P. Skokov, J. D. Moore, and O. Gutfleisch. Giant magnetocaloric effect driven by structural transitions. *Nano Mater.*, 11(7):620–626, 2012.

[38] M. A. Hamad. Magnetocaloric properties of $La_{0.6}Ca_{0.4}Mn_{O3}$. *J. Therm. Anal. Calorim.*, 113(2):609–613, 2008.

[39] A. He, V. Svitlyk, and Y. Mozharivskyj. Synthetic Approach for $(Mn,Fe)_2(Si,P)$ Magnetocaloric Materials: Purity, Structural, Magnetic, and Magnetocaloric Properties. *Inorg. Chem.*, 56(5):2827–2833, 2017.

[40] K. T. Matsumoto and K. Hiraoka. Magnetocaloric effect in $Gd_{1-x}Nd_xZn_2$. *J. Magn. Magn. Mater.*, 438:107–110, 2017.

[41] Z. Kutnjak, B. Roi, and R. Pirc. *Electrocaloric Effect: Theory, Measurements, and Applications* in Wiley Encyclopedia of Electrical and Electronics Engineering. John Wiley & Sons, New Jersy, 2015.

[42] L. Biao, W. XinHua, T. ZhenHua, L. Bo, T. Tao, X. ZhiWei, Z. TianFu, T. XinGui, X. Yong, L. Jie, and L. ShengGuo. Large electrocaloric effect in BaTiO3 based multilayer ceramic capacitors. *Sci. China Technol. Sci.*, 59(7):1054–1058, 2016.

[43] M. H. Park, H. J. Kim, Y. J. Kim, T. Moon, K. D. Kim, Y. H. Lee, S. D. Hyun, and C. S. Hwang. Giant Negative Electrocaloric Effects of $Hf_{0.5}Zr_{0.5}O_2$ Thin Films. *Adv. Mater.*, 283(36):7956–7961, 2016.

[44] H. Huang, G. Zhang, X. Ma, D. Liang, J. Wang, Y. Liu, Q. Wang, and L. Q. Chen. Size effects of electrocaloric cooling in ferroelectric nanowires. *J. Am. Ceram. Soc.*, 101(4):1566–1575, 2018.

[45] S. Qian, Y. Geng, Y. Wang, J. Ling, Y. Hwang, R. Radermacher, I. Takeuchi, and J. Cui. A review of elastocaloric cooling: Materials, cycles and system integrations. *Int. J. Refrig.*, 64:1–19, 2016.

[46] Y. Liu, I. C. Infante, X. Lou, L. Bellaiche, J. F. Scott, and B. Dkhil. Giant Room-Temperature Elastocaloric Effect in Ferroelectric Ultrathin Films. *Adv. Mater.*, 26(35):6132–6137, 2014.

[47] Y. J. Huang, Q. D. Hu, N. M. Bruno, J. H. Chen, I. Karaman, J. H. Ross Jr., and J. G. Li. Giant elastocaloric effect in directionally solidified NiMnIn magnetic shape memory alloy. *Scr. Mater.*, 105:42–45, 2015.

[48] A. Chauhan, S. Patel, and R. Vaish. Elastocaloric effect in ferroelectric ceramics. *Appl. Phys. Lett.*, 106(17):172901, 2015.

[49] A. Shen, D. Zhao, W. Sunb, J. Liub, and C. Li. Elastocaloric effect in a $Co_{50}Ni_{20}Ga_{30}$ single crystal. *Scr. Mater.*, 127:1–5, 2017.

[50] K. Niitsu, Y. Kimura, T. Omori, and R. Kainuma. Cryogenic superelasticity with large elastocaloric effect. *NPG Asia Mater.*, 10(1), 2018.

[51] G. E. W. Bauer, E. Saitoh, and B. J. V. Wees. Spin caloritronics. *Nature Mater.*, 11(5):391–399, 2012.

[52] F. K. Dejene, J. Flipse, and B. J. V. Wees. Verification of the Thomson-Onsager reciprocity relation for spin caloritronics. *Phys. Rev. B*, 90(8).

[53] H. Yu, S. D. Brechet, and J. P. Ansermet. Spin caloritronics, origin and outlook. *Phys. Lett. A*, 381:825–837, 2016.

[54] M. Zeng, Y. Feng, and G. Liang. Graphene-based Spin Caloritronics. *Nano Lett.*, 11(53):1369–1373, 2011.

[55] J. Linder and M. E. Bathen. Spin caloritronics with superconductors: Enhanced thermoelectric effects, generalized Onsager response-matrix, and thermal spin currents. *Phys. Rev. B*, 93(22):224509, 2016.

[56] C. Safranski, I. Barsukov, H. K. Lee, T. Schneider, A. A. Jara, A. Smith, H. Chang, K. Lenz, J. Lindner, Y. Tserkovnyak, M. Wu, and I. N. Krivorotov. Spin caloritronic nano-oscillator. *Nature Comm.*, 8:117, 2017.

[57] H. J. Goldsmid. *Introduction to Thermoelectricity*. Springer, Berlin, 2016.

[58] R. Wolfe and G. E. Smith. Experimental Verification of the Kelvin Relation of Thermoelectricity in a Magnetic Field. *Phys. Rev.*, 129(3):1086–1087, 1963.

[59] P. W. Bridgeman. *The thermodynamics of electrical phenomena in metals*. The Macmillan Company, New York, 1934.

[60] P. W. Bridgeman. The connections between the four transverse Galvanomagnetic and thermomagnetic Phenomena. *Phys. Rev.*, 24(6):644–651, 1924.

[61] A. Migliori, T. W. Darling, F. Freibert, S. A. Trugman, E. Moshopoulou, and J. L. Sarrao. Optimization of materials for thermomagnetic cooling. *MRS Online Proc. Library*, 478:231–242, 1997.

[62] J. P. Heremans, M. S. Dresselhaus, L. E. Bell, and D. T. Morelli. When thermoelectrics reached the nanoscale. *Nature Nanotechnol.*, 8:471–473, 2013.

[63] Y. Pei, H. Wang, and G. J. Snyder. Band Engineering of Thermoelectric Materials. *Adv. Mater.*, 24(46):6125–6135, 2012.

[64] A. F. Ioffe. *Semiconductor Thermoelements and Thermoelectric Cooling*. Infosearch, London, 1957.

[65] S. Wang, J. Yang, T. Toll, J. Yang, W. Zhang, and X. Tang. Conductivity-limiting bipolar thermal conductivity in semiconductors. *Sci. Rep.*, 5(1):10136, 2015.

[66] J. J. Gong, A. J. Hong, J. Shuai, L. Li, Z. B. Yan, Z. F. Ren, and J. M. Liu. Investigation of the bipolar effect in the thermoelectric material CaMg2Bi2 using a first-principles study. *Phys. chem. chem. phys.*, 18(24):16566–16574, 2016.

[67] A. C. Beer. *Galvanomagnetic Effects in Semiconductors*. Academic Press, New York, 1963.

[68] I. M. Tsidilkovskii. *Thermomagnetic Effects in Semiconductors*. Infosearch, London, 1962.

[69] C. Kittel. *Introduction to Solid State Physics*. John Wiley, New York, 1960.

[70] R. R. Heikes and R. W. Ure Jr. *Thermoelectricity: Science and Engineering*. Interscience, New York, 1961.

[71] C. Herring, T. H. Geballe, and J. E. Kunzler. Phonon-Drag Thermomagnetic Effects in n-Type Germanium. I. General Survey. *Phys. Rev.*, 111(1):36–57, 1958.

[72] H. B. Callen. *Thermodynamics and an Introduction to Thermostatistics.* John Wiley and Sons, New York, 1960.

[73] L. Onsager. Reciprocal Relations in Irreversible Process. I. *Phys. Rev.*, 37(4):405–426, 1931.

[74] P. Mazur. Onsager's reciprocal relations and Thermodynamics of irreversible processes. *Period. Polytech. Chem. Eng.*, 41(2):197–204, 1996.

[75] L. Onsager. Reciprocal Relations in Irreversible Process. II. *Phys. Rev.*, 38(12):2265–2279, 1931.

[76] R. Fieschi, S. R. De Groot, and P. Mazur. Thermodynamical theory of Galvanomagnetic and thermomagnetic phenomena. I: reciprocal relations in anisotropic metals. *Physica*, 20(1):67–76, 1954.

[77] R. Fieschi, S. R. De Groot, P. Mazur, and J. Vlieger. Thermodynamical theory of Galvanomagnetic and thermomagnetic phenomena. II: reciprocal relations for moving anisotropic mixtures. *Physica*, 20(1):245–258, 1954.

[78] R. Fieschi, S. R. De Groot, and P. Mazur. Thermodynamical theory of Galvanomagnetic and thermomagnetic phenomena. III: Explicit expressions for the measurable effects in isotropic metals. *Physica*, 20(1):259–273, 1954.

[79] W. H. Lucke. Reply to experiment in Thermoelectricity. *Am. J. Phys.*, 28:563, 1960.

[80] B. J. O'Brien, C. S. Wallace, and K. Landecker. Cascading of Peltier Couples for Thermoelectric Cooling. *J. Appl. Phys.*, 27(7):820–823, 1956.

[81] E. R. Washwell, S. R. Hawkins, and K. F. Cuff. The Nernst detector: fast thermal radiation detection. *Appl. Phys. Lett.*, 17(4):164–166, 1970.

[82] E. S. Rittner. On the Theory of the Peltier Heat Pump. *J. Appl. Phys.*, 30(5):702–707, 1959.

[83] C. F. Kooi, R. B. Horst, and K. F. Cuff. Thermoelectric-Thermomagnetic Energy Converter Staging. *J. Appl. Phys.*, 39(9):4257–4263, 1968.

[84] B. J. O'Brien and C. S. Wallace. Ettingshausen Effect and Thermomagnetic Cooling. *J. Appl. Phys.*, 29(7):1010–1012, 1958.

[85] C. F. Kooi, R. B. Horst, K. F. Cuff, and S. R. Hawkins. Theory of the Longitudinally Isothermal Ettingshausen Cooler. *J. Appl. Phys.*, 34(6):1735–1742, 1963.

[86] T. C. Harman, J. M. Honig, S. Fischler, A. E. Paladino, and M. J. Button. Oriented single-crystal bismuth nernst-ettingshausen refrigerators. *Appl. Phys. Lett.*, 4(4):77–79, 1964.

[87] Y. Tang, B. Cui, C. Zhou, and M. Grayson. p $\times$ n-Type Transverse Thermoelectrics: A Novel Type of Thermal Management Material. *J. Electron. Mater.*, 44(6):2095–2104, 2015.

[88] T. C. Harman, J. M. Honig, and B. M. Tarmy. Theory of Galvano-Thermomagnetic Energy Conversion Devices. V. Devices Constructed from Anisotropic Materials. *J. Appl. Phys.*, 34(8):2225–2229, 1963.

[89] O. Yamashita and S. Tomiyoshi. Effect of geometrical shape on magnetoPeltier and Ettingshausen cooling in Bi and Bi0.88Sb0.12 polycrystals. *J. Appl. Phys.*, 92(7):3794–3802, 2002.

[90] J. R. Madigan. A hybrid peltier-ettingshausen cooler for cryogenic temperatures. *Solid-State Electron.*, 7(9):643–654, 1964.

[91] K. Scholz, P. Jandl, U. Birkholz, and Z. M. Dashevskii. Infinite stage Ettingshausen cooling in Bi-Sb alloys. *J. Appl. Phys.*, 75(10):5406–5408, 1994.

[92] R. B. Horst and L. R. Williams. Application of solid-state cooling to spaceborne infrared focal planes. *Proc. 3rd Int. Conf. Thermoelectric Energy Conversion*, Arlington, TX, 1980.

[93] T. C. Harman and J. M. Honig. Theory of Galvano-Thermomagnetic Energy Conversion Devices. I. Generators. *J. Appl. Phys.*, 33(11):3178–3188, 1962.

[94] T. C. Harman and J. M. Honig. Theory of Galvano-Thermomagnetic Energy Conversion Devices. II. Refrigerators and Heat Pumps. *J. Appl. Phys.*, 33(11):3188–3194, 1962.

[95] T. C. Harman and J. M. Honig. Theory of Galvano-Thermomagnetic Energy Conversion Devices. III. Generators Constructed from Anisotropic Materials. *J. Appl. Phys.*, 34(1):189–194, 1963.

[96] T. C. Harman, J. M. Honig, and B. M. Tarmy. Galvano-Thermomagnetic Phenomena. IV. Application to Anisotropic Adiabatic Nernst Generators. *J. Appl. Phys.*, 34(8):2215–2224, 1963.

[97] R. D. Redin. *Thermomagnetic and Galvanomagnetic effects.* Iowa State College, Ames, IA, 1957.

[98] K. F. Cuff, R. B. Horst, J. L. Weaver, S. R. Hawkins, C. F. Kooi, and G. M. Enslow. The thermomagnetic figure of merit and Ettingshausen cooling in Bi-Sb alloys. *Appl. Phys. Lett.*, 2(8):145–146, 1963.

[99] Linseis. *Seebeck Coefficient / Electric Resistance Measuring System.* [Online], Available:https://www.linseis.com/fileadmin/_migrated/content_uploads/LSR3_-Seebeck_Resistivity.pdf.

[100] S. I. Tanuma and M. Sakurai. Magnetic field dependence of thermomagnetic effect of Bi88Sb12 alloy. *J. Adv. Sci.*, 7(3-4):163–167, 1995.

[101] M. Hyland, H. Hunter, J. Liu, E. Veety, and D. Vashaee. Magnetic field dependence of thermomagnetic effect of Bi88Sb12 alloy. *Appl. Energy*, 182:518–524, 2016.

[102] A. R. M. Siddique, R. Rabari, S. Mahmud, and B. V. Heyst. Thermal energy harvesting from the human body using flexible thermoelectric generator (FTEG) fabricated by a dispenser printing technique. *Energy*, 115(1):1081–1091, 2016.

[103] S. E. Jo, M. K. Kim, M. S. Kim, and Y. J. Kim. Flexible thermoelectric generator for human body heat energy harvesting. *Electron. Lett.*, 48(16):1013–1015, 2012.

[104] D. Madan, Z. Wang, A. Chen, P. K. Wright, and J. W. Evans. High-performance dispenser printed MA p-type Bi0.5Sb1.5Te3 flexible thermoelectric generators for powering wireless sensor networks. *ACS Appl. Mater. Interfaces*, 5(22):1187211876, 2013.

[105] Z. Cao, E. Koukharenko, M. J. Tudor, R. N. Torah, and S. P. Beeby. Screen printed flexible Bi2Te3-Sb2Te3 based thermoelectric generator. *J. Phys.: Conf. Series*, 476(Conference 1):012031, 2013.

[106] K. Behnia, A. Pourret R. Bel, K. Izawa, J. Flouquet, Y. Nakajima, Y. Matsuda, D. Kikuchi, Y. Aoki, H. Sugawara, and H. Sato. Gaint Nernst effect in heavy-electron metals. *J. Magnet. Magnet. Mater.*, 310:446–448, 2007.

[107] J. L. Cohn, B. D. White, C. A. M. D. Santos, and J. J. Neumeier. Gaint Nernst Effect and Bipolarity in the Quasi-One-Dimensional Metal Li0.9Mo6O17. *Phys. Rev. Lett.*, 108(5):056604, 2012.

[108] Z. Z. Alisultanov. Nernst-Ettingshausen Effect in Graphene. *JETP Lett.*, 99(12):702–705, 2014.

[109] S. A. Nemov, V. I. Proshin, G. L. Trrantasov, R. V. Parfen, D. V. Shamshur, and A. V. Charnyaev. Transverse Nernst-Ettingshausen effect, Resonant scattering, and Superconductivity in SnTe:In. *Phys. Solid State*, 51(3):491–494, 2009.

APPENDIX

Appendix A

Matlab files for simulation model

A.1 Main m-file

```
clc; clear all;

flag = 1;

% 1 -> dT_max vs current & length, and Temperature profile

% 2 -> dt_max vs shape factor

% 3 -> Qin_max and COP_max vs Length

% 4 -> Qin_max and COP_max vs Shape Factor

%Notes:

%x: the heat flow direction

%y: curect flow

%z: B field

%da: x axis step size

%a: length vector in x

%Eyy: electric field
```

```
global da a Eyy Thot shape_factor
da = 1e-3; %cm
Thot=150; %K
E_max=1;
Eyy = linspace(0,E_max,500); %V/cm
B_field = 1; % Tesla

%% \DelT_max vs Current, \DelT_max vs x_len and Temperature map
if (flag == 1)
shape_factor = 13;
x_len = 0.428; y_len = 2.54; z_len = 0.031; % Dimentions are taken from Book chapter
% x_len = 0.6; y_len = 2.62; z_len = 0.2; % Dimentions are taken from Book chapter
a = da:da:x_len;
Qin = 0; %W no heat load
% Defining the geometric structures for thick, thin, trapezoid and Harman's infinite stage
c_rect_thin = z_len*ones(1,length(a)); % thin rectangular
c_rect_thic = shape_factor*z_len*ones(1,length(a)); % thic rectangular
theta = atan(x_len/(0.5*(shape_factor - 1)*z_len)); % defining theta for trapezoid
c_trap = z_len*ones(1,length(a)) + 2*(a - a(1))./tan(theta); % trapezoid
c_harm = z_len*shape_factor.^(a/x_len); % Infinite
cond = 1; % 1 -> temp dependent material parameters, 0 -> temp independent param
[I_rect1,delT_rect1,dTmax_rect1,pos_rect1,Tprof_rect1,z_rect1,QJ_rect1,Qp_rect1] = multistage_NE(cond,y_len,c_rect_thin,B_field,Qin,0);
[I_rect2,delT_rect2,dTmax_rect2,pos_rect2,Tprof_rect2,z_rect2,QJ_rect2,Qp_rect2] = multistage_NE(cond,y_len,c_rect_thic,B_field,Qin,0);
```

```
[I_trap,delT_trap,dTmax_trap,pos_trap,Tprof_trap,z_trap,QJ_trap,Qp_trap] =
multistage_NE(cond,y_len,c_trap,B_field,Qin,0);
[I_harm,delT_harm,dTmax_harm,pos_harm,Tprof_harm,z_harm,QJ_harm,Qp_harm] =
multistage_NE(cond,y_len,c_harm,B_field,Qin,0);
[I_corr,delT_corr,dTmax_corr,pos_corr,Tprof_corr,z_corr,QJ_corr,Qp_corr] =
multistage_NE(cond,y_len,z_len,B_field,Qin,1);

figure(1);
plot(-0.5*fliplr(z_rect1),a,'r',0.5*fliplr(z_rect1),a,'r','linewidth',2.0); hold on;
plot(-0.5*fliplr(z_rect2),a,'g',0.5*fliplr(z_rect2),a,'g','linewidth',2.0); hold on;
plot(-0.5*fliplr(z_trap),a,'b',0.5*fliplr(z_trap),a,'b','linewidth',2.0); hold on;
plot(-0.5*fliplr(z_harm),a,'m',0.5*fliplr(z_harm),a,'m','linewidth',2.0); hold on;
plot(-0.5*fliplr(z_corr),a,'k',0.5*fliplr(z_corr),a,'k','linewidth',2.0); hold on;
plot(linspace(-0.5*z_corr(1),0.5*z_corr(1),10),a(1)*ones(1,10),'g',linspace(-0.5*z_corr(1),
0.5*z_corr(1),10),a(end)*ones(1,10),'g','linewidth',2.0); hold on;
plot(-0.5*fliplr(z_corr),a(1)*ones(1,length(a)),'g',-0.5*fliplr(z_corr),a(end)*ones(1,
length(a)), 'g',0.5*fliplr(z_corr),a(1)*ones(1,length(a)),'g',0.5*fliplr(z_corr),a(end)*
ones(1,length(a)),'g','linewidth',2.0);
xlabel('z axis —>');ylabel('<— x axis');title('Geometric structures of NE devices');

figure(2);
plot(I_rect1,delT_rect1,'r',I_rect2,delT_rect2,'g',I_trap,delT_trap,'b',I_harm,delT_harm,
'm',I_corr,delT_corr,'k','linewidth',2.0);
xlabel('Current (A)');ylabel('\DeltaT (K)');title('\DeltaT vs Current for Different
Shaped Structure');
```

```
legend('Thin rectangle','thick recatngle','Trapezoid','Harman infinite stage', 'This work')

figure(3);
plot(I_rect1,QJ_rect1,'r',I_rect2,QJ_rect2,'g',I_trap,QJ_trap,'b',I_harm,QJ_harm,'m',I_corr,
QJ_corr,'k','linewidth',2.0);
xlabel('Current (A)');ylabel('Joule Heat (W)');title('Joule Heat vs Current for Different
Shaped Structure');
legend('Thin rectangle','thick recatngle','Trapezoid','Harman infinite stage', 'This work')

figure(4);
plot(I_rect1,Qp_rect1,'r',I_rect2,Qp_rect2,'g',I_trap,Qp_trap,'b',I_harm,Qp_harm,'m',I_corr,
Qp_corr,'k','linewidth',2.0);
xlabel('Current (A)');ylabel('Ettingshausen Heat (W)');title('Ettingshausen Heat vs Cur-
rent for Different Shaped Structure');
legend('Thin rectangle','thick recatngle','Trapezoid','Harman infinite stage', 'This work')

figure(5);
plot(a,Tprof_rect1 - Tprof_rect1(1),'r',a,Tprof_rect2 - Tprof_rect2(1),'g',a,Tprof_trap -
Tprof_trap(1),'b',a,Tprof_harm - Tprof_harm(1),'m',a,Tprof_corr - Tprof_corr(1),'k');
xlabel('Device length in x-axis (cm)');ylabel('\DeltaT (K)');title('\DeltaT along x-axis
for Different geometries');
legend('Thin rectangle','thick recatngle','Trapezoid','Harman infinite stage', 'This work')

aa = repmat(a',1,length(a));
for i = 1:length(a)
```

```
cc_rect1(i,:) = linspace(-z_rect1(length(a)+1-i)/2,z_rect1(length(a)+1-i)/2,length(a));
TT_rect1(i,:) = Tprof_rect1(length(a)+1-i)*ones(1,length(a));
cc_rect2(i,:) = linspace(-z_rect2(length(a)+1-i)/2,z_rect2(length(a)+1-i)/2,length(a));
TT_rect2(i,:) = Tprof_rect2(length(a)+1-i)*ones(1,length(a));
cc_trap(i,:) = linspace(-z_trap(length(a)+1-i)/2,z_trap(length(a)+1-i)/2,length(a));
TT_trap(i,:) = Tprof_trap(length(a)+1-i)*ones(1,length(a));
cc_harm(i,:) = linspace(-z_harm(length(a)+1-i)/2,z_harm(length(a)+1-i)/2,length(a));
TT_harm(i,:) = Tprof_harm(length(a)+1-i)*ones(1,length(a));
cc_corr(i,:) = linspace(-z_corr(length(a)+1-i)/2,z_corr(length(a)+1-i)/2,length(a));
TT_corr(i,:) = Tprof_corr(length(a)+1-i)*ones(1,length(a));
end
figure(101);
surf(cc_rect2,aa,TT_rect2,'EdgeColor','None'), view(2), axis equal tight, colorbar
title('Temperature map of Rectangular Stage NE device');
figure(105);
surf(cc_rect1,aa,TT_rect1,'EdgeColor','None'), view(2), axis equal tight, colorbar
title('Temperature map of Rectangular Stage NE device');
figure(102);
surf(cc_trap,aa,TT_trap,'EdgeColor','None'), view(2), axis equal tight, colorbar
title('Temperature map of Trapeziodal Stage NE device');
figure(103);
surf(cc_harm,aa,TT_harm,'EdgeColor','None'), view(2), axis equal tight, colorbar
title('Temperature map of Harman Infinite Stage NE device');
figure(104);
surf(cc_corr,aa,TT_corr,'EdgeColor','None'), view(2), axis equal tight, colorbar
```

```
title('Temperature map of modified infinite stage NE device');
end

%% \DelT vs shape factor
if (flag == 2)
geometric_ratio = 1:2:201;
for sf = 1:length(geometric_ratio)
Qin = 0;
shape_factor = geometric_ratio(sf);
x_len = 0.428; y_len = 2.50; z_len = 0.031;
a = da:da:x_len;
c_rect_thin = z_len*ones(1,length(a));
c_rect_thic = shape_factor*z_len*ones(1,length(a));
theta = atan(x_len/(0.5*(shape_factor - 1)*z_len));
c_trap = z_len*ones(1,length(a)) + 2*(a - a(1))./tan(theta);
c_harm = z_len*shape_factor.^(a/x_len);
cond = 1;
[I_rect1,delT_rect1,dTmax_rect1(sf),pos_rect1,Tprof_rect1,z_rect1,QJ_rect1,Qp_rect1] =
multistage_NE(cond,y_len,c_rect_thin,B_field,Qin,0);
[I_rect2,delT_rect2,dTmax_rect2(sf),pos_rect2,Tprof_rect2,z_rect2,QJ_rect2,Qp_rect2] =
multistage_NE(cond,y_len,c_rect_thic,B_field,Qin,0);
[I_trap,delT_trap,dTmax_trap(sf),pos_trap,Tprof_trap,z_trap,QJ_trap,Qp_trap] =
multistage_NE(cond,y_len,c_trap,B_field,Qin,0);
[I_harm,delT_harm,dTmax_harm(sf),pos_harm,Tprof_harm,z_harm,QJ_harm,Qp_harm] =
multistage_NE(cond,y_len,c_harm,B_field,Qin,0);
```

```
[I_corr,delT_corr,dTmax_corr(sf),pos_corr,Tprof_corr,z_corr,QJ_corr,Qp_corr] =
multistage_NE(cond,y_len,z_len,B_field,Qin,1);
Irect1(sf) = I_rect1(pos_rect1);
Irect2(sf) = I_rect2(pos_rect2);
Itrap(sf) = I_trap(pos_trap);
Iharm(sf) = I_harm(pos_harm);
Icorr(sf) = I_corr(pos_corr);
end

figure(3);
plot(geometric_ratio,dTmax_rect1,'r',geometric_ratio,dTmax_rect2,'g',geometric_ratio,
dTmax_trap,'b',geometric_ratio,dTmax_harm,'m',geometric_ratio,dTmax_corr,'k');
xlabel('Shape factor');ylabel('\DeltaT_max (K)');title('\DeltaT_max vs Shape factor for
Different Shaped Structure');
legend('Thin rectangle','thick recatngle','Trapezoid','Harman infinite stage', 'This work')
figure(4);
plot(geometric_ratio,Irect1,'r',geometric_ratio,Irect2,'g',geometric_ratio,Itrap,'b',
geometric_ratio,Iharm,'m',geometric_ratio,Icorr,'k','linewidth',2.0);
xlabel('Shape factor');ylabel('I (A)');title('Current at \DeltaT_max vs Shape factor for
Different Shaped Structure');
legend('Thin rectangle','thick recatngle','Trapezoid','Harman infinite stage', 'This work')
end
```

A.2 M-file for Multistage NE devices

```
function [Itot,dT,dTmax,pos,Tprof,z_prof,QJ_prof,Qp_prof] =
multistage_NE(cond,y_len,z_len,B_field,Qload,flag_corr)
% Definition of all parameters:
% r at the end of all parameters for representing rectangular shape
% a,b,c = device dimensions (in cm)
% BNyx = B-field*Nernst (V/K)
% rhoyy = Resistivity (ohm/cm)
% kxxr = thermal conductivity (W/cm/K)
% alphayx = Seebeck co-efficient
% Qt = total heat flow (in W)
% Q = Heat flow density (in W/cm2̂)
% Qin = Input heat flow (W)
% Tc = Temp_profile from cold to hot side,
% delT_x = temperature gradient per legth along x-axis
% Jy = current density along y-axis
% Itot = Total current along y-axis
% Py = Joule heating along y-axis
global da a Thot Eyy shape_factor
c = z_len;
b = y_len;
x_len = a(end);
% initialization with zeros
QJ = zeros(length(Eyy),length(a)+1);
```

```
Qp = zeros(length(Eyy),length(a)+1);
Iy = zeros(length(Eyy),length(a)+1);
Py = zeros(length(Eyy),length(a)+1);
BNyx = zeros(length(Eyy),length(a)+1);
rhoyy = zeros(length(Eyy),length(a)+1);
kxx = zeros(length(Eyy),length(a)+1);
Rth = zeros(length(Eyy),length(a)+1);
R = zeros(length(Eyy),length(a)+1);
Itot = zeros(1,length(Eyy));
dT = zeros(1,length(Eyy));
N=length(a);
T(1,N+1)=Thot;
T(1,1)=Thot-30; %guess
T(1,:)=linspace(T(1,1),T(1,end),N+1); %linear guess
if flag_corr==0
c(N+1)=c(N);
else
c(1)=z_len(1);
a(N+1)=a(N);
end
i=1;
while i¡=length(Eyy) && T(i,1)¡=Thot
Ey=Eyy(i);
tolerance=1e60;
while tolerance¿1e-5
```

```
Told(i,:)=T(i,:);
if flag_corr==1
c = z_len(1)*exp((a*log(shape_factor)/x_len) + (0.5*(a/x_len).*(1-(a/x_len)).*((T(i,:)-
T(i,1))/T(i,1)).^2));
end
[BNyx(i,:),rhoyy(i,:),kxx(i,:)] = input_deck_BiSb(T(i,:),B_field,cond);
Rth(i,:)=da./kxx(i,:)./c/b;
R(i,:)=rhoyy(i,:)*b./c/da;
QJ(i,:)=(Ey*b).^2./R(i,:); %W
Qp(i,:)=Ey./rhoyy(i,:).*BNyx(i,:).*c*b.*T(i,:); %W
for j = N:-1:1
T(i,j)=T(i,j+1)+Rth(i,j)*( QJ(i,j)/2 + Qload - Qp(i,j) + sum(QJ(i,1:j-1)) ); %K
end
tolerance=abs(sum((T(i,:)-Told(i,:))));
end
Iy(i,:) = (Ey + BNyx(i,:).*gradient(T(i,:))/da )./rhoyy(i,:)*da.*c; %A
Itot(i) = sum(Iy(i,:));
Py(i,:) = Ey*b.*Iy(i,:); % Joule energy, J
dT(i) = Thot - T(i,1); % Tempearture gradient across the device
QJ_prof(i) = sum(QJ(i,:));
Qp_prof(i) = sum(Qp(i,:));
i=i+1;
T(i,:)=T(i-1,:);
end
Iy(i:end,:)=[];
```

```
Itot(i:end)=[];
Py(i:end,:)=[];
dT(i:end)=[];
[dTmax,pos] = max(dT);
Tprof = T(pos,:);
if flag_corr==1
z_prof = z_len(1)*exp((a*log(shape_factor)/x_len) + (0.5*(a/x_len).*(1-(a/x_len)).*
((T(pos,:)-T(pos,1))/T(pos,1)).^2));
else
z_prof = c;
end
end
```

A.3 Input file for material properties

```
function [B_Nyx resistivity thermal_cond] = input_deck_BiSb(x,y,cond)
% x = Temperature
% y = Magnetic field
% cond - indicates tempearature dependency of material parameter,
% cond = 0 -¿ T independent and cond = 1 -¿ Temperature dependent
if(cond == 0)
B_Nyx(1:length(x)) = 650*1e-6; % thermomagnetic power (V/K)
resistivity(1:length(x)) = 2.3*1e-3; % resistivity in ohm-cm
thermal_cond(1:length(x)) = 0.057; % thermal conductivity in w/cm/K
```

```
else
if y  = 1
disp('Material properties for B=1 were used. Update the porperties for accurate result.');
end
% Nyx parameters
xx=[0.0000 10.101 20.202 30.303 40.404 50.505 60.606 70.707 80.808 90.909 101.01 111.11
121.21 131.31 141.41 151.52 161.62 171.72 181.82 191.92 202.02 212.12 222.22 232.32
242.42 252.53 262.63 272.73 282.83 292.93 303.03 313.13 323.23 333.33 343.43 353.54
363.64 373.74 383.84 393.94 404.04 414.14 424.24 434.34 444.44 454.55 464.65 474.75
484.85 494.95 505.05 515.15 525.25 535.35 545.45 555.56 565.66 575.76 585.86 595.96
606.06 616.16 626.26 636.36 646.46 656.57 666.67 676.77 686.87 696.97 707.07 717.17
727.27 737.37 747.47 757.58 767.68 777.78 787.88 797.98 808.08 818.18 828.28 838.38
848.48 858.59 868.69 878.79 888.89 898.99 909.09 919.19 929.29 939.39 949.49 959.60
969.70 979.80 989.90 1000.00];
Nernstt=[0.001200 0.001200 0.001200 0.001200 0.0011886 0.0011587 0.001115 0.001051
0.0009893 0.0009084 0.0008307 0.0007542 0.00067695 0.00060092 0.00052781 0.00046364
0.0004076 0.0003516 0.0003079 0.00026514 0.00021624 0.00017613 0.00014419 0.00011857
9.8156e-05 8.1626e-05 6.8007e-05 5.7270e-05 4.8148e-05 4.0648e-05 3.5329e-05 3.1353e-05
2.8197e-05 2.5600e-05 2.3411e-05 2.1533e-05 1.9900e-05 1.8464e-05 1.7189e-05 1.6048e-05
1.5021e-05 1.4091e-05 1.3244e-05 1.2470e-05 1.1758e-05 1.1102e-05 1.0495e-05 9.9322e-06
9.4082e-06 8.9192e-06 8.4618e-06 8.0331e-06 7.6302e-06 7.2511e-06 6.8935e-06 6.5557e-06
6.2361e-06 5.9332e-06 5.6457e-06 5.3725e-06 5.1125e-06 4.8648e-06 4.6286e-06 4.4029e-06
4.1873e-06 3.9809e-06 3.7832e-06 3.5936e-06 3.4118e-06 3.2371e-06 3.0692e-06 2.9077e-06
2.7522e-06 2.6024e-06 2.4580e-06 2.3188e-06 2.1843e-06 2.0544e-06 1.9289e-06 1.8076e-06
1.6901e-06 1.5764e-06 1.4663e-06 1.3596e-06 1.2561e-06 1.1558e-06 1.0584e-06 9.6380e-07
```

8.7195e-07 7.8269e-07 6.9592e-07 6.0926e-07 5.2505e-07 4.4322e-07 3.6373e-07 2.8653e-07 2.1159e-07 1.3887e-07 6.8349e-08 7.5560e-22];

Nernst=interp1(xx,Nernstt,x,'pchip');

B_Nyx = Nernst*y;

% rhoyy

xx = [0.0000 10.101 20.202 30.303 40.404 50.505 60.606 70.707 80.808 90.909 101.01 111.11 121.21 131.31 141.41 151.52 161.62 171.72 181.82 191.92 202.02 212.12 222.22 232.32 242.42 252.53 262.63 272.73 282.83 292.93 303.03 313.13 323.23 333.33 343.43 353.54 363.64 373.74 383.84 393.94 404.04 414.14 424.24 434.34 444.44 454.55 464.65 474.75 484.85 494.95 505.05 515.15 525.25 535.35 545.45 555.56 565.66 575.76 585.86 595.96 606.06 616.16 626.26 636.36 646.46 656.57 666.67 676.77 686.87 696.97 707.07 717.17 727.27 737.37 747.47 757.58 767.68 777.78 787.88 797.98 808.08 818.18 828.28 838.38 848.48 858.59 868.69 878.79 888.89 898.99 909.09 919.19 929.29 939.39 949.49 959.60 969.70 979.80 989.90 1000.00];

rhoyyy = [30.359 25.722 21.793 18.460 15.629 13.219 11.167 9.4169 7.9249 6.6537 5.3484 4.2718 3.3930 2.6837 2.1178 1.6719 1.3247 1.0577 0.85444 0.70107 0.58503 0.49706 0.43067 0.38033 0.34180 0.31191 0.28829 0.26920 0.25343 0.24008 0.22865 0.21877 0.21012 0.20248 0.19566 0.18954 0.18402 0.17900 0.17442 0.17022 0.16635 0.16278 0.15947 0.15640 0.15353 0.15085 0.14834 0.14599 0.14378 0.14169 0.13972 0.13786 0.13610 0.13443 0.13284 0.13133 0.12989 0.12852 0.12721 0.12596 0.12477 0.12362 0.12253 0.12148 0.12047 0.11949 0.11856 0.11766 0.11680 0.11596 0.11516 0.11439 0.11364 0.11291 0.11221 0.11154 0.11088 0.11025 0.10963 0.10904 0.10846 0.10790 0.10735 0.10683 0.10631 0.10581 0.10533 0.10486 0.10440 0.10395 0.10351 0.10308 0.10266 0.10224 0.10184 0.10145 0.10107 0.10071 0.10035 0.10000];

rhoyy=interp1(xx,rhoyyy,x,'pchip');

resistivity = rhoyy*1e-3;

```
% thermal conductivity (ref: R B Horst)
xx=[0.0000 10.101 20.202 30.303 40.404 50.505 60.606 70.707 80.808 90.909 101.01 111.11
121.21 131.31 141.41 151.52 161.62 171.72 181.82 191.92 202.02 212.12 222.22 232.32
242.42 252.53 262.63 272.73 282.83 292.93 303.03 313.13 323.23 333.33 343.43 353.54
363.64 373.74 383.84 393.94 404.04 414.14 424.24 434.34 444.44 454.55 464.65 474.75
484.85 494.95 505.05 515.15 525.25 535.35 545.45 555.56 565.66 575.76 585.86 595.96
606.06 616.16 626.26 636.36 646.46 656.57 666.67 676.77 686.87 696.97 707.07 717.17
727.27 737.37 747.47 757.58 767.68 777.78 787.88 797.98 808.08 818.18 828.28 838.38
848.48 858.59 868.69 878.79 888.89 898.99 909.09 919.19 929.29 939.39 949.49 959.60
969.70 979.80 989.90 1000.00];
kxxx=[0.05100 0.05121 0.05146 0.05177 0.05222 0.05286 0.053662 0.054643 0.055746
0.05693 0.05811 0.05935 0.060615 0.06189 0.063135 0.06433 0.065451 0.066494 0.067443
0.068273 0.06901 0.06967 0.070264 0.07080 0.071285 0.071725 0.072128 0.072498 0.07284
0.07316 0.07346 0.073744 0.07401 0.074262 0.074501 0.074726 0.074941 0.075144 0.075338
0.075522 0.075698 0.07587 0.07603 0.07618 0.07633 0.076468 0.076603 0.076733 0.076858
0.07698 0.077094 0.07721 0.077313 0.07742 0.07752 0.077612 0.07771 0.077796 0.077883
0.07797 0.07805 0.07813 0.07821 0.07828 0.078352 0.078423 0.078491 0.078557 0.078621
0.078684 0.078745 0.078804 0.078862 0.078918 0.078973 0.07903 0.07908 0.07913 0.07918
0.079227 0.079274 0.07932 0.079365 0.07941 0.079452 0.079494 0.079535 0.07958 0.079614
0.079653 0.07969 0.07973 0.079765 0.079801 0.079836 0.07987 0.079904 0.07994 0.07997
0.08000];
kxx=interp1(xx,kxxx,x,'pchip');
thermal_cond = kxx;
end
```